INVESTIGATION OF SEISMIC SHEAR DESIGN PROVISIONS OF IRC CODE FOR RC BRIDGE PIERS USING DISPLACEMENT-BASED PUSHOVER ANALYSIS

A Thesis Submitted
in Partial Fulfillment of the Requirements
for the Degree of
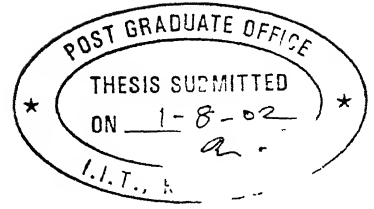
MASTER OF TECHNOLOGY

by

Rupen Goswami
Y010336

Department of Civil Engineering
Indian Institute of Technology Kanpur
August 2002
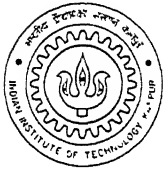
CERTIFICATE

It is certified that the work contained in this thesis entitled *"Investigation of Seismic Shear Design Provisions of IRC Code for RC Bridge Piers using Displacement-Based Pushover Analysis"* by Mr. Rupen Goswami (Roll No. Y010336), has been carried out under my supervision and that this work has not been submitted elsewhere for a degree.

(C. V. R. Murty)
Associate Professor
Department of Civil Engineering

August, 2002   Indian Institute of Technology, Kanpur

Abstract

Monotonic lateral load-deformation relationships of RC bridge piers bending in single curvature, designed as per the existing Indian standards, are analytically derived. For this, a static nonlinear displacement-based pushover analysis programme is developed. The analysis captures progression of plasticity, both along and across large pier sections using a fibre model. The effective shear stiffness considered accounts for both flexural translational and shear translational deformations of a general pier. Using an existing concrete confinement model, applicable for both circular and rectangular solid and hollow RC sections, appropriate hysteretic uniaxial constitutive relations for concrete and 'longitudinal' steel are developed to account for unloading and reloading in fibres during redistribution of stresses in the sections. Buckling of longitudinal steel is also accounted for.

From analysis of a number of piers, transverse reinforcement requirements are found to be inadequate; shear capacities of sections are found to be lower than the shear demand due to flexure, except in slender piers. Increasing transverse reinforcement increases the deformability and ductility of the pier. Increase in the level of axial load reduces the ductility but increases the shear demand on the section. Providing additional radial links in hollow circular sections increases the ductility of piers.

To my Parents..

Acknowledgments

My wholehearted gratitude go to my thesis supervisor, C.V.R. Murty, for the valuable guidance, critical technical discussions, and his care, affection and support towards me that eventually led to the completion of this thesis. I am indebted to Professor Sudhir K. Jain for his surprise surveillance on my progress and for giving me access to the vast resources of technical material in his office continuously throughout my stay. This has given me enough opportunity to read and learn, and has provided substantial amount of material much needed for this research.

I also thank Kiran J. Akella, (1999 M.Tech. Civil Engineering, IIT Kanpur) for sharing valuable knowledge on current bridge design practice in India. I also thank Professor Mahesh C. Tandon of TCPL, New Delhi and Sri. Atul Bhobe of S.N. Bhobe & Associates, Mumbai, for providing me important documents that helped understanding the bridge pier design strategy practiced in India. I also thank the faculty members of IIT Kanpur who have taught me and helped me increase my technical wisdom. In particular, I thank Professor Vinay K. Gupta for the initial tough days that he had put me in (!); it helped develop the confidence to face difficult situations in life. I also thank his family for the nice moments we all had spent together.

I remain ever grateful to all those who had rushed to *The Regency Hospital* and stayed there day and night...the days when I needed them the most. I also thank my Warden, Professor Keshav Kant for the help and quick arrangements he made, much required at that moment of crisis.

I thank Motilal and Malkhan for all the bottles of chilled water, and the warm cups of tea, and other stationary that they have supplied whenever I had asked for.

I can never forget the treasured company of my *friends*: Arindam, Sandip (*Sona*), Kaustubh (*Nati*), Roma, Balu, Rajrup, Jayanta, Santanu,... (the list goes on), and my very own batchmates: Anirudha, Santosh, Raghu, PK, Ramesh (*Chhotu*), Ajeet, Khanna *Sir,* Major *Saab*, and, Sona and Nati. They have not only provided the lighter moments that made the stay livelier, but have also pushed me harder towards my academic goals. In particular, my relationship with Nati saw so many technical and (more often!) non-technical matter being put in the right track by his constructive suggestions.

The company of Hemant and Snehal (with *misti* on a plate) has been very special. Among my seniors, the early wise words of Prabuddha-*da* are worth remembering. The company of Samit-*da* has helped me live through some very critical moments of my stay in this campus. Back here, Jaswant deserves a special mention not only for helping in completing this work by continuously reminding me of the deadlines, but also for sharing some important observations on *life*. And Ashutosh, one who ever smilingly spared so many evenings for me. His help in the final preparation of this thesis is highly acknowledged. I also thank Prishati, Prasenjit, Swagata and Ayan for the good moments I shared with them, that made my stay here in IIT Kanpur that much more memorable

... I have no words to express my appreciation for the unbound love and support from my parents. I recall their numerous sacrifices that made it possible for me to pursue my educational goals.

rupen

Table of Contents

List of Tables

...

List of Figures

•••

List of Symbols

Symbol	Description
A^c	Area of concrete fibre in fibre model
A_c	Core concrete area of pier
A_e	Effective shear area of pier (taken as $0.8\ A_g$)
A_g	Gross cross-sectional area of pier
A_i	Area of ith fibre in the Fibre Model
A_l	Area of longitudinal reinforcement in pier
A^s	Area of steel fibre in fibre model
A_s	Shear area of cross-section
A_{sh}	Total cross-sectional area of effective transverse reinforcement
A_{sv}	Cross-sectional area of each transverse steel bar
C	Centre-to-centre distance between adjacent longitudinal bars
D	Total depth of section in the considered direction of lateral force
D'	Core dimension in the direction under consideration
D_i, D_o	Inner and outer diameters of hollow sections
E	Young's modulus
E_c	Young's modulus of concrete
E_s	Young's modulus of steel
E_t	Tangent modulus of elasticity of material
E_{sec}	Secant modulus of elasticity confined concrete at ultimate stress
G	Bulk modulus of elasticity of material
I	Moment of inertia of RC section
I^*	Second moment of area of a fibre about effective centroidal axis
$^f[K]_t$	Tangent stiffness matrix of a fibre in the Fibre Model in global coordinates
$^f[K]_t^{GS}$	Geometric stiffness matrix of a fibre in the Fibre Model in global coordinates
$^f[K]_t^{TS}$	Truss stiffness matrix of a fibre in the Fibre Model in global coordinates
$^{ab}[K]_t$	Tangent stiffness matrix of a segment corresponding to axial and bending effects in the Fibre Model in global coordinates
$^{sh}[K]_t$	Tangent stiffness matrix of a segment corresponding to shear effects in the Fibre Model in global coordinates
$^{sh}[K]_t^l$	Tangent stiffness matrix of a segment corresponding to shear effects in the Fibre Model in local coordinates

Symbol	Description
$[K]_t^s$	Tangent stiffness matrix of a segment in global coordinates
$[K]_t$	Complete tangent stiffness matrix of member in global coordinates
L	Length of pier from point of maximum moment to the point of contraflexure; Length of fibre in the Fibre Model
M	Moment at a section
M_c	Moment resisted by a section at a general iteration level
M_{cal}	Calculated bending moment capacity of a section for a given curvature
M_u	Ultimate bending moment capacity of a section for a given axial load
N_f	Number of fibres a segment is discretised into in the Fibre Model
N_{fc}	Number of concrete fibres a segment is discretised into in the Fibre Model
N_{fs}	Number of steel fibres a segment is discretised into in the Fibre Model
N^*	Design axial load on pier at ultimate limit state in NZS 3101
P	Applied/Design axial load
P_c	Axial load resisted by a section at a general iteration level
P_{cal}	Calculated axial strength of a section for a given curvature
Q	First moment of area of a part of section above the fibre under consideration about the bending axis
$[R]$	Matrix relating the end-displacements and end-forces of a fibre to those of a segment in the Fibre Model in global coordinates
$[T]$	Transformation matrix relating displacements and forces in local and global coordinates
V_c	Nominal shear strength provided by concrete Total shear resisted by a segment at a general iteration level
V_n	Nominal shear strength of members
V_o	Shear demand in members based on overstrength shear
V_s	Nominal shear strength provide by transverse steel
V_u	Factored shear force in pier used in AASHTO
V_{uc}	Shear strength provided by concrete computed as per IS: 456-2000
V_{us}	Shear strength provided by transverse steel computed as per IS: 456-2000
b	Width of a section
b_c	Width of concrete core used in Kent-Park model
b_i, b_o	Inner and outer widths of a hollow rectangular section
b_v	Effective width of web
c_c	Modification factor on concrete shear capacity accounting effect of cyclic loading used in PWRI 1998
c_e	Modification factor on concrete shear capacity accounting effect of effective depth of section used in PWRI 1998

Symbol	Description
c_{pt}	Modification factor on concrete shear capacity accounting effect of longitudinal steel content used in PWRI 1998
d	Effective depth of section
d_l	Diameter of longitudinal bars
d_{tw}	Diameter of intermediate ties in a rectangular section
d_v	Depth of cross-section effective in resisting shear
d_w	Diameter of hoop in a rectangular section
$\{d\}$	End-displacement vector of a segment in the Fibre Model in global coordinate
f_c'	Characteristic compressive (cylinder) strength of concrete
f_c	Stress in concrete
f_{cc}'	Ultimate stress of confined concrete
f_{ck}	Characteristic compressive (cube) strength of concrete
f_{co}'	Ultimate stress of unconfined concrete
f_l	Lateral confining pressure
f_l'	Effective lateral confining pressure
f_{le}	Average equivalent average confining pressure
f_s	Stress in steel
f_{su}	Ultimate stress of steel
f_u	Ultimate stress of steel
f_y	Characteristic strength of steel defined in IS: 456-2000
f_{yl}	Nominal / specified yield stress of longitudinal steel
f_{yle}	Expected / actual yield stress of longitudinal steel
f_{yt}	Nominal / specified yield stress of transverse steel
f_{yte}	Expected / actual yield stress of transverse steel
$\{f\}$	End-force vector of a segment in the Fibre Model in global coordinates; External load vector on the member in global coordinates
$\{g\}$	End-displacement vector of a fibre in the Fibre Model in global coordinates
$\{h\}$	End-force vector of a fibre in the Fibre Model in global coordinates
k	A factor used in Saatcioglu-Razvi confinement model
k_1	Confinement coefficient
k_2	Effectiveness coefficient of confinement
k_s	Strength gain factor used in Sheikh-Uzumari model
l_e	Effective length of transverse reinforcement

Symbol	Description
m	Modular ratio
$\{p\}$	End-force vector of internal resistance of the member in global coordinates
r	A factor used in Saatcioglu-Razvi / Dasgupta confinement model
r'	A factor used in modifying the falling branch using Popovics' equation
$\{r\}$	End-force vector of a segment in the Fibre Model in local coordinate
$\{r_s\}$	Residual force vector in global coordinates
s	Longitudinal spacing of transverse reinforcement
s_l	Spacing of cross-ties in a rectangular section
$\{u\}$	End-displacement vector of a segment in the Fibre Model in local coordinate
w	Width of concrete fibres in the Fibre Model
x_u	Depth of neutral axis
x^*	Distance of effective centroidal axis from gross cross-section centroidal axis
y	Distance of midpoint of a fibre from gross cross-section centroidal axis
y^*	Distance of midpoint of a fibre from effective centroidal axis
α	Inclination of a segment in the global coordinate
β	A factor used in Sheikh-Uzumari confinement model; A factor used in calculation of concrete shear strength as per AASHTO LRFD Bridge Design Specifications; Relative ratio of pure flexural stiffness to pure shear stiffness
ε_{01}	Strain corresponding to ultimate stress of unconfined concrete
ε_{085}	Strain corresponding to 85% of ultimate stress of unconfined concrete in falling branch of stress-strain curve
ε_1	Strain corresponding to ultimate stress of confined concrete
ε_{20}	Strain corresponding to 20% of ultimate stress of confined concrete in falling branch of stress-strain curve
ε_{30}	Strain corresponding to 30% of ultimate stress of confined concrete in falling branch of stress-strain curve
ε_{50}	Strain corresponding to 50% of ultimate stress of confined concrete in falling branch of stress-strain curve
ε_{50u}	Strain corresponding to 50% of ultimate stress of unconfined concrete in falling branch of stress-strain curve
ε_{85}	Strain corresponding to 85% of ultimate stress of confined concrete in falling branch of stress-strain curve
ε_c	Strain in concrete
ε_s	Strain in steel
ε_{sl}	Minimum strain corresponding to ultimate stress of confined concrete

Symbol	Description
ε_{s2}	Maximum strain corresponding to ultimate stress of confined concrete
ε_{su}	Fracture strain of transverse steel
$\dot{\varepsilon}^f$	Net incremental axial strain on fibre f at global iteration level in the Fibre Model
γ	A factor used in Sheikh-Uzumari confinement model
ϕ	A resistance factor
φ	Curvature at a section
λ	Ratio of effectively confined core area at tie level to actual core area in Sheikh-Uzumari confinement model
μ_d	Target displacement ductility demand of a ductile member
ν	Poisson's Ratio of concrete-steel composite material
ν_c	Concrete shear strength used in CALTRANS
ρ_c	Area ratio of transverse reinforcement/ effective confinement
ρ_l	Percentage of longitudinal steel
ρ_s	Volumetric ratio of transverse reinforcement
ρ'_s	Ratio of total volume of transverse and longitudinal steel to volume of core concrete
ρ_t	Percentage of longitudinal steel in tension
σ_s	Stress in steel
σ_d	Design stress in transverse steel taken equal to $0.87 f_y$
$\sigma^1_{cr,b}$	Elastic buckling stress of longitudinal steel in piers
$\sigma^2_{cr,b}$	Inelastic buckling stress of longitudinal steel in piers
$\sigma_{cr,b}$	Critical stress for buckling of longitudinal steel in piers
σ^f	State of stress of fibre f in the Fibre Model at net incremental axial strain $\dot{\varepsilon}^f$ at a global iteration level
σ^c_i	State of stress of ith concrete fibre in the Fibre Model at global iteration level
σ^s_i	State of stress of ith steel fibre in the Fibre Model at global iteration level
τ_c	Design shear strength of concrete used in IS: 456-2000; Average shear stress in concrete in used in PWRI 1998

• • •

Chapter 1

Literature Survey

1.0 INTRODUCTION

Bridges are lifeline facilities that need to remain functional even after a major earthquake shaking, since their damage and collapse may not only cause loss of life and property, but also hamper post-earthquake relief and restoration activities. The damages or collapses of bridge structures during past earthquakes are attributed to failure of foundation (structural and geotechnical), substructure, superstructure, and connections between foundation and substructure and between substructure and superstructure. Moreover, in bridges, foundations are not accessible for retrofitting, while any inelastic action or failure of the superstructure renders the bridge dysfunctional for a long period. Connection failures are generally brittle in nature and are distressing. Hence, substructures are chosen as the components where inelasticity can be allowed and retrofitted. This thesis addresses the seismic design of reinforced concrete (RC) substructures.

RC bridge substructures, also called as *piers*, can be of four types (Figure 1.1). These are: (a) *Wall type*: compression members with a ratio of clear height to the maximum plan dimension less than *2 5* [AASHTO, 1998]; (b) *Single column type*: single compression members with a ratio of clear height to maximum plan dimension greater than *2.5* [AASHTO, 1998]; (c) *Multiple-column frame type*: when two or more column type piers are connected at the top by a cap beam resulting in frame action under lateral loads; and (d) *Linked-column frame type*: when two or more (usually four) tall column type piers are interconnected at intermediate levels by link beams to reduce displacements and design moments. Hereinafter in this thesis, the term *pier* shall be used

in general for both individual column type and wall type substructures.

The superstructure-to-pier connection can be either a moment-resisting one or a bearing one. The framed or multicolumn piers have higher redundancy and hence there is less ductility demand on individual plastic hinges at the critical sections. However, single column piers with the superstructure simply rested on them, are vertical cantilevers with no redundancy. Hence, their overall response critically depends on the satisfactory performance of the single plastic hinge at the base of the column. Thus, single column piers are most vulnerable, but they are most commonly used due to good aesthetics.

1.1 PERFORMANCE OF BRIDGE PIERS IN SOME MAJOR EARTHQUAKES

One of the earthquakes during the early part of the century that severely hit bridges was the 1923 Kanto earthquake. Masonry piers supporting bridges crumbled during the shaking. Based on damages to highway bridges caused by the earthquake, seismic forces were formally taken into account since 1926 in the design of highway bridges in Japan, and the equivalent static Seismic Coefficient Method was introduced for analysis of bridge systems subjected to lateral load caused by earthquakes.

In USA, the 1971 San Fernando earthquake is significant form the point of view of seismic design of bridges. Span collapses due to relative movement of piers exposed the inadequate seat width provisions. Linkage restrainer bolts across the movement joints failed and also led to the collapse of a span. Substructure columns primarily failed in shear, both outside and within the plastic hinge region. The failure outside the plastic hinge region was due to the flexural strength based shear demand exceeding the shear strength capacity and due to lack of confinement from inadequate transverse reinforcement. The failure inside the plastic hinge region was due to the shear strength in the plastic hinge region being less than that in the portion outside the hinge. This initiated

intensive research on the effect of flexural ductility demand on the shear capacity of reinforced concrete sections. Piers also showed inadequate flexural ductility. Due to inadequate transverse reinforcement, crushing of concrete in the plastic hinge region extended into the core of the section as soon as concrete strain reached unconfined concrete strain, and longitudinal steel buckled resulting in rapid strength degradation; eventually this led to the inability of the pier to support even the gravity load. In addition, lap splicing of transverse reinforcement resulted in opening up of the reinforcement and accelerating the failure process. A pullout failure of column, due to inadequate length and straight-bar anchorage detailing of column reinforcement into the footing caused the failure of another bridge. The 1971 San Fernando Earthquake served as a major turning point in the development of seismic design criteria for bridges in United States, prior to which, specifications for the seismic design of bridges were primarily based on the then existing lateral force requirements for buildings. These developments are discussed in Sections 1.5.2 and 1.5.3.

The 1989 Loma Prieta Earthquake in California caused widespread damage to the region's highways and bridges, including the collapse of more than a mile of an elevated roadway, namely the Cypress Street Viaduct. Insufficient anchorage of cap beam reinforcement into the columns was one reason that caused the failure of the Cypress Viaduct. In addition, lack of properly designed joint shear reinforcement caused extensive cracking at joint regions; this joint shear failure is generally accepted as a major contributor to the collapse of the viaduct. Inadequate lap-splice lengths of longitudinal bars caused bond failure in columns. Underestimation of seismic displacements resulted in inadequate clearance of *150mm* between the lower roadway and the independent columns supporting the upper-level deck at the China Basin / Southern Viaduct in San Francisco. This led to pounding of the lower roadway on the adjacent column. Further,

vertical oscillations of concrete deck slabs caused some support columns to punch through the deck, and resulted in tilting and collapse of the bridge.

In the 1995 Hyogo-Ken Nanbu (Kobe) Earthquake, highway structures were severely affected, particularly the single column type reinforced concrete piers. Most concrete piers failed due to lack of (a) sufficient transverse reinforcement for shear strength, (b) confinement, and (c) lateral support to longitudinal bars. Premature termination of longitudinal reinforcement caused a number of columns to develop flexure-shear failures at mid-height. The superstructures were mostly simply supported over steel pin bearings, and with short seat lengths. Dislodging of girders off the bearings was common. The stiff tension-link restrainers failed and unseated a number of spans. At some locations, lateral spreading of weak soil aggravated the relative displacement of piers, again resulting in unseating of spans. Bridges with multiple-column frame type substructures generally performed better than single column type ones. The highway bridge specification [PWRI, 1990], published in 1990 by Japan Road Association was revised in 1996 [JRA, 1996] in view of the extensive damage caused by the 1995 Hyogo-Ken Nanbu (Kobe) earthquake. The various modes of undesirable structural damage (e.g., shear failure, opening up of transverse tie, buckling of longitudinal reinforcement, and crushing of concrete in the plastic hinge region) to bridge piers under strong seismic shaking are schematically shown in Figure 1.2.

1.2 PAST STUDIES RELATED TO RC BRIDGE PIERS

A major part of damage and collapse of bridges during past earthquakes was due to failure of piers. Bridge piers, even today, are sometimes [*e.g.*, IRC 21, 1987] designed primarily as axially loaded members. However, one of the early professional documents identified that piers are vulnerable in shear in strong earthquakes [ASCE-ACI, 1973] as was emphatically demonstrated by the numerous collapses of large number of reinforced

concrete piers during the 1971 San Fernando earthquake. In that document, two failure types were highlighted. These are (a) flexural-shear failure, and (b) axial compression failure. The first type occurs in slender columns with low axial loads and manifests as flexural cracking, and the second type occurs in stocky columns with high axial loads and manifests as complete destruction of the column core prior to any diagonal shear cracking. In the past, a number of experimental and analytical investigations were carried out to understand the seismic behaviour of bridge piers, the primary test variables being pier slenderness, axial load level, and longitudinal and transverse steel.

1.2.1 Experimental Studies

Tests on bridge piers carried out in Japan and New Zealand include three *1:3* scale model RC bridge piers with different shear span ratios subjected to simulated seismic loading [Davey, 1975], and RC columns deformed in double curvature under reversed cyclic loading at the Building Research Institute in Japan (1975, 1978). A shake table study was also conducted on a *1:6* scale model RC bridge pier in 1976 [Munro *et al.*, 1976]. In general, these are the three types of experiments conducted on bridge piers.

In an experimental programme, four RC columns (*550mm* square cross-section; *3.3m* high; twelve *24mm* diameter Grade 380 steel deformed bars as longitudinal reinforcement; *10mm* or *12mm* diameter Grade 275 steel plain round bars as transverse reinforcement) were subjected to lateral loading [Park *et al.*, 1982]. The columns had a M/VD ratio of *2.46*, where M and V are respectively the design moment and shear capacities, and D is the characteristic depth. The test variables were the level of axial load and the amount of transverse hoop reinforcement. Transverse hoops were designed as per the then revised draft of the New Zealand Concrete Design Code [NZ 3101, 1978]. All columns showed stable ductile behaviour under simulated seismic loading up to a displacement ductility factor of at least *6*. Maximum compressive strain in confined

concrete was in the range *0.016* to *0.026*, and considerably higher flexural strengths were observed than those computed as per ACI code provisions [ACI 318-77, 1977] (particularly for columns with high axial load levels).

From a study of nearly full-scale columns of circular, square and rectangular cross-sections with various arrangements of lateral reinforcements subjected to lateral loading, it was concluded that the most important parameter that influences the shape of moment-curvature curve for all sectional shapes is the amount of confining reinforcement [Mander *et al.*, 1988b]. As the ratio of volume of lateral reinforcement to that of confined concrete increases, the peak strain of confined concrete increases and the slope of falling branch reduces. The maximum longitudinal strain in the core concrete was reported as *0.05* at the instance of hoop fracture. Later, a theoretical stress-strain model for confined concrete was developed by equating the strain energy required for fracture of the first lateral reinforcement to that stored in the confined concrete [Mander *et al.*, 1988a].

In another study, *25* columns of *1:3* scale (*400mm* diameter; M/VD ratios of *1.5*, *1.75*, *2.0* and *2.5*) were subjected to a sequence of imposed displacements to investigate the shear strength of circular bridge columns bending in single curvature [Ang *et al.*, 1989]. Longitudinal reinforcements were either *16* or *24mm* diameter deformed steel bars with nominal yield strength of either *275* or *380MPa*. Plain round bars of *6, 10* or *12mm* diameter were used as transverse spiral reinforcement. Shear strength was found to reduce with increasing flexural deformation in columns with displacement ductility factors in excess of *2.0*

Experimental investigations were carried out to determine strength and deformability of circular columns primarily in shear [Wong *et al.*, 1993]. Sixteen *400mm* diameter columns with aspect ratio of *2* were tested under quasi-static lateral loading with constant axial compression. All the columns were reinforced with *20* deformed bars of

16mm diameter, *i.e.*, with *3.2%* of longitudinal reinforcement. Three levels of axial compression load, ranged between $0.10 - 0.39 f_c' A_g$, were applied. The study concluded that shear deformation in stout columns with small or no axial compression load is significant and should be included in the initial stiffness estimate so that dependable ductility and drift values are obtained. Biaxial loading patterns lead to more severe degradation of stiffness and strength. Hysteretic response and ductility capacity are distinctly improved with increase in spiral steel content.

Thin-walled hollow circular columns with only one layer of transverse reinforcement were tested to ascertain the flexural behaviour of such columns [Zahn *et al.*, 1990]. Six columns were subjected to axial compression and cyclic flexure primarily to investigate the effects of the ratio of inner and outer diameters and of the axial load on ductility. All columns had an outer diameter of *400mm*. Two columns with diameter ratios *0.53, 0.63* and *0.73* each were subjected to different levels of axial loads. The total amount of longitudinal steel was kept the same, namely *16* bars of *16mm* diameter of *275* grade steel, in all the columns. Thus, columns with thinner wall had a higher percentage of longitudinal steel. The maximum cantilever displacement ductility obtained was *12.4* when the transverse reinforcement volumetric ratio was *1.13%*. The most important factor to control the ductile behaviour of this type of sections was identified as the location of neutral axis with respect to the inside compression face, when ultimate flexural strength is reached. Columns with neutral axis closer to the inside compression face at the ultimate flexural strength proved to be more ductile than those with neutral axis near the geometric centroid of the section. Columns with thicker wall, lower longitudinal steel ratio and lower level of axial load were more ductile, because in them the neutral axis lies near the inner compression face.

An experimental investigation to study the flexural capacity and ductility of

square high strength concrete columns [Azizinamini and Kuska, 1994] showed the adequacy of the ACI-318-89 design provisions. The investigation addressed the effects of compressive strength of concrete, axial load on the column, and the amount, spacing and yield strength of the transverse reinforcement, on flexural strength and ductility of high-strength concrete columns. Square concrete columns (*305mm* side; *2.44m* height) were subjected to three levels of axial load, *i.e.*, *20%*, *30%* and *40%* of nominal column direct compression capacity. The cylinder strength of concrete ranged from *26-104MPa*, and the longitudinal and transverse steels were of *414* grade. The volumetric ratio of transverse steel was varied from *2.36* to *3.82%* by varying the longitudinal spacing. It was concluded that high-strength concrete columns that had axial load below *20%* of the axial load capacity and that were designed as per the seismic provisions in ACI-318-89, possessed adequate curvature and displacement ductilities. However, the code provisions over-estimate their flexural capacities.

In another experimental study, two large-scale columns (*610mm* diameter; *1829mm* high) with low longitudinal reinforcement ratio of *0.0053* (about one-half of the lower limit specified by ACI-318-89) and *0.0106* (the lower limit specified by ACI-318-89) were tested under cyclic inelastic lateral displacement loading [Priestley and Benzoni, 1996]. Column 1 consisted of *12 #4* (*12.7mm* diameter) longitudinal bars with plain round *#2* (*6.35mm* diameter) spirals at *76.2mm* vertical pitch, whereas Column 2 had *24 #4* bars with *#2* spirals at *127mm* vertical pitch. The reinforcement yield strengths were *462MPa* for *#4* longitudinal bars and *361MPa* for *#2* spirals. Concrete strength was *30MPa*, and columns were axially loaded to *503kN* corresponding to an axial load ratio of $P/f_c'A_g = 0.057$. Column 1 exhibited stable flexural response with high-ductility shear failure at a displacement ductility of *10*. Column 2 suffered shear failure at displacement ductility of *2.5*. It was concluded that lower limits of ACI for

longitudinal steel ratio could be reduced without detrimental influence on flexural response, and that the shear strength of concrete component may be considered independent of longitudinal reinforcement ratio. Also, the average of the flexural rigidity of the two columns measured at the point of first yield of tension steel was *0.23EI$_{gross}$*, considerably lesser than *0.5EI$_{gross}$* generally used in estimating the natural periods and displacements of RC structures.

In a shake table test, *14* one-sixth scale RC cantilever columns were tested to determine the effect of various parameters [Dodd and Cooke, 2000]. All columns were *200mm* in diameter and had *18* uniformly spaced *6mm* diameter deformed bars in the longitudinal direction (average yield stress of *450MPa*) with a concrete cover of *11mm*. Spiral steel was either of *3.15mm* diameter or of *4mm* diameter round bars (average yield stress of *250MPa* and *260MPa*, respectively). The transverse reinforcement required in the potential plastic hinge zone was calculated based on methods proposed in the literature [Ang *et al.*, 1989] for low and high axial load columns. Spirals at maximum spacing of six longitudinal bar diameters were used. Columns with aspect ratios of *4, 7* and *10* with axial loads of *0.05/f$_c'$A$_g$* and *0.4/f$_c'$A$_g$* were subjected to cyclic lateral displacement loading. Low axial-load columns typically failed by fracture of longitudinal steel and high-axial load columns by fracture of spiral reinforcement after about *20%* drop in flexural strength. However, both failure modes were initiated by buckling of longitudinal reinforcement. Also, due to dynamic action, flexural strength was higher than that predicted by ACI-318-95 or CALTRANS specification [CALTRANS, 1999] by about *10%*; the effect was larger for high axial-load columns.

In a real-life retrofit project, two *1:2.5* scale bridge piers with structural flares were tested [Saiidi *et al.*, 2001]. The actual columns had irregular octagonal cross-sections with a smooth parabolic flare in the transverse direction of the bridge. The two

specimens, namely *HS* and *LS*, had *16mm* diameter deformed bars as longitudinal reinforcement of *1.79%* and *1.02%* respectively. The lateral steel comprised of *6mm* diameter deformed steel ties and cross-ties at a spacing of *64mm*. The average tensile yield stresses of longitudinal and transverse steel were *438MPa* and *455MPa*, respectively. The concrete compressive strength was *51.7MPa*. As the flexural capacity varied along the column height, theoretical moment-curvature relations for different cross-sections were derived beforehand and idealised plastic moments were derived. The analysis with axial loads of *713kN (160kip)* and *632kN (142kip)* for the two columns, included effects of confinement, crushing of cover concrete and strain hardening of main steel. The variation of flexural capacity along the height was prepared for the two columns, and shear forces required to develop a plastic hinge were estimated (Figure 1.3). The theoretical plastic hinge locations were *737mm (29inch)* above the footing for both the columns. During experiments, the failure of Column *HS* was initiated by buckling of longitudinal bars at *737mm* above the footing; the maximum displacement ductility achieved was *6*. The failure of Column *LS* was also initiated by longitudinal bar buckling at *813mm*; the maximum displacement ductility achieved was *8*. Thus, in these RC columns with structural flares, the plastic hinge occured at locations away from the end connection. Also, the shear capacity estimated as per CALTRANS Specifications [CALTRANS, 1995] was lesser than the actual capacity by about *25%*. A reasonably accurate estimate of shear capacity was obtained for non-circular columns by adding the shear capacity contribution due to arch action [Priestley *et al.*, 1994] equal to *20%* of the applied axial load.

1.2.2 Analytical Studies

In contrast to the extensive experimental studies conducted, relatively lesser effort was expended on analytical studies to assess strength and ductility of RC members.

In an attempt to estimate the load-deflection response of centrally loaded beam specimens [Park *et al.*, 1972], moment-curvature $(M - \varphi)$ relations were developed considering hysteretic stress-strain curves for both steel and concrete including effect of confinement. From the moment-curvature relations, the transverse deflection Δ_{AB} of any point A on the beam from the tangent to the axis of the member at another point B, was computed as

$$\Delta_{AB} = \int_{A}^{B} x\varphi \ ds , \qquad\qquad (1.1)$$

where x is the distance of element ds from A, and φ is the curvature in the segment. This technique is very commonly used in estimating the load-deformation relation of RC members.

A non-linear finite element approach was presented to quantify the inelastic dynamic response of RC vertical chimneys subjected to ground shaking [Maiti and Goyal, 1996]. The chimney was idealised as an assemblage of beam elements along the height. The cross section was discretised into a number of strips parallel to the neutral axis. Hysteretic behaviour of an unconfined concrete model and a bi-linear backbone stress-strain relation for reinforcing steel was used to obtain the element stiffness matrices. This structural model was subjected to strong ground motions and a non-linear time history analysis was done to evaluate the response histories of displacements at the nodal points. From the displacement history, stress resultants at the nodes along the height of the assemblage were computed based on the material models. It was shown that failure or collapse of the chimney does not occur even after significant yielding of one section as maximum earthquake forces act for short duration and are reversible.

An analytical procedure was developed to model the formation and progression of flexural hinging in solid RC columns [Razvi and Saatcioglu, 1999b]. The procedure was

used to compute column drift capacity from the moment-curvature relation through a second order analysis procedure for concrete columns subjected to the combined action of constant axial force and monotonically increasing lateral load. Inelastic effects, like concrete confinement, reinforcement strain hardening, anchorage slip and reinforcement bar buckling, were incorporated in the analysis. A displacement- based design procedure for confined columns was proposed and design aids developed. The design parameters included amount of transverse steel, yield strength of transverse steel, spacing and arrangement of transverse reinforcement, concrete strength, gross area to confined area ratio of the section, percentage of longitudinal steel, and column aspect ratio. Design aid charts were developed for the drift capacity of columns as a function of these design parameters. Separate charts were drawn for drift capacities corresponding to *20%* decay in lateral load resistance and *20%* decay in moment resistance of the column. This design procedure was believed to offer a more rational performance criterion for design than that employed in ACI-318-95. It incorporates axial force and drift as design parameters, and recognises the importance of tie arrangement in column confinement. As a result, it brought flexibility to design, allowing for trade-off amongst spacing, volumetric ratio, yield strength and arrangement of confining reinforcement, and promoting more favourable tie arrangements for improved seismic performance.

Post-peak behaviour of tall hollow bridge piers was predicted [Masukawa *et al.,* 2000] in another study considering spalling of cover concrete and buckling of longitudinal reinforcement. An analytical model proposed in an another earlier study [Suda *et al.,* 2000] to quantify these two phenomena that may initiate a column failure, was used in the analysis. In that model, longitudinal compressive steel bars were idealised as fixed-fixed beams subjected to compressive force and supported by hoops and cross-ties. The hoops and cross-ties were themselves modelled as elasto-plastic

springs. The concrete cover was modelled as a series of springs with tensile strengths that decrease with deformation. Longitudinal steel was assumed to buckle over a length covering a number of layers of hoops. A mathematical expression was proposed to estimate this buckling length, and this length was used to derive the critical stresses on the longitudinal bars. The models for predicting spalling of cover concrete and buckling of reinforcement were implemented in a three-dimensional finite element computer program for analysis of RC piers. Also, a hollow square specimen was tested under the action repeated cyclic forces. Spalling of cover concrete was observed at different locations at different levels of ductility. Analytically obtained responses matched with those obtained from experiments with high degree of accuracy for the RC hollow piers that predominantly experienced bending failure.

In another study, three hollow circular bridge columns were subjected to a constant axial load and reversed cyclic horizontal load. [Yeh *et al.*, 2001]. The inner and outer diameters of columns were of *1500mm* and *900mm* respectively. Two columns were *5.5m* high while the third one was *3.5m*. All columns had *64 22mm* diameter longitudinal bars (yield strength of *418.2MPa*; ultimate strength of *626.5MPa*). The transverse reinforcement (yield strength of *410MPa*) in the columns was different; (a) Column 1- *13mm* diameter bars at *100mm* centres, (b) Column 2- *13mm* diameter bars at *300mm* centres, and (c) Column 3- *10mm* diameter bars at *200mm* centres. Columns 1 and 3 had additional cross-ties. Column 1 was designed as per ACI-318-95. The longitudinal reinforcement bars in Column 2 were spliced in the plastic hinge region. The transverse reinforcement of Column 3 was *40%* of that required by ACI-318-95. The cylinder compressive strength of concrete used in Columns 1, 2 and 3 were *31.7MPa*, *33 8MPa* and *30.9MPa* respectively. The constant axial load applied was *3600kN*. Column 1 exhibited a stable flexural behaviour and a displacement ductility of *9.9*.

Column 2 sustained bond failure of longitudinal bars and a displacement ductility of only *2.8*. The ultimate performance of column 3 was influenced by the low shear capacity. The concrete at the base was crushed on reaching a displacement ductility of *5.3*. An analytical model was also developed to predict the load-displacement relationship of the columns. Existing models for confined concrete were used. Stress-strain relationship of longitudinal steel incorporated the phenomenon of low-cycle fatigue. Moment-curvature relationships for the sections were developed and the load-displacement relationship was determined using the moment area method and the curvature diagram of the column along the length. The proposed model satisfactorily predicted the load-displacement path for column with stable flexural behaviour.

The above studies reveal that the overall load-deflection relationship of RC member is generally achieved through integration of the sectional curvature over small lengths [Park *et al.*, 1972, Yeh *et al.*, 2001]. This procedure requires generation of moment-curvature relation of a number of sections along the member length, especially if the member is non-prismatic [Saiidi *et al.*, 2001], which is computationally intensive. Also, the procedure requires a accurate estimation of the bending moment at a section in the deformed configuration of the RC pier. This is done through the conventional elastic analysis procedure often neglecting geometric nonlinearity effect. In two studies [Razvi and Saatcioglu, 1999b, Masukawa *et al.*, 2000], the effect of longitudinal bar buckling was taken into consideration, which significantly influenced the limiting response of the column. In addition, the simultaneous differential response of cover concrete and confined core concrete is not always accounted for [Maiti and Goyal, 1996]. Furthermore, in stocky piers, there can be considerable shear deformation, which was not considered in the above studies. This shear deformation, together with spalling of cover concrete and subsequent buckling of longitudinal bars can significantly alter the overall

response of the column and may even induce brittle failure well before the flexural capacity at a section is reached. Thus far, no analytical work is reported to predict the overall load-deflection relationship and final response behaviour of such cantilever compression members considering all the above-mentioned feasible effects.

1.3 DISTRIBUTED PLASTICITY MODEL: FIBRE MODEL

For bridge piers with large cross-sections, the general approach of idealising the member by its centroidal axis and defining the inelastic action of the whole cross-section in a lumped sense, does not accurately model the spread of inelasticity both along the member length and across the cross-section. Partial yielding and elastic unloading of a portion of the cross-section and the complex stress distribution across the cross-section was accounted for by discretising a RC member into a number of finite-sized discrete areas across the cross-section [Warner, 1969]. This approach permits the use of any desired stress-strain relation for concrete and steel. Thus, the representation of the concrete stress block by a highly linearised idealisation receded, and the effects of strain hardening in steel and unloading of concrete at high strains became amenable to detailed investigation. In addition, irregularities in geometry of the cross-section and in the arrangement of steel reinforcement could be modelled. A similar discretisation approach was adopted [Santhathadaporn and Chen, 1972] in a study on steel compression members under biaxial bending; a general procedure was presented for obtaining tangent stiffness matrix of a segment composed of such discrete areas or *fibres*. However, such models were restricted to monotonic loading only and do not capture the complex stress distribution within the segment cross-section that may be generated through partial unloading during general cyclic loading. Thus, a need was felt for a distributed plasticity model that is general enough to cover any arbitrary cross-section, loading conditions, material properties, and, to capture the geometric nonlinearities. Such a *Fibre Model* was

developed for steel frame members [Murty and Hall, 1994].

1.3.1 Geometric Model Description

In the fibre model [Murty and Hall, 1994], the member was discretised into N_s segments along the length, and each segment into N_f *fibres* across the cross-section (Figure 1.4). Each fibre was modelled by its geometric centroidal axis and capable of withstanding axial load applied normal to its cross-section. Thus, the axial strain and axial stress in each fibre were calculated as average values at its centroid. A uniaxial cyclic constitutive law for the material was used to control the loading and unloading of the fibres. It was assumed that the fibres do not buckle under compression. Thus, the model does not incorporate local buckling in the member, though it includes the overall buckling of the member. Geometric nonlinearities of the segment are modelled by updating the deformed configuration in line with the Updated Lagrangian Approach. A one-dimensional load-deformation relation was written to capture the behaviour of each fibre independently. The flexural load-deformation relation of the segment was obtained by combining the axial load-deformation relationships of the fibres constituting the segment. There was no strength interaction of the shear force with bending moment or axial load in the segment; fibres carried the shear force elastically. Thus, the fibre model was general enough to incorporate irregular geometry, material nonlinearity, geometric nonlinearity and cyclic loading. In addition, the irregular geometry could be incorporated through proper discretisation of the member.

1.3.2 Load-Deformation Relation

For analysis involving material and geometric nonlinearity, incremental equilibrium equations are required. These relations between incremental stress resultants and incremental deformations, namely the *incremental* or *tangent load-deformation*

relations, were derived for all the fibres, which were combined to form the incremental equilibrium equation for a segment (Figure 1.5). Finally, the incremental equilibrium equation of the entire member was obtained by assembling those of its segments. *Large displacements* but *small strains* were considered.

1.3.2.1 Incremental Load-Deformation Relation of a Fibre

Each fibre was treated as an axial member with no flexural property. Thus, only two in-plane translational degrees of freedom were considered at the end of each fibre (Figure 1.5a). Hence, the fibre incremental matrix load-deformation equation is of order four. The fibre incremental equilibrium equation in global coordinates was written as

$$^f[K]_t \{\dot{g}\} = \{\dot{h}\},$$
(1.2)

where

$$^f[K]_t = {}^f[K]_t^{TS} + {}^f[K]_t^{GS} ,$$
(1.3)

$$^f[K]_t^{TS} = \frac{E_t A}{L} \begin{bmatrix} a^2 & ab & -a^2 & -ab \\ & b^2 & -ab & -b^2 \\ & & a^2 & ab \\ Sym & & & b^2 \end{bmatrix},$$
(1.4)

$$^f[K]_t^{GS} = \frac{P}{L} \begin{bmatrix} b^2 & -ab & -b^2 & ab \\ & a^2 & ab & -a^2 \\ & & b^2 & -ab \\ Sym & & & a^2 \end{bmatrix},$$
(1.5)

$$\{\dot{g}\}^T = \langle \dot{g}_1 \quad \dot{g}_2 \quad \dot{g}_3 \quad \dot{g}_4 \rangle,$$
(1.6)

$$\{\dot{h}\}^T = \langle \dot{h}_1 \quad \dot{h}_2 \quad \dot{h}_3 \quad \dot{h}_4 \rangle,$$
(1.7)

$$a = \cos\alpha , \text{ and}$$
(1.8a)

$$b = \sin\alpha .$$
(1.8b)

In Eq.(1.2), $^f[K]_t$ is the tangent stiffness matrix, $\{\dot{g}\}$ is the incremental end-displacement vector and $\{\dot{h}\}$ is the incremental end-force vector of the fibre in global

coordinate. ${}^f[K]_t^{TS}$ and ${}^f[K]_t^{GS}$ are the truss stiffness matrix and geometric stiffness matrix. E_t is the tangent modulus of elasticity of the material. The axial load P is positive for tensile load, and L is the length of each fibre, which is equal to the height h of the segments discretised along the length of the pier. Here, α is the inclination of the segment, and hence of the fibres, in the global coordinates.

1.3.2.2 Incremental Load-Deformation Relation of a Segment

The segment incremental load-deformation relation was obtained by assembling those of the constituent fibres given in Section 1.3.2.1. However, since the fibres are not coupled to each other through interface flexural shear, the shear stiffness of the segment was added separately.

(a) Incremental Relation without Shear Stiffness

For each fibre, the translations at the end of the fibre correspond to the translation at its centroidal axis. The Euler-Bernoulli kinematic assumption, that *plane sections normal to the centroidal axis before bending, remain plane and normal to it even after bending,* was made. The end-displacement and end-force quantities of a segment in global coordinate were taken as $\{d\}$ and $\{f\}$ respectively (Figure 1.5b). If y is the distance of the fibre centroid from the centroidal axis of the cross section, then the incremental fibre end-displacement vector $\{\dot{g}\}$, and the incremental segment end-displacement vector $\{\dot{d}\}$ were related through fibre transformation matrix $[R_f]$, as

$$\left\{ \{\dot{g}\} \right\} = \left[[R_f] \right] \{\dot{d}\}, \tag{1.9}$$

where

$$
[R_f] = \begin{bmatrix} 1 & 0 & y\cos\alpha & 0 & 0 & 0 \\ 0 & 1 & y\sin\alpha & 0 & 0 & 0 \\ 0 & 0 & 0 & 1 & 0 & y\cos\alpha \\ 0 & 0 & 0 & 0 & 1 & y\sin\alpha \end{bmatrix},
\tag{1.10}
$$

$$
\{g\}^T = \langle \dot{g}_1 \quad \dot{g}_2 \quad \dot{g}_3 \quad \dot{g}_4 \rangle, \text{ and}
\tag{1.11}
$$

$$
\{d\}^T = \langle \dot{d}_1 \quad \dot{d}_2 \quad \dot{d}_3 \quad \dot{d}_4 \quad \dot{d}_5 \quad \dot{d}_6 \rangle.
\tag{1.12}
$$

Further, the fibre incremental end-force vector $\{\dot{h}\}$ and the segmental incremental

end-force vector $\{\dot{f}\}$ were also related through the same transformation matrices $[R_f]$ as

$$
\{\dot{f}\} = \begin{bmatrix} \cdot & \cdot & [R_f]^T & \cdot & \cdot \end{bmatrix} \begin{Bmatrix} \vdots \\ \{\dot{h}\} \\ \vdots \end{Bmatrix},
\tag{1.13}
$$

where

$$
\{\dot{h}\}^T = \langle \dot{h}_1 \quad \dot{h}_2 \quad \dot{h}_3 \quad \dot{h}_4 \rangle \text{ and}
\tag{1.14}
$$

$$
\{\dot{f}\}^T = \langle \dot{f}_1 \quad \dot{f}_2 \quad \dot{f}_3 \quad \dot{f}_4 \quad \dot{f}_5 \quad \dot{f}_6 \rangle.
\tag{1.15}
$$

Assembling the incremental equations of all fibres and using Eqs.(1.9) and (1.13), the

segment incremental equilibrium equation in global coordinate was obtained as

$$
{}^{ab}[K]_t \{\dot{d}\} = \{\dot{f}\},
\tag{1.16}
$$

where ${}^{ab}[K]_t$ is the tangent stiffness matrix of a segment corresponding to axial and

bending effect, given by

$$
{}^{ab}[K]_t = \sum \begin{bmatrix} [\Lambda] & -[\Lambda] \\ -[\Lambda] & [\Lambda] \end{bmatrix},
\tag{1.17}
$$

in which

$$[\Lambda] = \frac{E_t A}{L}\begin{bmatrix} a^2 & ab & ah \\ ab & b^2 & bh \\ ah & bh & h^2 \end{bmatrix} + \frac{P}{L}\begin{bmatrix} b^2 & -ab & 0 \\ -ab & a^2 & 0 \\ 0 & 0 & 0 \end{bmatrix}. \tag{1.18}$$

(b) Incremental Relation for Shear Stiffness

In the model, to obtain the shear stiffness, the Euler-Bernoulli kinematic assumption was partially relaxed. Thus, *plane sections normal to the centroidal axis before bending, remain plane after bending though not normal to it*. If G is the bulk modulus of elasticity and A_s the segment cross-sectional area effective in resisting shear, the incremental equilibrium equation of the segment for shear in local coordinates (Figure 1.6) was written as

$$^{sh}[K]^l_t\{\dot{u}\} = \{\dot{r}\}, \tag{1.19}$$

where $^{sh}[K]^l_t$ is the tangent stiffness matrix of a segment corresponding to shear deformation in local coordinates, and given by

$$^{sh}[K]^l_t = GA_s\begin{bmatrix} 0 & 0 & 0 & 0 & 0 & 0 \\ & \dfrac{1}{L} & -\dfrac{1}{2} & 0 & -\dfrac{1}{L} & -\dfrac{1}{2} \\ & & \dfrac{L}{4} & 0 & \dfrac{1}{2} & \dfrac{L}{4} \\ & & & 0 & 0 & 0 \\ & & & & \dfrac{1}{L} & \dfrac{1}{2} \\ Sym. & & & & & \dfrac{L}{4} \end{bmatrix}. \tag{1.20}$$

Here, $\{\dot{u}\}$ is incremental end-displacement vector, and $\{\dot{r}\}$ is the incremental end-force vector of the segment in the local coordinates. If α is the inclination of the segment in the global coordinate, $\{\dot{u}\}$ and $\{\dot{r}\}$ were then related to the respective global quantities $\{\dot{d}\}$ and $\{\dot{f}\}$, through the coordinate transformation matrix $[T]$ as

$$\{\dot{u}\} = [T]\ \{\dot{d}\}, \text{ and} \tag{1.21a}$$

$$\{\dot{f}\} = [T]^T\ \{\dot{r}\}, \tag{1.21b}$$

where

$$[T] = \begin{bmatrix} a & b & 0 & 0 & 0 & 0 \\ -b & a & 0 & 0 & 0 & 0 \\ 0 & 0 & 1 & 0 & 0 & 0 \\ 0 & 0 & 0 & a & b & 0 \\ 0 & 0 & 0 & -b & a & 0 \\ 0 & 0 & 0 & 0 & 0 & 1 \end{bmatrix},$$ (1.22)

a and b are as defined in Eq.(1.8).

Thus, the incremental equilibrium equation of the segment for shear in global coordinates is

$$^{sh}[K]_t \{\dot{d}\} = \{\dot{f}\}$$ (1.23)

where

$$^{sh}[K]_t = [T]^T \,^{sh}[K]_t [T] = GA_s \begin{bmatrix} \dfrac{b^2}{L} & -\dfrac{ab}{L} & \dfrac{b}{2} & -\dfrac{b^2}{L} & \dfrac{ab}{L} & \dfrac{b}{2} \\ & \dfrac{a^2}{L} & -\dfrac{a}{2} & \dfrac{ab}{L} & -\dfrac{a^2}{L} & -\dfrac{a}{2} \\ & & \dfrac{L}{4} & -\dfrac{b}{2} & \dfrac{a}{2} & \dfrac{L}{4} \\ & & & \dfrac{b^2}{L} & -\dfrac{ab}{L} & -\dfrac{b}{2} \\ & & & & \dfrac{a^2}{L} & \dfrac{a}{2} \\ \text{Sym.} & & & & & \dfrac{L}{4} \end{bmatrix}.$$ (1.24)

(c) Complete Incremental Equation of a Segment

Using the tangent stiffness matrices $^{ab}[K]_t$ and $^{sh}[K]_t$ corresponding to the axial and bending effects, and to the shear effects, from Eqs.(1.17) and (1.24) respectively, the complete segment incremental equilibrium equation in global coordinates was written as

$$[K]_t^S \{\dot{d}\} = \{\dot{f}\}$$ (1.25)

where

$$[K]_t^S = \,^{ab}[K]_t + \,^{sh}[K]_t,$$ (1.26)

$$\{\dot{d}\}^T = \langle \dot{d}_1 \quad \dot{d}_2 \quad \dot{d}_3 \quad \dot{d}_4 \quad \dot{d}_5 \quad \dot{d}_6 \rangle, \text{ and}$$

$$\{\dot{f}\}^T = \langle \dot{f}_1 \quad \dot{f}_2 \quad \dot{f}_3 \quad \dot{f}_4 \quad \dot{f}_5 \quad \dot{f}_6 \rangle.$$

In Eq.(1.25), $[K]_t^s$ is the segment tangent stiffness matrix in global coordinate. Since, the shear response was assumed to be elastic and uncoupled from the axial load and bending effects, the above linear superposition was conducted even under nonlinear and inelastic conditions.

1.3.2.3 Incremental Equilibrium Equation of the Member

The incremental equilibrium matrix equation of the whole member was formed by assembling those of all its segments. Symbolically, if $[K]_t$ is the complete global tangent stiffness matrix of the member, $[K]_t^s$ is the segment global tangent stiffness matrix from Eq.(1.26), and $\sum$ is the assembly operator, then

$$[K]_t = \sum_{s=1}^{N_s} \left\{ [K]_t^s \right\}, \tag{1.27}$$

where N_s is the number of segments in the member.

1.4 MATERIAL MODELS: CONSTITUTIVE LAWS

Each *fibre* in the fibre model is essentially a one-dimensional member with its entire area concentrated at its centroid. Its load-deformation relationship is derived using material constitutive law. In RC structures, the two different material fibres, namely of concrete and of reinforcing steel, require two different models for material constitutive law. Brief descriptions of some of the material constitutive law models of concrete and reinforcing steel available in literature are discussed in the following sub-sections.

1.4.1 Reinforcing Steel

Stress-strain relations of reinforcing steels used in different countries can be defined by different constitutive models. In India, the most widely used reinforcing steel is HYSD bars conforming to IS: 1786-1979. A model representing the virgin stress-strain curve for HYSD bars was developed [Dasgupta, 2000] through curve fitting on experimental data from uniaxial tensile tests.

Uniaxial test data of reinforcing bars show differences in the responses in tension and compression; these differences are affected by the coordinate system used to represent the data. However, if stresses and strains are defined in the true coordinate system, the differences disappear and tension-and compression stress-strain curves practically coincide upto the ultimate stress [Balan *et al.*, 1998]. Thus, in a study on strength and ductility of hollow RC sections [Dasgupta, 2000], the virgin curve in compression was taken as a symmetric image of the curve in tension about the stress-strain axes.

The load-carrying capacity of compression reinforcement in RC piers is significantly affected by the unsupported length of the longitudinal bars, which is the spacing of the transverse ties that provide lateral support and thereby prevent buckling of the longitudinal reinforcement bars. If s and d_b are the longitudinal spacing of transverse reinforcement and diameter of the longitudinal reinforcement, it was observed [Mau, 1990] that at $s/d_b < 5$, steel reaches its peak stress f_u, while for $s/d_b > 10$, the steel can at best carry a stress of f_y. For the range $5 < s/d_b \le 10$, the peak stress sustained varies between f_u and f_y. Thus, for bars under monotonic loading, an average critical spacing of $6d_b$ is reported in the literature [Mander *et al.*, 1988; Mau, 1990; Bayrak *et al.*, 2001] to prevent inelastic buckling of longitudinal reinforcement.

1.4.2 Confined and Unconfined Concrete

Experimental studies proved that both strength and ductility of RC members, in general, are greatly enhanced by having more transverse reinforcement. Transverse reinforcement induces a confining pressure on the core concrete. Thus, analytical models were developed to define the constitutive relations for confined concrete.

Originally, a stress-strain model was proposed for confined concrete consisting of a second-order parabola as the ascending branch and a linear segment as the descending branch (Figure 1.7) [Kent and Park, 1971]. It was assumed that the confining steel had no effect on the shape of the ascending parabola or on the strain corresponding to the maximum stress. Maximum stress was also taken as the unconfined concrete cylinder strength f_c'. The effect of confinement was reflected only in the slope of the falling branch, which flattened with the increase in confinement. The descending branch falls upto a stress of $0.2f_c'$ and after that, the stress remains constant as a residual stress. The entire stress-strain curve as per this model was defined as

$$
f_c = \begin{cases}
f_c'\left[\dfrac{2\varepsilon_c}{0.002}-\left(\dfrac{\varepsilon_c}{0.002}\right)^2\right] & \varepsilon_c \leq 0.002 \\[4mm]
f_c'\left[1-\dfrac{0.5(\varepsilon_c-0.002)}{\varepsilon_{50u}+\varepsilon_{50h}-0.002}\right] & 0.002 \leq \varepsilon_c \leq \varepsilon_{20} \ , \\[4mm]
0.2f_c' & \varepsilon_c \geq \varepsilon_{20}
\end{cases}
\tag{1.28}
$$

where

$$
\varepsilon_{50u}=\frac{3+0.002f_c'}{f_c'-1000} \quad \text{and} \quad \varepsilon_{50h}=\frac{3}{4}\rho_s\sqrt{\frac{b_c}{s}}.
\tag{1.29}
$$

Here, ρ_s is the volumetric ratio of transverse steel, b_c is the width of confined core and s is the spacing of hoops. Later, this curve was modified [Park *et al.*, 1982] to

incorporate the enhancement in concrete strength due to presence of confinement, which was taken to be the product of volumetric ratio and the yield strength of the transverse reinforcements. So, the confined concrete strength was given as

$$f'_{cc} = f'_c + \rho_s f_{yt},$$ (1.30)

where f_{yt} is the yield strength of transverse steel.

Another model considering the effectiveness of confinement was proposed around the same time [Sheikh and Uzumeri, 1982]. In this model, the effective confined core area was assumed less than the actual core area within the centrelines of the perimeter hoops. The effective confined core area was determined from the distribution of longitudinal bars, and the configuration and spacing of ties. The stress-strain curve of confined concrete was given by (Figure 1.8)

$$f_c = \begin{cases} k_s f'_c \left[\dfrac{2\varepsilon_c}{\varepsilon_{s1}} - \left(\dfrac{\varepsilon_c}{\varepsilon_{s1}} \right)^2 \right] & \varepsilon_c \le \varepsilon_{s1} \\ k_s f'_c & \varepsilon_{s1} \le \varepsilon_c \le \varepsilon_{s2} \\ \dfrac{0.15 k_s f'_c}{\varepsilon_{85} - \varepsilon_{s2}} (\varepsilon_c - \varepsilon_{s2}) & \varepsilon_{s2} \le \varepsilon_c \le \varepsilon_{85} \\ 0.3 k_s f'_c & \varepsilon_{85} \ge \varepsilon_{30} \end{cases}$$ (1.31)

where k_s is the strength gain factor given by

$$k_s = 1 + \frac{\lambda}{f'_c} \beta \left(\rho_s f_{yt} \right)^\gamma.$$ (1.32)

Here, λ is the ratio of the effective core area at tie level and the actual core area, while β and γ are constants; ε_{s1} and ε_{s2} are the minimum and maximum strains corresponding the peak stress, respectively, and are given by

$$\varepsilon_{s1} = 80 k_s f'_c \times 10^{-6}, \text{ and}$$ (1.33)

$$\varepsilon_{s2} = \varepsilon_{01} \left[1 + \frac{248}{C} \left\{ 1 - 5 \left(\frac{s}{b_c} \right)^2 \right\} \right] \frac{\rho_s f_{yt}}{\sqrt{f_c'}}, \qquad (1.34)$$

where ε_{01} is the strain corresponding to the ultimate stress of the unconfined concrete and C is the distance (in *mm*), between adjacent longitudinal bars. In the Eq.(1.31), ε_{85} is the strain corresponding to *85%* of ultimate stress in the falling branch and given by

$$\varepsilon_{85} = \varepsilon_{s2} + 0.225 \rho_s \sqrt{\frac{b_c}{s}}. \qquad (1.35)$$

This model was further modified [Sheikh and Yeh, 1992] by introducing the enhancement in ductility due to strain gradient and dependence of concrete strength on the level of axial load. For axial loads larger than the balance axial load, concrete strength reduced with increase in axial load, which was verified by experimental results.

The first comprehensive stress-strain model for confined concrete applicable to both circular and rectangular cross-sections with or without supplementary crossties was proposed in 1988 [Mander *et al.*, 1988a]. The model accounted for cyclic loading and effect of strain rate. The influence of transverse and longitudinal reinforcement configurations was accounted for by defining an effective lateral confining stress that depended on the configuration of the transverse and longitudinal reinforcement. A "five parameter" multi-axis failure surface available in literature [William and Warnke, 1975] was adopted to define the compressive strength of confined concrete as

$$f_{cc}' = f_{co}' \left(-1.254 + 2.254 \sqrt{1 + \frac{7.94 f_l'}{f_{co}'}} - 2 \frac{f_l'}{f_{co}'} \right), \qquad (1.36)$$

where f_l' is the effective lateral confining stress that involves the stirrup configuration through an effectiveness coefficient. A single equation [Popovics, 1973] was used to define the stress-strain curve over the entire range of strain, given by

$$f_c = \frac{f_{cc}' x r}{r - 1 + x^r},$$ (1.37)

where

$$x = \frac{\varepsilon_c}{\varepsilon_1}, \text{ and } \varepsilon_1 = \varepsilon_{01}\left[1 + 5\left(\frac{f_{cc}'}{f_{co}'} - 1\right)\right].$$ (1.38)

Here ε_1 is the strain corresponding to the peak stress f_{cc}' in confined concrete.

An energy balance approach was used to predict the longitudinal strain in confined concrete by equating the strain energy stored in the transverse steel to that stored in the core concrete and longitudinal steel. Thus, the loss of strain energy in confining steel at first hoop fracture was equated to the gain in strain energy in concrete due to confinement (the shaded portion in Figure 1.9) plus the additional energy required to maintain yield in the longitudinal steel in compression.

Later, keeping this original stress-strain model, maximum confined strength, and corresponding strain at maximum strength, a conservative estimate of maximum confined concrete strain was proposed [Paulay and Priestley, 1992] as

$$\varepsilon_{c\,max} = 0.004 + \frac{1.4\rho_s f_{yt}\varepsilon_{su}}{f_{cc}'},$$ (1.39)

where ε_{su} is the fracture strain of the confining steel.

A new approach to modelling concrete stress-strain path emerged when a model based on area ratio of confining steel was proposed [Saatcioglu and Razvi, 1992] instead of the volumetric ratio used until then. Confined concrete ultimate stress f_{cc}', corresponding strain ε_1, and strain ε_{85} at which stress falls to 85% of ultimate strength were expressed in terms of equivalent uniform confining pressure f_{le} as

$$f_{cc}' = f_{co}' + k_1 f_{le}$$ (1.40)

$$\varepsilon_1 = \varepsilon_{01}(1 + 5k), \text{ and} \tag{1.41}$$

$$\varepsilon_{85} = \varepsilon_{085} + 260\rho_c\varepsilon_1. \tag{1.42}$$

An effectiveness coefficient, similar to those used in earlier models, was used to convert the average confining pressure to equivalent uniform confining pressure. The stress-strain curve consisted of a parabolic ascending part, followed by a straight falling branch and a straight line residual stress branch (Figure 1.10), and given by

$$f_c = \begin{cases} f'_{cc}\left[\dfrac{2\varepsilon_c}{\varepsilon_1} - \left(\dfrac{\varepsilon_c}{\varepsilon_1}\right)^2\right]^{\frac{1}{1+2k}} & 0 \leq \varepsilon_c \leq \varepsilon_1 \\[4mm] f'_{cc}\left[1 - \dfrac{0.15(\varepsilon_c - \varepsilon_1)}{\varepsilon_{85} - \varepsilon_1}\right] & \varepsilon_1 \leq \varepsilon_c \leq \varepsilon_{20} \\[4mm] 0.2f'_{cc} & \varepsilon_c \geq \varepsilon_{20} \end{cases} \tag{1.43}$$

The model is applicable to circular, square and rectangular sections confined with spirals, rectilinear hoops, cross ties, welded wire fabric and a combination of these. This model allowed for a superposition of individual effects of different types of lateral reinforcements. Later, this model for normal strength concrete was modified [Razvi and Saatcioglu, 1999a] to include high strength concrete. In this modified version, the ascending branch was defined by Eq.(1.37).

Out of the above models, only two [Mander *et al.*, 1988a; Saatcioglu and Razvi, 1992, 1999a] are applicable to solid sections of square, rectangular, circular and wall-type columns. The first analytical model applicable to hollow sections was proposed [Dasgupta, 2000] as an extension to an existing model [Razvi and Saatcioglu, 1999a]. It addressed a new situation, wherein the outer and inner hoops of a circular section are tied by links leading to two distinctly different confining actions, namely hoop action and the direct action of links. In the model, the concrete stress-strain curve for the whole range of

strain was again defined by the single equation [Popovics, 1973] given in Eq.(1.37) with

$$r = \frac{E_c}{E_c - E_{\sec}}, \; E_{\sec} = \frac{f_{cc}'}{\varepsilon_1}, \; E_c = 3320\sqrt{f_c'} + 6900. \tag{1.44}$$

The maximum strength of confined concrete f_{cc}' and corresponding strain ε_1 were given by

$$f_{cc}' = f_{co}' + k_1 f_{le}, \text{ and} \tag{1.45}$$

$$\varepsilon_1 = \varepsilon_{01}(1 + 5k_3 K), \tag{1.46}$$

where f_{co}' is the unconfined concrete (bending) compressive strength in member taken as 0.68 times the concrete cube strength, ε_{01} is the unconfined concrete strain at peak stress f_{co}', f_{le} is the equivalent confining pressure, and k_1, k_3 and K are confining coefficients defined as

$$k_1 = 6.7 f_{le}^{-0.17}, \tag{1.47}$$

$$k_3 = \frac{40}{f_{co}'} \le 1.0, \text{ and} \tag{1.48}$$

$$K = \frac{k_1 f_{le}}{f_{co}'}. \tag{1.49}$$

Apart from the static monotonic confinement models discussed above, various cyclic loading tests on unconfined and confined concrete to predict the hysteretic behaviour of concrete are reported in the literature. Plain concrete, when subjected to repeated uniaxial compressive loading produce an *envelope* curve that is approximately same as the complete stress-strain curve obtained under uniaxial monotonic loading [Sinha *et al.*, 1967]. Spirally confined normal weight and light weight concrete also show similar behaviour under cyclic loading [Shah *et al.*, 1983]. Under random cyclic loading, the unloading and reloading curves do not coincide and are not parallel to the initial

loading curve. The average slope of the unloading and reloading curves is inversely proportional to the plastic strain, thereby implying stiffness degradation for the entire strain range [Bahn *et al.*, 1998]. Such hysteretic rules can be applied on the above confinement models as required.

1.5 SEISMIC DESIGN OF BRIDGES: CODE PROVISIONS

1.5.1 Overview

Seismic design includes both force design and displacement design. In the former, probable forces on the members are estimated and designed for, while in the latter, relative displacements due to out-of-phase response of different parts of the bridge are addressed. Force design was the primary focus in international codes on seismic design of bridges until some failures attributed to relative displacement effects were observed in some past earthquakes (*e.g.*, 1964 Alaska; 1971 San Fernando; 1995 Kobe).

The design and detailing of substructures warrants some requirements that not only directly affect the capacity of the member, but also at times, govern the overall behaviour of the member, and of the structure as a whole. For example, it is a common practice to limit the longitudinal reinforcement quantity in reinforced concrete columns. Primarily, the upper and lower limits were specified from non-seismic considerations. The upper limit is generally specified to avoid excessive congestion of reinforcement in the columns, which may cause difficulties in proper concreting. And, the lower limit is specified to cover the following aspects: (a) to control creep and shrinkage redistribution of axial stress in columns, which may induce high compressive stresses in reinforcements, and (b) to ensure that the ultimate flexural strength of the column section exceeds its cracking strength.

However, in seismic design, other aspects also come into force. In the past

earthquakes, a large number of piers have failed in shear (*e.g.*, 1971 San Fernando; 1995 Kobe). A maximum limit on longitudinal reinforcement restricts the maximum overstrength moment-based shear demand on the pier, and hence, may prevent a brittle behaviour. Also, in piers with low longitudinal reinforcement, early tension stiffening may result in increase in the cracked-section stiffness and attract additional shear force resulting in early brittle damage. Moreover, in columns with low longitudinal reinforcement and low axial load levels, high tensile strains with considerable strain hardening can occur in reinforcement resulting in high overstrength factors. In small diameter longitudinal bars associated with low longitudinal steel ratio, strain penetration leads to additional rotation and subsequent additional displacement. In extreme cases, fracture of longitudinal reinforcement could result at relatively low displacement ductility levels. Thus, minimum and maximum limits to longitudinal reinforcement are important for satisfactory performance of piers even under seismic shaking.

The transverse reinforcement in reinforced concrete columns is supposed to serve a three-fold function, namely (a) confining the compressed core concrete, (b) preventing lateral buckling of the longitudinal compression reinforcement, and (c) providing shear resistance and minimising the potential for a column shear failure. These primary conditions serve as guidelines for the specifications related to minimum transverse bar diameter, longitudinal and transverse spacing, and amount of transverse reinforcement required to prevent brittle failures in piers.

A summary of bridge seismic design provisions in various international and national codes, in particular, related only to strength design of piers is presented in the following sub-sections.

1.5.2 CALTRANS Seismic Design Criteria

The California Department of Transportation Seismic Design Criteria [CALTRANS, 1999] specifies requirements for Ordinary Standard Bridges with spans less than *90m* constructed with normal weight concrete superstructure and pier elements on soil that are not susceptible to liquefaction, lateral spreading or scour.

The design philosophy requires that structures be designed to resist internal forces generated when the structure reaches its *collapse limit state*, a condition when sufficient number of plastic hinges are formed to create a local or global collapse mechanism. All columns are required to have a minimum lateral flexural capacity, based on actual material properties, to resist a lateral load of *10%* of the tributary dead load applied at the vertical centre of mass of the superstructure. The column shear demand is to be taken as the shear force associated with the overstrength column moment; CALTRANS recommends Capacity Design. All capacity-protected members, such as footings, all joints and girders, are required to remain essentially elastic. The column overstrength moment, associated shear demand, and moment distribution characteristics of the system determine the design stress resultants for these capacity-protected components adjacent to columns. However, the column overstrength moment is to be modified with an overstrength magnifying factor of *1.2* to account for the material strength variations between columns and adjacent members, with the column moment capacity being greater than the idealised plastic moment capacity.

The capacity of concrete components to resist seismic demands, except for *shear*, is to be based on most probable (expected) material properties and not the nominal material strengths. Furthermore, separate stress-strain Mander's Models (Mander, 1988) are recommended for confined and unconfined concrete to determine the actual local capacity of ductile concrete members. Seismic shear capacity is to be conservatively

determined based on the nominal material strengths only.

CALTRANS recommends that seismic forces and displacement demands on structures be evaluated by either of the two analysis methods, namely (a) Equivalent Static Analysis (ESA), and (b) Elastic Dynamic Analysis (EDA). ESA is recommended for structures or individual frames with balanced spans and uniformly distributed stiffness where the overall response can be predicted by a single translational mode of vibration. The equivalent static horizontal force computed as the product of the spectral acceleration and the tributary weight is to be applied at the vertical centre of mass of the superstructure.

The EDA is recommended where ESA does not adequately cover the dynamic behaviour of the structure. A linear elastic multi-modal spectral analysis is required with at least *90%* mass participation; the modal analysis results are to be combined using the complete quadratic combination (CQC) rule.

The design seismic load is to be determined from an elastic acceleration response spectrum. The horizontal mean spectral acceleration for a maximum credible earthquake is defined by a *5%* damped elastic response spectrum. The response spectrum includes the peak rock acceleration, site modification factor depending on the soil profile types and soil amplification factors. These depend on the moment magnitude of the maximum credible earthquake and the distance of the site from a major fault.

The horizontal earthquake load effects in two mutual orthogonal directions are to be combined to form two general load cases, namely (i) response from *100%* of load in one direction with the response from *30%* of load in its orthogonal direction, and, (ii) response from *30%* of load in the first direction with the corresponding response from *100%* of load in its orthogonal direction. In the analysis, CALTRANS recommends the use of effective section properties that reflect the cracking that occurs before the yield

limit state is reached. Further, minimum target displacement ductility demands μ_d are specified for each substructure. Foundation flexibility is also accounted for in the analysis. In addition, the $P - \Delta$ effect is required to be considered if the product $P \times \Delta$ is greater than *20%* of the column plastic moment capacity.

CALTRANS specifies that the plastic moment capacity of all ductile concrete members be calculated by $M - \varphi$ analysis based on expected material strengths. The seismic shear demand V_o be based on this overstrength plastic moment capacity and the nominal shear capacity V_n of the ductile concrete members be governed by

$$\phi V_n \geq V_o , \tag{1.50}$$

where

$$V_n = V_c + V_s , \tag{1.51}$$

in which V_c and V_s are shear strength offered by concrete and steel reinforcement respectively. ϕ is a resistance factor taken as *0.85*.

For members under net axial tension, shear capacity V_c offered by concrete is ignored. For those under compression, it is a product of shear strength v_c and effective concrete area A_e (taken as *80%* of the gross cross-sectional area A_g), *i.e.*,

$$V_c = v_c A_e \tag{1.52}$$

where

$$v_c \begin{cases} = Factor1 \times Factor2 \times \sqrt{f_c'} \quad (MPa), \\ \leq 0.33\sqrt{f_c'} \end{cases} \tag{1.53}$$

$$Factor1 \begin{cases} \geq 0.025 \\ = \dfrac{\rho_s f_{yt}}{12.5} + 0.305 - 0.083\mu_d \ , \ \text{and} \\ < 0.25 \end{cases} \tag{1.54}$$

$$Factor2 \begin{cases} = 1 + \dfrac{P}{13.8 \times A_g} \\ \leq 1.5 \end{cases} \quad . \tag{1.55}$$

P is the applied compressive axial load (in *Newton*). For sections outside the potential plastic hinge region, *Factor1* is taken as *0.25*.

The shear capacity V_s offered by reinforcement is given by

$$V_s = \frac{\pi}{2} \frac{A_{sv} f_{yt} D'}{s} \quad \text{for circular sections, and} \tag{1.56}$$

$$V_s = \frac{A_{sh} f_{yt} D'}{s} \quad \text{for rectangular wall sections in weak direction,} \tag{1.57}$$

where D' is the cross-sectional dimension of the confined core concrete measured between the centreline of the peripheral hoop or spiral, f_{yt} is the nominal yield strength of the transverse steel reinforcement, A_s is the cross-sectional area of transverse hoop or spiral, A_{sh} is the total area of effective transverse reinforcement in the rectangular sections, and s is the centre-to-centre spacing of transverse reinforcement set along the longitudinal axis of the pier.

In the strong direction, wall piers are required to resist a shear demand that is dependent on their boundary condition. It is recommended that wall piers with fixed-fixed end conditions be designed to resist a shear generated by the unreduced elastic acceleration response spectrum demand or *130%* of the ultimate shear capacity of the foundation. Pier walls with fixed-pinned connection are to be designed for *130%* of the larger of either the shear capacity of the pinned connection or the ultimate capacity of the foundation. In addition, the thickness (width) of the pier wall shall be so proportioned that the average shear stress is less than $0.67\sqrt{f_c'}$.

CALTRANS specifies a minimum area $(A_v)_{\min}$ (in mm^2) of shear reinforcement

for each individual core of columns confined by interlocking spirals or hoops given by

$$\left(A_v\right)_{\min} \geq 0.17\frac{sD'}{f_{yt}}. \tag{1.58}$$

It also specifies the maximum area $\left(A_v\right)_{\max}$ (in mm^2) of shear reinforcement given by

$$\left(A_v\right)_{\max} \leq \frac{V - V_c}{0.67\sqrt{f_c'}A_e}, \tag{1.59}$$

where V is the total shear to be resisted.

In addition, the maximum spacing of transverse reinforcement set is restricted to the minimum of (a) one-fifth of the least dimension of cross-section for columns or one-half of the least cross-section dimension of piers, (b) six times the nominal diameter of longitudinal reinforcement, and (c) *203 mm*.

For compression members, the maximum area of longitudinal reinforcement is prescribed as *4%* of gross cross-sectional area, and the minimum as *1%* for columns and *0 25%* for wall piers. The maximum nominal bar diameter in columns is specified from flexural bond considerations as

$$d_l = 2.1\sqrt{f_c'}\,\frac{L_b}{f_{yle}}, \tag{1.60}$$

where $L_b = L - 0.5D$. Here, L is the length of column from point of maximum moment to the point of contra-flexure, and D is the total depth of section in the direction of interest.

1.5.3 AASHTO Bridge Design Specifications

The American Association of State Highway and Transportation Officials LRFD Bridge Design Specifications (SI Edition) [AASHTO, 1998] are applicable to the design, evaluation and rehabilitation of fixed and movable highway bridges. In general, bridges are required to be designed for specified limit states that include (a) Service Limit State,

(b) Fatigue and Facture Limit State, (c) Strength Limit State, and (d) Extreme Event Limit State. In particular, the provisions of the seismic design correspond to the Extreme Event Limit State.

Seismic design philosophy requires (a) small to moderate earthquakes to be resisted by structural components within the elastic range without significant damage, and (b) exposure to shaking from large earthquakes to cause no collapse of all or part of the bridge, but damages that occur to be readily detectable and accessible for inspection and repair.

The force effects on the components and connections are to be determined primarily by elastic analysis methods, although the resistance is to be determined, in many cases, based on inelastic behaviour. Apart from the load enhancement applied, the load effects on the structure or on its components are also to be modified depending on the ductility level desired, the redundancy and the operational importance of the structure. Finally, the load effect is required to be less than $\phi \times R_n$, where R_n is the nominal resistance or capacity and ϕ is a resistance factor.

The design earthquake load is to be calculated based on an elastic response coefficient and the equivalent weight of the structure on a component through an appropriate analysis method. The analysis procedures recognised include (a) uniform load elastic method, (b) single-mode spectral method, and (c) multi-mode spectral method. The choice of the procedure depends on the importance of the bridge, hazard level of the concerned seismic zone, and irregularities of the bridge. Further, for critical bridges in seismic zone of highest seismic hazard, a comprehensive time history analysis is recommended. In the multi-mode method, for a particular mode of vibration, the response coefficient is a function of the ground acceleration coefficient depending on the seismic zone, site coefficient to account for the four possible soil profile types, and the

associated period of vibration of the mode. The importance criterion is taken care of by suitably using the input ground motion for design earthquake, *i.e.*, critical bridges are designed for large earthquakes with a higher return period unlike essential and other bridges. The horizontal earthquake load effects in two mutual orthogonal directions (longitudinal and transverse) are to be combined to form two general load cases as (i) combination of response from *100%* of the load along first direction with that from *30%* of the load along the second, and (ii) combination of response from *100%* of the load along the second direction with that from *30%* of the load along the first.

The seismic design force effects on the different components obtained from the elastic analysis are divided by a response modification factor R to get the design seismic forces. The response modification factors for substructures are greater than *1.0*, while those for all connections between parts of structures are less than *1.0*. Thus, the specifications require the substructures to deform inelastically, while the connections are required to perform essentially within the elastic limit. However, when an inelastic time history analysis is used, the response modification factor R is always taken as *1.0* for both substructure and connections.

The AASHTO specifications are intended to ensure that a substructure is provided with adequate ductility and is forced to yield in flexure and that the chances of brittle modes of failure are minimised. Accordingly, substantial requirements for compression members are introduced.

The maximum area $(A_l)_{\max}$ of non-prestressed longitudinal reinforcement for compression members is stated as *8%* of the gross area of cross-section, and the minimum area $(A_l)_{\min}$ requirement for non-prestressed steel is given by

$$\frac{(A_l)_{\min} f_{yl}}{A_g f_c'} \geq 0.135, \tag{1.61}$$

where f_{yl} is the specified yield stress (in *MPa*) of longitudinal reinforcing bars. The compressive strength of concrete f_c' appears in this specification as bending primarily controls the dimensioning of the column and the amount of reinforcement. However, for bridges in higher seismic zones, the maximum and minimum areas of longitudinal reinforcement are fixed at *6%* and *1%*, respectively, of the gross cross-section area A_g.

The columns are required to be designed biaxially for both minimum and maximum axial load levels. However, when the factored axial load level exceeds $0.20 f_c' A_g$, the resistance factor ϕ is reduced to *0.50* from the normal value of *0.90* for flexure in RC components, to account for the reduction in ductility capacity at high axial load levels. In wall-type piers, the minimum reinforcement ratio in both vertical and horizontal direction is specified as *0.0025*. The vertical reinforcement ratio can be more than the horizontal reinforcement ratio, with a maximum spacing of *450mm* in both horizontal and vertical direction. However, in such cases, the response reduction factor is not applicable to get the design forces.

The column factored shear resistance ϕV_n shall be greater than or equal to the factored shear force V_u along each principal axis of the column. The nominal shear resistance V_n is given by the lesser of

$$V_n = V_c + V_s, \text{ and} \tag{1.62a}$$

$$V_n = 0.25 f_c' b_v d_v, \tag{1.62b}$$

where V_c is shear strength provided by concrete; V_s is shear strength provided by transverse reinforcement; b_v is the effective web width taken as the minimum web width within the depth d_v; and d_v is the effective shear depth taken as the distance measured perpendicular to the neutral axis, between the resultants of the tensile and compressive

forces due to flexure, subjected to a minimum value equal to the greater of *0.9d* and

0.72D, where *d* is the effective depth from extreme compression fibre to the centroid of

the tensile force in the tension reinforcement and *D* is the overall depth of the section.

The concrete shear capacity V_c and reinforcement shear capacity V_s are given by

$$V_c = 0.083\beta\sqrt{f'_c}b_v d_v \text{, and} \tag{1.63}$$

$$V_s = \frac{A_{sh}f_{yt}d_v}{s}, \tag{1.64}$$

where β is a factor depending on the applied loading and the properties of the section.

The nominal transverse reinforcement requirement for piers specifies minimum

bar diameter as (a) *32mm* diameter bars for *102mm* or smaller diameter longitudinal bars,

and (b) *41mm* diameter bars for *114mm* or larger diameter longitudinal bars. The

maximum spacing of transverse reinforcement set along the longitudinal axis of the

member needs to be the lesser of (a) least cross-sectional dimension of the compression

member, and (b) *300mm.*

Transverse ties are to be so arranged that every corner and alternate longitudinal

bar has lateral support provided by the corner of a tie having an included angle of not

more than *135°*. When the column is designed based on plastic hinging capability, the

maximum spacing of longitudinal bars needs to be such that no longitudinal bar is farther

than *150mm* clear on each side along the tie of a laterally supported bar. When the bars

are located around the periphery of a circle, a complete circular tie is to be used, provided

the splicing of the ties are staggered.

The transverse reinforcement at the potential plastic hinge regions for circular

columns needs to be such that the minimum volumetric ratio of spiral reinforcement is

the greater of

$$\rho_s = 0.45\left(\frac{A_g}{A_c} - 1\right)\left(\frac{f'_c}{f_{yt}}\right), \text{ and} \tag{1.65a}$$

$$\rho_s = 0.12\left(\frac{f'_c}{f_{yt}}\right). \tag{1.65b}$$

For rectangular columns, the gross total area A_{sh} of rectangular hoop is to be larger than

$$A_{sh} = 0.30sD'\left(\frac{A_g}{A_c} - 1\right)\left(\frac{f'_c}{f_{yt}}\right), \text{ and} \tag{1.66a}$$

$$A_{sh} = 0.12sD'\left(\frac{f'_c}{f_{yt}}\right), \tag{1.66b}$$

where D' is the column core dimension in the direction under consideration. The maximum spacing of such transverse reinforcement is to be the minimum of (a) one-quarter of the minimum member dimension, and (b) *100mm.*

1.5.4 NZS Bridge Design Specifications

The earthquake resistant design standard for bridges in New Zealand [NZS 3101, 1995] accepts the philosophy that small to moderate earthquakes are to be resisted within the elastic range of the structure, and large earthquakes through inelastic ductile action. However, bridges are not to collapse during strong shaking. They are to remain usable, at least by light traffic, after the design earthquake has occurred. Further, structural damage is to be visible and accessible for inspection and repair. The piers are to be designed to behave in a ductile manner to dissipate the earthquake induced energy. The philosophy emphasises that the structure should posses both sufficient strength and adequate ductility.

However, the structure and its components are categorised into three types, namely (a) fully-ductile, (b) partially-ductile, and (c) non-ductile, depending on the force-

deformation characteristics and the hysteretic energy dissipation capability. This is driven by the economics of the project. For example, in bridges where short piers or abutments provide transverse restraint to superstructures, or in one- or two-span bridges where longitudinal restraint is necessarily at abutments, a plastic mechanism is unlikely to form in the piers even under extreme earthquake shaking; here, the investment to ensure a ductile behaviour becomes unjustifiably large as the design forces generated in a particular direction become too large in a part or all of the bridge. In such cases, a lower standard of earthquake resistance is accepted in the form of a reduced post-elastic behaviour, but not by an appreciable increase in risk of collapse.

In design, the concept of capacity design is used. First, through an elastic analysis under the specified loads, the minimum flexural strength requirements for the plastic hinges are to be determined and the plastic hinge sections are to be designed for such moments. Then, the overstrength flexural capacity of the plastic hinges are to be determined; the structure is re-analysed assuming all potential plastic hinges to have developed their overstrength flexural capacities and the associated moment and shear demands on all structural components other than those with the plastic hinges are to be determined and designed for. The members with plastic hinges are to be designed for the shear corresponding to the state when flexural hinges are formed.

The earthquake load acting on the bridge is to be computed based on a seismic coefficient, which varies with the fundamental period of the structure, the seismic hazard level of the site, and the seismic zone. In addition, the seismic coefficient depends on the expected ductility level of the structure. Thus, the coefficient values for non-ductile structures are higher than the fully-ductile ones. Furthermore, an importance factor is to be applied to arrive at the design seismic force level. Thus, the design earthquake load is the product of the seismic coefficient, importance factor, and the weight of the structure.

New Zealand Standards for concrete structures [NZS 3101,1995] specifies the requirements for longitudinal and transverse steel for the structural design of RC ductile piers under seismic loading. For both columns ad piers, the minimum and maximum area of longitudinal reinforcement are specified as *0.8%* and *8%* respectively of the gross cross-sectional area of the member. However, in potential plastic hinge regions, the maximum area of longitudinal reinforcement is to be limited to $18A_g/f_{yl}$. The maximum centre-to-centre spacing of such cross-linked longitudinal bars across the pier cross-section is to be limited to the lesser of (a) one-fourth of the lateral dimension of the cross-section in the direction of spacing, and (b) *200mm*. In any row of bars, the smallest bar diameter needs to be at least *2/3* of the largest bar diameter used.

For spiral or circular hoops, the minimum diameter is specified as *5mm*. For rectangular hoops and ties, it is to be the maximum of (a) *5mm* for longitudinal bars less than *20mm* in diameter, (b) *10mm* for longitudinal bars from *20* to *32mm* in diameter, and (c) *12mm* for longitudinal bars larger than *32mm* in diameter.

The minimum volumetric ratio of spiral or circular hoop reinforcement in compression members needs to be greater than

$$\rho_s = \frac{(1-\rho_l m)}{2.4}\left(\frac{A_g}{A_c}\right)\left(\frac{f_c'}{f_{yt}}\right)\left(\frac{N^*}{\phi f_c' A_g}\right) - 0.0084 \text{ , and} \qquad (1.67a)$$

$$\rho_s = \frac{A_{sl}}{155D'}\left(\frac{f_{yl}}{f_{yt}}\right)\left(\frac{1}{d_l}\right), \qquad (1.67b)$$

where N^* is the design axial load at the ultimate limit state. The minimum total effective area of non-circular hoop or tie reinforcement in each principal direction within spacing s in compression members is to be greater than

$$A_{sh} = \frac{(1-\rho_l m)sD'}{3.3}\left(\frac{A_g}{A_c}\right)\left(\frac{f_c'}{f_{yt}}\right)\left(\frac{N^*}{\phi f_c' A_g}\right) - 0.0065sD'. \qquad (1.68)$$

Further, the minimum area $\left(A_{sv}\right)_{\min}$ of an individual leg of a stirrup or tie is specified as

$$\left(A_{sv}\right)_{\min} = \frac{\sum A_l f_{yl}}{135 f_{yt}}\left(\frac{s}{d_l}\right), \tag{1.69}$$

where $\sum A_l$ is the sum of the areas of the longitudinal bars reliant on the tie whose maximum centre-to centre spacing across the cross-section is lesser than one-third of the lateral dimension of the cross-section in the direction of spacing or *200mm*. The maximum centre-to centre spacing of transverse reinforcement set along the member subjected to earthquake effects is to be the lesser of (a) one-third of the least lateral dimension of the cross-section, and (b) *10* times the diameter of the longitudinal bar to be restrained.

In potential plastic hinge regions, Eqs.(1.67) and (1.68) are replaced by Eqs.(1.70) and (1.71) respectively, which are

$$\rho_s = \frac{\left(1.3 - \rho_l m\right)}{2.4}\left(\frac{A_g}{A_c}\right)\left(\frac{f_c'}{f_{yt}}\right)\left(\frac{N^*}{\phi f_c' A_g}\right) - 0.0084, \tag{1.70a}$$

$$\rho_s = \frac{A_{sl}}{110D'}\left(\frac{f_{yl}}{f_{yt}}\right)\left(\frac{1}{d_l}\right), \text{ and} \tag{1.70b}$$

$$A_{sh} = \frac{\left(1.3 - \rho_l m\right)sD'}{3.3}\left(\frac{A_g}{A_c}\right)\left(\frac{f_c'}{f_{yt}}\right)\left(\frac{N^*}{\phi f_c' A_g}\right) - 0.0065sD'. \tag{1.71}$$

In addition, the maximum centre-to-centre spacing of transverse reinforcement set along the member in the potential plastic hinge region is to be the lesser of (a) one-fourth of the least lateral dimension of the cross-section, and (b) *6* times the diameter of the longitudinal bar to be restrained. The required minimum quantity of transverse reinforcement outside the potential plastic hinge region is *70%* of that required in the potential plastic hinge region.

In piers of limited-ductility capacity, the quantity of transverse reinforcement in the potential plastic hinge region is to be given by Eq.(1.70) and Eq.(1.71). However, the maximum centre-to centre spacing of transverse reinforcement set along the member in the potential plastic hinge region shall be the lesser of (a) one-fourth of the least lateral dimension of the cross-section, and (b) *10* times the diameter of the longitudinal bar to be restrained. Thus, there is reduction in the transverse steel content for sections of partial-ductility capacity as compared to sections that are fully-ductile.

1.5.5 PWRI Design Specifications for Highway Bridges

The Public Works Research Institute Design Specifications of Highway Bridges in Japan provides specifications [PWRI, 1998] for seismic design of bridges. For bridges of span less than *200m*, it requires the structure to be primarily designed for two levels of seismic demand; one corresponding to an earthquake that is highly probable during the service period of the bridge, and another stronger seismic motion that is less probable during the service period of the bridge. Also, bridges are classified into two groups of importance, namely standard and high.

The seismic design philosophy requires that under the highly probable seismic event, no damage is caused to either group of bridges, while under the strong seismic event, the target seismic performance is to prevent fatal damage to bridges of standard importance group, and limit damage in bridges of high importance group. In no case, collapse of the bridge is allowed.

Seismic loads on the structure are to be estimated by seismic coefficient method and ductility design method. For the highly probable seismic events, seismic coefficient method is recommended with allowable stress intensities, allowable displacements, safety factors, or a combination of these. And, for strong seismic event, ductility design method is required, which considers horizontal capacities, allowable ductility factors, residual

displacements or a combination of these. However, for important bridges with irregularities that may behave in a complicated manner, dynamic time history response analysis or response spectrum analysis is required to check the design done as per the seismic coefficient method and ductility design method. Site conditions and satisfactory seismic performance of the entire bridge system including the bearing supports and unseating prevention system are to be considered in design.

In the ductility design method prescribed in PWRI specifications, piers are required to have a lateral capacity greater than the equivalent lateral load equal to product of equivalent lateral force coefficient and tributary weight on it. In addition, the residual displacement of the pier is to be less than the allowable residual displacement, namely *1/100* of the height from the bottom edge of the pier to the point where the inertial force acts on the superstructure.

The PWRI provisions recommend that horizontal inertial forces be considered in two mutual orthogonal directions. However, the inertial forces in the two horizontal directions are to act separately. In the design of substructures, inertial forces in the vertical direction are also to be considered.

The capacity of the section is to be calculated based on a stress-strain model of concrete considering the restraining effect of ties. The section is to be discretised into a number of fibres in the direction in which the inertia force acts, and the bending moment, axial load and section curvature demands are to be estimated for the design seismic load.

The shear capacity V_n of the section is given by Eq.(1.51), where concrete shear capacity V_c and shear reinforcement capacity V_s are given by

$$V_c = c_c c_e c_{pt} \tau_c bd \text{ , and}$$

(1.72)

$$V_s = \frac{A_{sh} f_{yt} d}{1.15s},$$

(1.73)

where c_c, c_e, and c_{pt} are modification factors. τ_c is the average shear stress that concrete can bear and is a function of the grade of concrete. c_c accounts for decline of average shear stress borne by concrete due to the effect of cyclic loading. c_e accounts for the 'scale effect', wherein the average shear strength in concrete decreases with increase in effective depth. c_{pt} accounts for increase in average shear stress that concrete can bear with increase in longitudinal tension steel. However, such increase is restricted to a maximum of *1%* of tension steel as it is not desirable to increase the tension steel ratio to enhance V_c.

The PWRI provisions recommend the minimum bar diameter of hoops to be *13mm* and the maximum centre-to-centre spacing to be *150mm*. However, outside the potential plastic hinge region, spacing may be increased gradually. In hollow sections, intermediate ties are to hold the hoop ties on the outer and inner sides to increase the effect of hoop ties. An upper limit of *1.8%* is imposed on the volumetric ratio of amount of transverse reinforcement. Under cyclic plastic deformation, excessive increase in confining force on concrete reduces the length of plastic hinge, fractures the longitudinal reinforcement, and reaches the ultimate state; the upper limit on transverse steel controls these factors.

1.5.6 IRC and IS Specifications for Road Bridges

The general loading and stresses, including those of seismic effects, for the design and construction of road bridges in India are specified in the Indian Road Congress specification IRC:6-2000 [IRC 6, 2000]. The Indian Standards Institution's Criteria for Earthquake Resistant Design of Structures IS:1893-1984 [IS 1893, 1984] also has loading criteria for bridges in India. However, these same specifications for seismic force are reiterated in IRC:6-2000. Additional design provisions specifically for concrete structures

are specified in IRC:21-1987 [IRC 21, 1987] and special provisions for foundations and substructures in IRC:78-1983 [IRC 78, 1983].

The seismic design philosophy behind these provisions primarily covers force design. The horizontal design earthquake load on bridges with span length less than *150m* is to be calculated based on a seismic coefficient. The coefficient depends on the seismic hazard level of the site, and is applicable for structures standing on soils or rocks that will not settle or slide due to loss of strength during vibrations. The lateral load is to be further modified based on soil-foundation system type and the importance of the bridge. The equivalent static horizontal seismic load on the bridge is specified as the product of the modified horizontal seismic coefficient and the weight acting at the vertical centre of mass of the structure. The design procedure does not consider the flexibility and dynamic behaviour of the bridge or its components.

RC members are required to be designed by the Working Stress Method. A *50%* increase in permissible stresses is allowed in seismic events. The analysis for forces and stresses is to be based on gross cross-sectional properties of components. However, if the resultant tension at any section due to the combined action of direct compression and bending is greater than a specified permissible tensile stress, cracked section analysis is recommended with the specified permissible stresses. For compression members, there are no provisions of design for transverse shear.

There are no special provisions for confinement of concrete. However, requirements for nominal reinforcements are specified. The minimum diameter of transverse reinforcement (*i.e.*, lateral ties, circular rings or helical reinforcement) is to be the larger of (a) one-quarter of the maximum diameter of longitudinal reinforcement, and (b) *8mm*. The maximum centre-to-centre spacing of such transverse reinforcement along the member length is to be the lesser of (a) least lateral dimension of the compression

member, (b) *12* times the diameter of the smallest longitudinal reinforcement bar in the compression member, and (c) *300mm*.

IRC:78-1983 specifies an additional requirement for transverse reinforcement in walls of hollow RC piers. The minimum area of such reinforcement is given as *0.3%* of the sectional area of the wall. Such reinforcement is to be distributed on both faces of the wall: *60%* on the outer face and the remaining *40%* on the inner face.

The minimum and maximum areas of longitudinal reinforcement for columns are specified to be *0.8%* and *8%* respectively, of the gross cross-sectional area of the member. The minimum and maximum specified nominal longitudinal bar diameters for columns are *12mm* and *40mm*, respectively. IRC:21-1987 requires that every corner and alternate longitudinal bar to have lateral support provided by the corner of a tie having an included angle of not more than *135 °*, and no longitudinal bar to be farther than *150mm* clear on each side along the tie of a laterally supported bar. When the bars are located on the periphery of a circle, a complete circular tie is to be used.

A comparison of the IRC provisions for seismic design of RC bridge piers with those of the other codes/specifications reveals that IRC provisions do not consider the possibility of plastic hinge formation in an extreme seismic event. Also, preventing buckling of longitudinal reinforcement and confining the core concrete for a stable post-yield response are not addressed. Hence, a thorough investigation of the response of substructures designed as per the current IRC specifications for seismic load effects is warranted.

1.6 NOMINAL SHEAR CAPACITY OF SOLID CIRCULAR AND RECTANGULAR RC PIERS

Satisfactory seismic behaviour of reinforced concrete structures requires that the brittle form of failures be prevented. This requires that the nominal shear capacity be

greater than the overstrength moment-based shear demand on the structure. The nominal shear capacity V_u comprises of shear strength provided by concrete V_{uc}, by transverse steel V_{us}, and that by longitudinal steel V_{ul}. The shear V_{ul} resisted by longitudinal steel is through its direct shear capacity under the existing axial stress, and by dowel action. However, a clear quantification of these actions is not available in any of the codes of practice. Currently, V_{uc} indirectly accounts for the longitudinal steel content. Thus, the nominal shear capacity is given by [IS:456-2000]

$$V_u = V_{uc} + V_{us}. \tag{1.74}$$

Shear strength provided by concrete V_{uc} is equal to an effective area A_e times the nominal shear stress τ_c. For rectangular sections, AASHTO recommends an A_e as the product of width b and effective shear depth d_v, where d_v is the distance between resultants of tensile and compression forces due to flexure. However, for circular sections, A_e is not stated. CALTRANS recommends A_e as *0.8* times the gross cross-section area for general ductile concrete members; this is also supported elsewhere in the literature [Priestley *et al.*, 1996]. The nominal shear stress τ_c is a function of grade of concrete and the percentage of tension steel ρ_t. For pier sections with generally well-distributed longitudinal steel and with at least half the section cracked under seismic action, ρ_t is generally taken as $0.5\rho_l$, where ρ_l is the percentage of longitudinal steel [Priestley *et al.*, 1996].

In deriving the shear strength V_{us} provided by transverse steel, it is assumed that the potential shear crack crosses the transverse reinforcement at *45°* to the member axis. Thus, for solid rectangular sections, V_{us} is given by

$$V_{us} = \sigma_d A_{sh} \frac{D'}{s}, \tag{1.75}$$

where σ_d is the design tensile stress in steel, s is the spacing of vertical transverse reinforcement along the pier axis, D' is the centre-to-centre distance of peripheral transverse reinforcement (Figure 1.11a), and A_{sh} is the total area of transverse reinforcement cut by the potential shear crack.

In solid circular sections, the total shear resisted by transverse hoops [Ang *et al.*, 1989] is given by

$$V_{us} = \frac{\pi}{2} A_{sv} \sigma_d \frac{D'}{s},$$
(1.76)

where A_{sv} is the cross-sectional area of the hoop, and D' is the centre-to-centre distance of peripheral transverse reinforcement (Figure 1.10b). However, shear resisted by transverse steel in hollow circular or rectangular sections are not available in the specifications/standards.

1.7 PRESENT STUDY

The primary objective of this study is to assess the post-yield lateral load-deformation relation of RC bridge piers designed as per Indian bridge design provisions. Four types of generally used pier sections, solid and hollow, as well as circular and rectangular, are designed as per the specifications of IRC. In the analytical study, pier cross-section type, slenderness ratio and axial load level are changed. A new feature of using additional radial links in hollow circular pier sections is also investigated. However, general provisions on detailing of reinforcement (such as splicing, lapping of longitudinal and hoop bars, and specifications for hooks), are not discussed in the present analytical study, though these features significantly affect the final response of the pier under seismic shaking.

As no previous analytical tools are available to assess the global load-deformation

relationship of piers with either solid or hollow cross-sections, with due consideration to concrete confinement, longitudinal bar buckling and shear deformation in the cross-section, a comprehensive analytical procedure is developed. To account for spread of plasticity, both along the member height and across the section, an existing fibre model [Murty and Hall, 1994] is modified to properly account for the effective shear stiffness to account for the lateral translational stiffness of both squat and slender members. An existing concrete confinement model [Dasgupta. 2000] applicable to both hollow and solid as well as circular and rectangular sections is used. The stress-strain curve for steel, empirically derived based on laboratory test data, conforming to IS:1786-1979 is taken from a previous study [Dasgupta, 2000]. The constitutive models of concrete and steel are modified for appropriate hysteretic behaviour during partial unloading and subsequent reloading. A displacement-based pushover analysis procedure is developed to capture the overall global monotonic load-deformation response of cantilever compression members bending in single curvature under lateral loading. A computer program is written for the analysis.

The study estimates the overstrength plastic moment hinge-based maximum shear demand and the possible drift capacity of Indian Code designed bridge piers, and investigates the primary mode of failure, namely ductile flexural failure or brittle shear failure.

• • •

Chapter 2

Displacement-Based Pushover Analysis

2.0 INTRODUCTION

In the present study, an analytical procedure is developed for the assessment of inelastic drift capacity of (circular and square, solid and hollow) RC piers bending in single curvature. Finite element analysis approach is used; the pier is discretised into smaller segments along the length of the member and each segment into fibres across the cross-section. The segment incremental load-deformation relations are computed based on a fibre model, using available material models for reinforcing steel and concrete (confined or unconfined). The pier is pushed at the top in displacement increments and the updated deformed geometry is computed, and the internal resistance developed is calculated from the current segment orientation and inelastic material properties.

2.1 EFFECTIVE UNCRACKED SHEAR AREA AND BULK MODULUS IN RC PIERS

In this study, the effective area A_s of the initial *uncracked* RC sections resisting shear is calculated by numerically evaluating the integral in the expression given below [Ghali and Neville, 1997]

$$A_s = \frac{I^2}{\int_A \frac{Q^2}{b^2} dA}, \qquad (2.1)$$

where I is the second moment of the complete area of cross-section about the considered axis of bending, Q is the first moment of the area of the part of the section above the fibre under consideration about the axis of bending, b is the width of the cross-section at the fibre under consideration parallel to the axis of bending, and dA is the area of the

differential element above the fibre under consideration (Figure 2.1). For this numerical integration, the cross-section is discretised into a number of concrete (both core and cover) and steel fibres (Figure 2.2). The area of the steel fibres are transformed to equivalent concrete fibres through the modification factor defined as

$$m = \left(\frac{E_s}{E_c} \right)_{initial},$$

(2.2)

where E_s and E_c are the modulus of elasticity of longitudinal reinforcing steel and concrete. Thus, the second moment of area of the section about the axis of bending, taken as the centroidal axis of the gross cross-section, is

$$I = \sum_{i=1}^{N_{fc}} \left(A_i^c y_i^2 + \frac{1}{12} w_i t^3 \right) + \sum_{j=1}^{N_{fs}} \left(A_j^s (m-1) y_j^2 \right),$$

(2.3)

where A^c and A^s are the area of each concrete and steel fibres, w is the width of the concrete fibres and t is the thickness of the fibres after discretisation of the section. N_{fc} and N_{fs} are the total number of concrete and steel fibres respectively. Hence, the effective area resisting shear is given by

$$A_s = \frac{I^2}{\sum_{i=1}^{N_{fc}} \left\{ \frac{\left(\sum_{j=1}^{i^*} A_j y_j \right)}{w_i^{*2}} A_i^* \right\}},$$

(2.4)

where A_j in the denominator of Eq.(2.4) includes the appropriate equivalent concrete area in case of steel fibres under consideration. The width w_i^* and the differential area A_j^* correspond to full width and area of concrete fibres, *i.e*, inclusive of both the cover and core concretes at the same distance from the centroidal axis of the section. i^* in Eq.(2.4) is number of the last fibre (concrete or steel) above the fibre under consideration.

The bulk modulus of elasticity G of the composite RC material is computed as an effective modulus as stated below. The moduli of elasticity E of longitudinal reinforcing steel, core concrete and cover concrete are different. Hence, an effective modulus of elasticity E_{eff} of the composite material is numerically evaluated under the action of load of superstructure and the self-weight from the effective flexural rigidity $(EI)_{eff}$ of the whole section, computed as

$$(EI)_{eff} = \sum_{i=1}^{N_f} E_i I_i^* , \tag{2.5}$$

where E_i is the tangent modulus of the concrete or steel fibre at the uniform axial strain level under the action of superstructure gravity load and the self-weight. and I_i^* is the second moment of area of fibre i about the centroidal axis of the cross-section. In this case, the actual areas of steel fibres are considered. The effective modulus of elasticity E_{eff} of the composite material is then calculated as

$$E_{eff} = \frac{(EI)_{eff}}{I} , \tag{2.6}$$

where $(EI)_{eff}$ and I are as defined in Eq.(2.5) and Eq.(2.3) respectively. From E_{eff}, the effective bulk modulus of elasticity G_{eff} of the composite material is then computed as

$$G_{eff} = \frac{E_{eff}}{2(1+v)} . \tag{2.7}$$

In the present study, a value of 0.15 is used for the Poisson's Ratio v for the composite material, *i.e.*, reinforced concrete.

2.2 MATERIAL CONSTITUTIVE LAW MODELS USED

The load-deformation relationship of each fibre is derived using material constitutive law. In RC structures, the two different material fibres, namely reinforcing steel and concrete, require two different material constitutive law models. The core concrete fibres are *confined* and the cover concrete *unconfined*. Also, the *longitudinal* and *transverse* steels can be different. However, the transverse steel only affects the confinement of the core concrete and influences its axial stress-strain relation. Only the longitudinal steel directly plays a role in the axial, bending and shear resistance of the section. Thus, only longitudinal steel is modelled.

During pushover analysis, initially all the fibres are in compression under the action of gravity load (loading in compression). As curvature in the section is gradually increased, compressive strain in some fibres increases, while in others, the compressive strain decreases and eventually becomes tensile (unloading in compression and subsequent loading in tension). Again, after spalling of cover concrete, redistribution of stresses occurs within the section. As such, there is possibility of further partial or full unloading and reloading in tension or compression for both concrete and steel fibres.

2.2.1 Longitudinal Steel

A model representing the virgin stress-strain curve for high yield strength deformed (HYSD) bars conforming to IS:1786-1979 developed earlier [Dasgupta, 2000] is used. The associated equations are reproduced in Appendix A. In this study, the virgin curve in compression is taken as a symmetric image of the curve in tension about the stress-strain axes.

In the monotonic pushover analysis, exhaustive hysteretic models for reinforcing steel may not be required. Simple loading, unloading and reloading rules are therefore

prescribed (Figure 2.3). The following are the salient features of the model used:

a) All unloading and initial reloading slopes, upto yield, are equal to the initial elastic modulus E_s; there is no stiffness degradation.

b) There is no strength deterioration.

c) As the material unloads from the virgin curve, the whole stress-strain curve translates along the strain axis, the total translation being dependent on the plastic strain history; a kinematic hardening approach is utilised with translation of the stress-strain path with no change of size or shape, but with accumulation of plastic strain.

To account for buckling of longitudinal reinforcement, the following algorithm is implemented in the present study. The critical buckling stress $\sigma_{cr,b}^1$ at elastic stage of a longitudinal reinforcement is given by Euler's buckling theory for a compression member under clamped-clamped condition, as

$$\sigma_{cr,b}^1 = \frac{\pi^2 E_s}{4(s/d_b)^2},\qquad(2.8)$$

where s and d_b are the longitudinal spacing of transverse reinforcement and diameter of longitudinal reinforcement. To prevent inelastic buckling, a critical spacing of $6d_b$ is commonly used [CALTRANS, 1999]. However, for steels with high ultimate to yield ratio of about *1 5*, this specification is reasonable, but is inadequate for steels with lower ratio (*e.g.*, HYSD bars conforming to IS:1786-1979 with $f_u / f_y \approx 1.25$). For such steels, in absence of other experimental data, the critical stress for inelastic buckling is taken as

$$\sigma_{cr,b}^2 = \begin{cases} f_u & \text{for} & \left(\dfrac{s}{d_b}\right) < 5 \\[2mm] f_y - \dfrac{(f_u - f_y)}{5}\left(\dfrac{s}{d_b} - 5\right) & \text{for} & 5 < \left(\dfrac{s}{d_b}\right) < 10 \\[2mm] f_y & \text{for} & \left(\dfrac{s}{d_b}\right) > 10 \end{cases}.\qquad(2.9)$$

Thus, the overall critical stress for buckling or stability of compression bars is given by (Figure 2.4)

$$\sigma_{cr,b} = Min\left[\sigma_{cr,b}^1 ; \sigma_{cr,b}^2\right] . \tag{2.10}$$

2.2.2 Concrete

In this study, the existing models [Dasgupta, 2000] for uniaxial stress-strain constitutive laws of confined and unconfined concrete in hollow circular and rectangular sections are modified in the post-ultimate range and enhanced to include unloading and further reloading. In the original model [Dasgupta, 2000], a single equation [Popovics, 1973] was used to define the stress-strain curve over the entire range of strain, given by Eq.(1.37). However, the falling branch defined by the above equation is too flat and remains above the experimental uniaxial stress-strain data. Hence, in this study, the equation is modified beyond the strain corresponding to the peak stress (Figure 2.5) as

$$f_c = \frac{f_{cc}' x r_o}{r_o - 1 + x^{r_o}}, \tag{2.11}$$

where

$$r_o = r^{(1+1/r)}, \tag{2.12}$$

where r is given by Eq.(1.44).

For the purposes of monotonic pushover analysis of large pier sections, simple unloading and reloading rules are employed. The salient features of the concrete model used are (Figure 2.6):

a) Linear unloading and reloading occur with tangent modulus equal to the initial modulus.

b) The residual strain capacity is calculated from the accumulated plastic strain.

c) The tensile strength of concrete is neglected.

2.3 PURE TRANSLATIONAL STIFFNESS OF A SEGMENT

For a prismatic segment of length L, second moment of area about geometric centroidal axis I, area resisting shear A_s, with elastic modulus E and bulk modulus G, the pure flexural lateral translational stiffness is $12EI/L^3$, while the pure shear translational stiffness is equal to GA_s/L (Figure 2.7). From Eq.(1.19), the incremental shear force on the segment is given by

$$\dot{V} = \frac{GA_s}{L}(\dot{u}_2 - \dot{u}_5) - \frac{GA_s}{2}(\dot{u}_3 + \dot{u}_6). \tag{2.13}$$

For pure incremental lateral translation without any incremental flexural rotations at the ends of the element, the lateral translational stiffness comes out to be GA_s/L, independent of whether the member is slender or stocky. But, this stiffness of GA_s/L is true only for stocky members with pure shear deformations. Therefore, a correction is introduced using β, the relative ratio of flexural lateral translational stiffness and shear stiffness, $\left(12EI/L^3\right)/\left(GA_s/L\right)$. Eq.(2.13) is then modified by the factor $\beta/(1+\beta)$ as

$$\dot{V} = \frac{GA_s}{L}\left(\frac{\beta}{1+\beta}\right)(\dot{u}_1 - \dot{u}_4) - \frac{GA_s}{2}\left(\frac{\beta}{1+\beta}\right)(\dot{u}_3 + \dot{u}_6), \tag{2.14}$$

to cover any general case of piers with varying relative flexural and shear deformations. Thus, Eqs.(1.20) and (1.24) are replaced by

$$^{sh}[K]^l_t = GA_s\left(\frac{\beta}{1+\beta}\right)\begin{bmatrix} 0 & 0 & 0 & 0 & 0 & 0 \\ & \dfrac{1}{L} & -\dfrac{1}{2} & 0 & -\dfrac{1}{L} & -\dfrac{1}{2} \\ & & \dfrac{L}{4} & 0 & \dfrac{1}{2} & \dfrac{L}{4} \\ & & & 0 & 0 & 0 \\ & & & & \dfrac{1}{L} & \dfrac{1}{2} \\ \text{Sym.} & & & & & \dfrac{L}{4} \end{bmatrix}, \text{ and} \tag{2.15}$$

$$
{}^{sh}[K]_t = GA_s\left(\frac{\beta}{1+\beta}\right)
\begin{bmatrix}
\dfrac{b^2}{L} & -\dfrac{ab}{L} & \dfrac{b}{2} & -\dfrac{b^2}{L} & \dfrac{ab}{L} & \dfrac{b}{2} \\[2mm]
 & \dfrac{a^2}{L} & -\dfrac{a}{2} & \dfrac{ab}{L} & -\dfrac{a^2}{L} & -\dfrac{a}{2} \\[2mm]
 & & \dfrac{L}{4} & -\dfrac{b}{2} & \dfrac{a}{2} & \dfrac{L}{4} \\[2mm]
 & & & \dfrac{b^2}{L} & -\dfrac{ab}{L} & -\dfrac{b}{2} \\[2mm]
 & & & & \dfrac{a^2}{L} & \dfrac{a}{2} \\[2mm]
Sym. & & & & & \dfrac{L}{4}
\end{bmatrix}.
\qquad (2.16)
$$

The β factor is modified as cracking takes place in the cross-section through the use of cracked values of EI and GA_s in the expression for β.

2.4 DISPLACEMENT-BASED PUSHOVER ANALYSIS

The structure is subjected to increasing displacement in one direction until final collapse of the pier. The force required to sustain the specified displacement is calculated considering the residual strength of the material, the deformation of the structure and the progression of internal cracking. Thus, the full load-deformation relationship of the pier is available. From this, the overstrength shear demand, the drift capacity and the displacement-ductility capacity of the RC pier bending in single curvature, are extracted.

To begin with, a small displacement increment is imposed at the tip of the cantilever pier. Corresponding to this tip displacement, an initial deformed profile is assumed. Usually the deformed shape of an elastic cantilever with only bending deformations considered under the action of a concentrated load at the tip, is a good approximation. Thus, the initial lateral transverse displacement x_y and rotation θ_y at a distance y from the bottom support, for a displacement Δ_o at the tip of a cantilever of length L and flexural rigidity EI (Figure 2.8) are given by

$$x\big|_y = \frac{y^2}{2L^3}(3L - y)\Delta_o, \text{ and}$$ (2.17a)

$$\theta\big|_y = \frac{3y}{2L^3}(2L - y)\Delta_o.$$ (2.17b)

The change in length of the cantilever is considered while estimating the internal resistance of the pier.

For the assumed displacement profile along the height of the pier, the internal resistance $\{p\}$ is calculated. The external load vector $\{f\}$ consists of vertical concentrated load at the top of the pier from the gravity load of the superstructure and vertical dead loads at all intermediate nodes from the dead load of the pier segments. The unbalance force $\{f_u\} - \{p_u\}$ along all unknown degrees of freedom is calculated. The assumed deformed geometry of the pier is corrected using the additional incremental deformation $\{x_u\}$ in the unknown degrees of freedom which is obtained by solving

$$[K_{uu}].\{\dot{x}_u\} = \{f_u\} - \{p_u\},$$ (2.18)

where $[K_{uu}]$ is the iterating sub-matrix corresponding to the unknown degrees of freedom. It is extracted from the partitioned initial tangent stiffness matrix $[K]_t$ of the pier, given by

$$[K]_t = \begin{bmatrix} [K_{uu}] & [K_{us}] \\ [K_{su}] & [K_{ss}] \end{bmatrix}.$$ (2.19)

$[K]_t$ is obtained as in Eq.(1.27) but with the modification suggested at Eqs.(2.15) and (2.16). The net incremental deformation in global coordinate $\{\dot{x}_u\}$ is updated and the new internal resistance $\{p_u\}$ is re-calculated for this revised geometry of the pier segments. The procedure is repeated until the force unbalance is within the specified tolerance.

2.4.1 Iteration Scheme

Pushover analysis is iterative computation owing to the nonlinearities in the member constitutive relations and due to geometric effects. Modified Newton-Raphson Method is used for the iterations. At the global iteration level, at displacement step r and iteration level k, the incremental deformation vector along the unknown displacement directions $^r\{\dot{x}_u\}_k$ is obtained from

$$^{r-1}[K_{uu}]\,^r\{\dot{x}_u\}_k = \{f_u\} - {}^r\{p_u\}_k, \qquad (2.20)$$

where $^{r-1}[K_{uu}]$ is the iterating matrix based on the cracked section properties at the end of the last displacement step $(r-1)$, and $^r\{p_u\}_k$ is the internal resistance vector. The net incremental deformation vector $^r\{\dot{x}\}_k^{net}$ in the displacement step r and up to iteration k is then obtained as

$$^r\{\dot{x}\}_k^{net} = {}^r\{\dot{x}\}_{k-1}^{net} + {}^r\{\dot{x}\}_k, \qquad (2.21)$$

where $^r\{\dot{x}\}_k$ is the incremental deformation vector along all, known and unknown degrees of freedom. $^r\{\dot{x}\}_k^{net}$ is then decomposed to form the global incremental end-deformation vector $^r\{\dot{d}\}^s$ for each segment s. Hence, if $\overset{s}{\prod}$ is the decomposition operator that depends on the connectivity array of the degrees of freedom at the ends of the segment s, then

$$^r\{\dot{d}\}^s = \overset{s}{\prod} {}^r\{\dot{x}\}_k^{net}. \qquad (2.22)$$

Based on the new deformation profile updated using the node coordinates at the end of the displacement step r, the net global incremental end-deformations and the coordinate transformation $[T]$ are updated. The net incremental deformation vector $^r\{\dot{u}\}^s$ in local coordinate for each segment s, is obtained as

$$^r\{\dot{u}\}^s = [T] \; ^r\{\dot{d}\}^s \, , \tag{2.23}$$

where

$$\left(^r\{\dot{u}\}^s\right)^T = \{\dot{u}\}^T = \langle \dot{u}_1 \quad \dot{u}_2 \quad \dot{u}_3 \quad \dot{u}_4 \quad \dot{u}_5 \quad \dot{u}_6 \rangle . \tag{2.24}$$

2.4.1.1 Internal Resistance due to Imposed Deformation

In the calculation of $^r\{p_u\}_k$, the following procedure is employed. The net incremental axial strain $\dot{\varepsilon}^f$ in fibre f at a normal distance y from the centroidal axis of the gross cross-section of the segment before deforming, is calculated as

$$\dot{\varepsilon}^f = \frac{(\dot{u}_1 - \dot{u}_4) + (\dot{u}_3 - \dot{u}_6)y}{L} , \tag{2.25}$$

where L is the length of the fibre.

Given the state of the fibre at the end of the previous displacement step $(r\text{-}1)$ and the net incremental axial strain $\dot{\varepsilon}^f$, the new stress state σ^f of the fibre is obtained using the cyclic constitutive laws of steel and concrete described in Section 2.2.

From the stresses of all the fibres in the cross-section of the segment, the total internal resistance, namely the axial resistance P_c and the bending moment M_c resisted by the section (segment), are calculated from

$$P_c = \sum_{i=1}^{N_{fc}} \sigma_i^c A_i^c + \sum_{j=1}^{N_{fs}} \sigma_j^s A_j^s \, , \text{ and} \tag{2.26}$$

$$M_c = \sum_{i=1}^{N_{fc}} \sigma_i^c A_i^c y_i + \sum_{j=1}^{N_{fs}} \sigma_j^s A_j^s y_j \, , \tag{2.27}$$

and the total shear $^r V_c^s$ resisted by the segment s in the displacement step r, is obtained using Eq.(2.14) as

$$^r V_c^s = {}^{(r\text{-}1)} V_c^s + GA_s \left(\frac{\beta}{1+\beta} \right) \left\{ \frac{(\dot{u}_2 - \dot{u}_5)}{L} - \frac{(\dot{u}_3 + \dot{u}_6)}{2} \right\} , \tag{2.28}$$

where $^{(r\text{-}1)} V_c^s$ is the segment shear force at the end of the previous displacement step.

Thus, the components of the end-force vector $^r\{r\}^s$ in local coordinate for the segment s are obtained as

$$r_1 = P_c \qquad (2.29a)$$

$$r_2 = {^rV_c^s} \qquad (2.29b)$$

$$r_3 = M_c - \frac{{^rV_c^s}L}{2} \qquad (2.29c)$$

$$r_4 = -P_c \qquad (2.29d)$$

$$r_5 = -{^rV_c^s} \qquad (2.29e)$$

$$r_6 = -M_c - \frac{{^rV_c^s}L}{2} \qquad (2.29f)$$

Using the coordinate transformation $[T]$, the segment end-force vector in global coordinate, $\{p\}^s$ is computed by

$$^r\{p\}^s = [T]^T {^r\{r\}^s} . \qquad (2.30)$$

The assembly of these $\{p\}^s$ vectors of each segment results in the updated complete member residual force vector $\{p\}^C$. Collecting the forces along the unknown degrees of freedom $\{p_u\}$, the residual force vector $\{r_s\}$ is then computed as

$$\{r_s\} = \{f_u\} - \{p_u\}. \qquad (2.31)$$

The above procedure is reiterated until the residue $\{r_s\}$ is within the tolerance. Upon convergence, the global coordinates of the nodes and the segment end forces are updated. The target deformed geometry for the next displacement step $(r+1)$ is computed based on the next lateral increment at the tip of the cantilever pier (Figure 2.9). And again, the new global coordinates and segment end-forces are obtained.

2.4.1.2 Cracked Section Properties

With increasing section curvature associated with increasing pier drift, the

compressive strain increases in some fibres and decreases in the others. Eventually, the latter fibres become tensile. Tensile strength of concrete is neglected in this study. Thus, concrete fibres with tensile axial stresses are considered *cracked* and are neglected in the subsequent analysis. New cracked section properties are calculated and used. In addition, at high deformation levels, reinforcement yielding occurs and the tangent modulus of steel drops from the initial elastic value.

Further, for non-uniform compressive strain across the full cross-section, even at low drift levels, the net rigidities of the section decrease due to the reduction in tangent modulus of the concrete fibres. An *effective* centroidal axis (Figure 2.10) that is not coincident with the original gross cross-section centroidal axis is conceivable. This effective centroidal axis is at a distance x^*, measured positive if above the centroidal axis into the compression zone of the section, from the gross cross-section centroidal axis such that

$$\sum_{i=1}^{N_f} E_i A_i y_i^* = 0,$$
(2.32)

where y_i^* is the distance of the fibre i from the effective centroidal axis. When the section is uniformly strained with uniform steel reinforcement, this effective centroidal axis coincides with the gross cross-sectional centroidal axis.

The effective axial rigidity $(EA)_{eff}$ reflecting the extent of concrete cracking and reinforcement yielding is computed as

$$(EA)_{eff} = \sum_{i=1}^{N_f} E_i A_i,$$
(2.33)

where E_i is the tangent modulus of the concrete or steel at its current state. The, effective shear rigidity $(GA_s)_{eff}$ based on the effective shear area is also required to reflect the increased shear deformations in flexurally cracked RC members. However, the numerical

procedure defined at Eq.(2.4) to compute the effective area resisting shear cannot be applied for cracked RC sections. In this study, the effective shear rigidity is taken to be proportional to the axial rigidity as

$$(GA_s)_{eff} = GA_s \frac{(EA)_{eff}}{EA}.$$ (2.34)

2.5 TOLERANCE LIMITS

In the displacement based non-linear analysis, the convergence of the iterations within a displacement load step is assessed based on the magnitudes of the force and moment quantities in the residual force vector $\{r_s\}$, as explained earlier. For practical finite precision, the iterations are declared to have converged if the residual force quantities are less than some prescribed *tolerance*. Since the residual force vector contains forces and moments, separate limits are set for the tolerance associated with each of them. In the present study, tolerance limits of *0.1kN* and *0.1kNm* are adopted for the force and moment quantities respectively.

2.6 COMPUTER PROGRAM

Based on the formulations discussed, a computer program (in ForTran) is developed for the displacement based pushover analysis of piers bending in single curvature.

2.7 DISCRETISATION OF PIER INTO SEGMENTS

First, the effect of discretisation of pier along the length is studied. A *305mm* diameter, *1375mm* long specimen column section is discretised into *5, 6, 9, 10* and *11* segments (N_s) along the length. Figure 2.11 shows the lateral load-deformation diagram for the different cases. The results are in good agreement with each other as far as the

lateral load demand is considered, but the maximum deformation capacity gradually

converges along discretisation with *9*, *10* and *11* segments. This shows that with

discretisation resulting in segment length to sectional dimension in the direction of

bending, of about *0.42* to *0.5*, the solution converges. Hence, a ratio of segment length to

sectional dimension in the direction of bending of approximately *0.5* is used in the

numerical analyses presented in this thesis.

2.8 NUMERICAL VALIDATION OF DISPLACEMENT-BASED PUSHOVER ANALYSIS

A computer program is developed in line with displacement-based pushover

analysis described in Section 2.4. The analytical estimates of lateral load-deformation

relations of two piers are compared with experimental results reported in literature.

A solid rectangular column A1, *380mm* by *610mm* in cross-section with a

moment arm of *2355mm* was subjected to monotonic lateral loading [Wehbe *et al.*, 1996].

The column had *18* longitudinal reinforcement bars of *19mm* diameter. The transverse

reinforcement, at *110mm* centre-to-centre spacing along the axis of the column, in the

bottom *930mm* length of the column consisted of one *6mm* diameter perimeter hoop, two

6mm diameter cross-ties in long direction, and two *10mm* diameter cross-ties in the short

direction. In the remaining length, *10mm* diameter perimeter hoop and cross-ties are

provided. The stress-strain curve of longitudinal reinforcing steel bars used are given in

the literature. The salient parameters of the steel model used in this study are tuned to

estimate this. This stress-strain curve is represented by a model for mild steel having a

linear initial part, a yield plateau, and a third curvilinear part represented by the cubic

ellipsoidal model given in Eq.(A-1) in Appendix A. In addition, the literature provides

only average compressive strength of the concretes used in specimens. The stress-strain

curve of concrete used in this study (described in Section 2.2.3) is tuned to emulate this

average data. The details of the specimen used in the analysis are given in Table 2.1, and the experimental setup is shown in Figure 2.12. The experimental and analytical monotonic load-deformation curves are shown Figure 2.13. The salient quantities of these curves are presented in Table 2.2. In the experiment, spalling of cover concrete occurred at drift of about *46mm*, while in the analytical study, spalling of cover concrete is observed at drift of *30mm*. Also, in the experiment, the peak lateral load and ultimate lateral drift were obtained as *361kN* and *122mm*, while the analysis predicts a maximum lateral load of *310.8kN* and an ultimate drift of about *100mm*. Moreover, in the second and third cycle of *122mm* drift, opening of transverse tie, buckling of longitudinal reinforcement, and crushing of concrete were observed during the experiment. The computer program developed does not capture opening of ties; thus this feature does not appear in the analytical prediction. Buckling of longitudinal reinforcement is also not observed in the analytical study. Yet, the initiation of compression failure of core concrete is estimated by the analysis at a drift level of *100mm*. The analysis predicts the maximum overstrength based shear and probable ultimate drift within *14%* of the experimental values.

A hollow circular pier PI2-C with additional radial links [Yeh *et al.*, 2001] was also subjected to monotonic displacement loading. The pier had *64* longitudinal bars of *22mm* diameter equally distributed along outer and inner periphery. It had inner and outer hoops and *32* radial links of *10mm* diameter as transverse reinforcement at *200mm* centre-to-centre spacing. The details of the specimen are given in Table 2.1. In the analytical model, different yield strengths of longitudinal and transverse reinforcement could not be taken and hence a single value of *410MPa* is used. Also, since the ultimate strain capacity of reinforcing bars was not available in the reference, an ultimate strain of *0.20* is used in the analysis. The experimental and analytical monotonic load-deformation

curves are shown in Figure 2.14, and their salient features recorded in Table 2.2. In the experimental study, tension yielding of longitudinal reinforcement was reported at *40mm* drift with corresponding lateral load of *1840.1kN*, while in the analysis, tension yielding is observed at drift of *15-20mm* at an average lateral load of around *2100kN*. Thus, the analysis overestimates the initial stiffness. The first concrete crushing (spalling) in the experimental study was reported at drift of *40mm*, while in the analysis, spalling of cover concrete occurred at *35mm* drift. In the experiment, the maximum lateral load was *2356.4kN* and was achieved at drift of *80mm*, while in the analysis, the maximum lateral load is *2488.6kN* and is attained at *85mm* drift. Further, in the experiment, at drift of *100mm*, longitudinal bars ruptured (due to low cycle fatigue) after buckling. However, in the monotonic analysis, only buckling of longitudinal reinforcement is observed at drift of *85mm*. Also, at *100mm* drift, heavy concrete spalling was reported in the experiment, while in the analysis, at drift of *105mm*, the lateral load decreased drastically due to compression failure of core concrete. In general, the analytical prediction is close to the experimental value.

The computer program developed for the monotonic displacement-based pushover analysis is thus seen to predict the salient features of the lateral load-deformation relation of RC piers with reasonable accuracy. The analysis results are very sensitive to the material properties input, namely the actual concrete compressive strength and steel uniaxial tensile test data. Since only average test data are available for the above two specimens, the difference between the experimental values and analytical estimates is therefore understandable.

<center>• • •</center>

Chapter 3

Numerical Studies

3.0 OVERVIEW

Using the formulations discussed in Chapter 2, the overall load-deformation curves are obtained for a number of piers designed as per existing Indian bridge seismic design standards and subjected to monotonic lateral displacement loading. The shear demand when overstrength moment capacity is reached is in focus. This is compared with nominal shear capacity obtained again as per code specified procedures, and the failure mode of the code-designed piers identified.

3.1 NOMINAL SHEAR CAPACITY OF HOLLOW CIRCULAR AND RECTANGULAR RC PIERS

Extending the method of computation of shear strength provided by transverse steel V_{us} for solid sections, discussed in Section 1.6, to hollow sections, the total shear resisted by transverse reinforcement in a bi-symmetric hollow rectangular section is given by

$$V_{us} = \sigma_d \left[A_1 \frac{\left(D^{'} - D^{''}\right)}{s} + A_2 \frac{D^{'}}{s} \right],$$

(3.1)

where $D^{'}$ and $D^{''}$ are the centre-to-centre distances of outer and inner transverse rectangular hoops (Figure 3.1a). It is considered that both inner and outer rectangular hoops and intermediate ties are at equal spacing s along the pier axis. In Eq.(3.1), A_1 is the total area of stirrup legs in a layer in the direction of the shear in one flange, and A_2 is the total area of stirrup legs in a layer in the direction of the shear in the two webs.

Similarly, shear resisted by circular hoops in hollow circular section with outer

and inner hoops of bar diameters A_{sv1} and A_{sv2} respectively, at equal spacing s along

the pier axis is given by

$$V_{us} = \sigma_d \frac{\pi}{2} \left[A_{sv1} \frac{D'}{s} + A_{sv2} \frac{D''}{s} \right], \tag{3.5}$$

where D' and D'' are the centre-to-centre distances of outer and inner transverse circular

hoops (Figure 3.1b). The effect of radial links is not included in the estimation of V_{us} and

hence of V_u. However, neglecting its contribution is only conservative from capacity

design point of view.

Thus, the nominal shear capacities V_u of piers with hollow circular and

rectangular cross-sections are computed as per Eq.(1.74). Further, in calculating V_{uc},

(a) A_e is taken as *0.8* times the gross cross-section area of solid and hollow sections,

whether circular or rectangular; and (b) τ_c is taken from Table 19 of IS:456-2000

corresponding to $\rho_t = 0.5\rho_l$. In calculating V_{us}, the design stress in steel σ_d is taken as

0.87 f_y, where f_y is the characteristic strength of HYSD bars.

3.2 PARAMETRIC STUDIES

To begin with, the adequacy of strength design provisions is investigated for solid

and hollow RC piers of circular and rectangular cross-sections. Piers of typical height *5m*

are designed as per the strength design methodology outlined in IRC:21-1987. The

approximate initial choice of section size (cross-sectional area) and probable load on the

piers are taken from field data of existing bridge piers. The piers are subjected to a

superstructure gravity load of *6500kN*, and the lateral and vertical seismic loads are

calculated based on the seismic coefficient method outlined in IRC:6-2000 for seismic

zone V, with importance coefficient of *1.5* and soil foundation system coefficient of *1.0*.

There is no provision for shear design of piers or compression members in IRC:21-1987. Thus, only nominal transverse reinforcement is provided in first four piers (one each of solid circular, solid rectangular, hollow circular and hollow rectangular; hereinafter called a *set*) designed as per the code provisions. These are named as CSWG, RSWG, CHWG and RHWG. However, provisions for shear design in beams and slabs are outlined in IRC:21-1987; the entire shear is attributed to the transverse steel only. Hence, an additional set of four more piers (namely CSSG, RSSG, CHSG and RHSG) is designed for shear as per the shear design provisions outlined in IRC:21-1987. The monotonic lateral load-deformation response of all the *8* piers are ascertained. In addition, nominal shear capacities of the sections are computed as per IS:456-2000 by the procedures discussed in Sections 1.6 and 3.1; both concrete and transverse steel contribute to the shear strength of the section.

Next, the effect of pier slenderness on overall response is investigated. The set of four piers is designed for each of the three slenderness ratios, namely *2, 6*, and, *10*. The piers (namely CSWL-2, CSWL-6, CSWL-10, RSWL-2, RSWL-6, RSWL-10, CHWL-2, CHWL-6, CHWL-10, RHWL-2, RHWL-6 and RHWL-10) are designed for the same superstructure gravity load of *6500kN*, and a transverse load of *650kN* with nominal transverse reinforcement. In all piers, the cross-sectional area is kept at approximately *4.8m²*, giving a compression force of about $0.042 f_c' A_g$. Pushover analysis is performed for all the *12* piers to compare the lateral shear demand with the nominal shear capacity of the sections.

Then, the effect of level of axial load on the overall response of piers is investigated. For this, a *10m* diameter solid circular pier is designed for superstructure gravity load of *5050kN* and lateral load of *505kN*. The pier has 44Y28 longitudinal bars and circular hoop of diameter *8mm* at *300mm* centre-to-centre. The pier is then subjected

to axial compression loads of $0.05 f_c' A_g$, $0.10 f_c' A_g$ and $0.30 f_c' A_g$ and lateral pushover analysis performed (analysis cases CSWP-05, CSWP-10 and CSWP-30). The circular hoops in the pier are enhanced to *10mm* and *12mm* diameters at *130mm* centres, and the lateral load-deformation response of the three axial load levels are traced for these additional two transverse reinforcement types also.

Finally, the effect of additional radial links on the load-deformation behaviour of hollow circular piers is investigated. The hollow circular piers with no radial links in the first (CHWG) and second (CHWL-2) investigations are re-analysed with *19* and *28* radial links of *8mm* diameter HYSD steel bars, and the load-deformation responses are compared with the corresponding original ones.

The nomenclature used in designating the various piers in the above analyses is explained here. The first character (*i.e.*, 'C' or 'R') indicates piers of *circular* or *rectangular* cross-section. The second character (*i.e.*, 'S' or 'H') indicates *solid* or *hollow* sections. The third character (*i.e.*, 'W' or 'S') indicates piers *without* and *with* shear design. The fourth character (*i.e.*, 'G', 'L', or 'P') indicates type of investigation undertaken on the piers, namely effect of *geometry*, *slenderness* or *axial load*. The fifth set of numbers in the investigation on effect of slenderness (*i.e.*, '2', '6', '10') indicates slenderness of the piers, while that in the investigation on effect of axial load level (*i.e.*, '05', '10', '30') indicates the axial load ratio. In the investigation on effect of axial load, the last numeral (*i.e.*, '1', '2', or '3') indicates 1st, 2nd, and 3rd run for the pier with three different transverse reinforcement. In the investigation on effect of additional radial links, the last character (i.e., 'L') indicates presence of additional radial links. The character 'C' in the graphical representations of responses indicates *nominal shear capacity* of the pier.

In all numerical studies, concrete cover of *40mm* and concrete grade of *40MPa*

are used. Circular pier with helical reinforcement is not very common in Indian practice, and hence not considered in this study. When the resultant tension due to direct compression and bending exceeds permissible stress given in IRC:21-1987, cracked section analysis is carried out for the sections using an already available computer program deriving the P-M curve with permissible stresses given in IRC:21-1987. An increase in permissible stresses by *50%* (in seismic condition) is considered in the analyses as per recommendation of IRC:6-2000.

3.3 RESULTS AND OBSERVATIONS

Global lateral load-deformation responses of piers obtained are graphically represented in Figures 3.2 to 3.8. The nominal shear capacities of the sections are also shown with the shear demand. In addition, the volumetric ratio of transverse reinforcement provided and that required for the shear demand are listed in Tables 3.2, 3.4, and 3.6. The following observations are made from these investigations.

The investigation on effect of geometry showed that short piers (with slenderness ratio of about *2-3*) with solid sections perform better than the hollow ones with approximately same cross-sectional area. Hollow sections require larger section dimension and draws in more lateral force, thereby increasing the overstrength-based seismic shear demand, without any appreciable increase in deformability in piers with circular cross-section. In piers with rectangular cross-section, the pier with hollow cross-section shows increased deformability, apart from the expected increased shear demand (Figure 3.2). This is due to the IRC:21-1987 requirement that, in rectangular sections, every corner and alternate longitudinal bar be laterally supported by the corner of a tie, and that no longitudinal bar be farther than *150mm* from such a laterally supported bar. This introduces additional intermediate ties in both directions in the hollow rectangular sections, which enhance the effective confinement of concrete (compare volumetric ratio

of transverse reinforcement in Table 3.2) and increases the maximum strain in concrete. This also results in increased deformability of the hollow rectangular section compared to the solid rectangular section. On the other hand, piers with solid cross-sections with additional transverse shear reinforcement (through shear design) show more stable post-yield behaviour with enhanced deformability and displacement ductility (Figure 3.3).

The shear capacities of circular and rectangular sections, whether solid or hollow, with nominal transverse reinforcement as recommended by IRC:21-1987 are insufficient for the shear demands due to flexure for short piers (Tables 3.1 and 3.2). Premature shear failure of piers is predicted before they achieve the full flexural strength or lateral deformation. For piers of same height and cross-sectional area, and subjected to the same axial compression, the shear capacity of solid circular piers is least among the four types of piers discussed. This is attributed to the presence of only a single circular hoop in solid circular piers. In rectangular sections, additional intermediate ties in both the directions enhance the shear capacity. Thus, the ratio of transverse reinforcement required (to prevent shear failure) to that provided is maximum (*6.67*) in pier with solid circular section and least (*1.15*) in pier with hollow rectangular section (Table 3.2).

Also, in hollow sections, the additional requirement of minimum area of transverse steel equal to *0.3%* of the wall cross-section exceeds the nominal reinforcement requirement, and often, exceeds the transverse steel requirement from shear design as outlined in IRC:21-1987 (Table 3.1). Even this transverse steel of *0.3%* is however inadequate in short piers to cater for resisting the overstrength moment-based shear demand in short piers (Table 3.2).

In most piers where nominal transverse reinforcement is provided, buckling of longitudinal reinforcement occurred (Table 3.1), resulting in sudden loss of load carrying capacity. This is due to the large spacing of transverse reinforcement adopted along the

member length, which is the minimum of (a) *12* times the diameter of smallest longitudinal reinforcement bar, and (b) *300mm*, as per IRC:21-1987.

The investigation on effect of pier slenderness reveals that the nominal transverse reinforcement requirements are inadequate for short piers (slenderness ratio of *2*). On the other hand, for slender piers (slenderness ratio of *6* and *10*), the nominal shear capacity is higher than the demand (Tables 3.3 and 3.4). Thus, slender piers exhibit a ductile behaviour. In large hollow rectangular piers, better distribution of longitudinal steel and enhanced concrete confinement due to additional intermediate links cause very stable post-yield response, compared to other three types of sections considered in the study (Figure 3.4). In addition, in general, with increasing slenderness, the shear demand reduces and deformability increase (Figure 3.5). This is due to increased flexibility of piers with increased slenderness. Thus, the target deformability of a pier seems to be a function of its slenderness. However, as in the first study, failure is primarily initiated by buckling of longitudinal steel (Table 3.3).

The investigation on effect of axial load shows that with increase in axial load level, ductility reduces while the shear demand increases (Figure 3.6). With increase in axial load, tension yielding of steel is delayed increasing the yield displacement, while the ultimate displacement is reduced due to lesser residual flexural strain capacity of the fibres. This causes a reduction in ductility. In addition, with increase in axial load level, flexural cracking of concrete fibres is delayed, thereby increasing the net uncracked section area. This increases the section rigidity and thus draws in more lateral shear, thereby increasing the shear demand. In addition, with increase in amount of transverse reinforcement, the deformability increases (Figure 3.7). This is again due to increase in confinement of concrete and corresponding increase in ultimate strain capacity. These observations suggest that with increase in axial load level, for an expected drift capacity,

higher amount of transverse reinforcement is required to prevent shear failure (Tables 3.5 and 3.6).

The study on radial links reveals that providing additional radial links in hollow circular sections increase ductility of piers (Table 3.7, Figure 3.8). By providing nominal radial links of Y8 bars (increase of *25%* to *40%* in volumetric ratio of transverse reinforcement), the drift capacity increases by at least about *1%* even in short piers with slenderness ratio of *2*. This is because the additional links not only increase the amount of transverse reinforcement and affect the concrete confinement, but also cause transfer of tension from outer hoop to the inner hoop and thereby prevent compression failure of inner hoop. Moreover, links also prevent buckling of longitudinal steel and the inner hoop by reducing the unsupported lengths.

In addition, critical conditions in the form of (a) tension yielding, (b) and buckling of longitudinal reinforcement, (c) spalling of cover concrete, and (d) compression failure of core concrete, are traced along the lateral load-deformation response of the piers. For instance, in the solid circular pier CSWG, the first tension yielding of longitudinal reinforcement occurs at drift level of *0.52%* in the bottom *0.55D* length of the pier (last segment length considered in the analysis), where *D* is the section dimension. Subsequently, spalling of cover concrete and buckling of compression longitudinal reinforcement occur at drift of *1.16%* in the bottom *0.55D* length of the pier. Finally, spalling of cover concrete in the bottom *1.67D* length and compression failure of core concrete in the bottom *0.55D* length of the pier occur at drift of *1.30%*, leading to failure. Details of such critical conditions of pier CSWG and all other piers considered in this study are given in Table 3.8.

3.5 IMPLICATIONS OF RESULTS FROM ANALYTICAL STUDIES ON IRC PROVISIONS

The results of the investigations reported in Section 3.4 provide significant insight into the effectiveness of IRC provisions to prevent brittle shear failure. The implications of these results are important in light of the large stock of bridge piers that are to be built as part of the ongoing National Highway Development Project in India. These are:

a) IRC Code prescribed shear capacities are lower than the corresponding shear demand due to flexure for short piers; in general, nominal transverse reinforcement requirements prescribed in IRC Code need to be enhanced up to *6* times the current Code values.

b) Increasing the amount of transverse reinforcement increases displacement ductility of piers, and produces improved post-yield response; transverse reinforcement requirement in IRC Code can be made a function of the required displacement ductility of piers.

c) Buckling of longitudinal reinforcement occurs resulting in rapid strength loss and subsequent failure of piers; maximum limit on the spacing of transverse reinforcement prescribed in IRC Code is grossly inadequate in preventing buckling of longitudinal steel and subsequent failure of piers under strong seismic shaking.

d) Piers under higher axial compression require more transverse reinforcement for expected displacement ductility; transverse reinforcement requirement in IRC code can be made a function of the probable maximum axial load on the pier and the required displacement ductility.

e) Providing additional radial links in hollow circular piers increases displacement ductility; new specification for use of radial links needs to be urgently incorporated in the IRC Code.

•••

Chapter 4

Summary and Conclusion

4.0 GENERAL

Piers are critical components of earthquake-resistant bridges; these are the only locations where inelasticity can be allowed to dissipate the seismic energy input into RC bridges during strong earthquake shaking. During past earthquakes, damages or collapses of bridges have also occurred due to failure of these substructures. The failures include flexural-shear failure, axial compression failure, or brittle bond failure. Also, apart from the conventional solid sections, bridge piers are now often made hollow to reduce the seismic mass amongst other reasons. Indian bridge design provisions have not kept abreast with the state of the art. Hence, a detailed investigation is warranted into the strength design and lateral load-deformation relation of piers of different cross-sections.

4.1 SUMMARY

A review of the existing IRC provisions for bridge pier design reveals that the formation of plastic hinge is not ensured through design; brittle shear failures can occur in Indian bridges. Confinement of concrete for a stable post-yield response and buckling of longitudinal steel are also not considered in the design process. An analytical study is carried out to trace the response of piers designed as per the current IRC seismic design specifications.

A displacement-based monotonic pushover analysis algorithm is developed for investigating monotonic lateral load-deformation relationships of single column piers bending in single curvature. A fibre model is used to capture the progression of plasticity both along and across large pier sections. An effective shear stiffness is considered,

which accounts for both flexural translational and shear translational deformations depending upon the overall slenderness of the pier and the level of flexural cracking induced in it. An existing concrete confinement model of the monotonic stress-strain curve, applicable to both hollow and solid as well as circular and rectangular sections is used. Appropriate hysteretic uniaxial constitutive relations for concrete and steel are developed to incorporate unloading and reloading in fibres during redistribution of stresses in the sections. An analytical model for buckling of longitudinal steel is also included in the algorithm.

Using a computer program developed based on the algorithm, lateral displacement-based pushover analyses of a number of code-designed bridge piers are carried out. Nominal shear capacities are computed and compared to the overstrength flexural shear demands. The exercise is repeated for piers of different sections and over a practical range of slenderness. Also, the possible influence of axial load is investigated on a solid circular pier. The role of additional radial links on lateral load-deformation relation of hollow circular piers is also investigated.

4.2 CONCLUSIONS

The salient conclusions drawn from the study described in this thesis are:

a) Capacity Design based shear design of piers is required to ensure a ductile response of bridge piers.

b) Transverse reinforcement requirements in IRC:21-1987 need to be enhanced to ensure ductile response of RC piers.

c) The maximum spacing requirement of transverse reinforcement needs to be made more stringent to prevent buckling of longitudinal reinforcement and subsequent failure or piers.

d) Radial links are vital for realising ductile performance of hollow circular RC piers.

4.3 POSSIBLE FUTURE WORK

In this study, the analyses included effect of shear deformation in large pier sections in the computation of flexural shear demand and drift capacity. The nominal shear capacity was considered to remain constant throughout the load-deformation curve, and was calculated separately. This was used to predict the failure mode of the code-designed piers. However, the actual available shear capacity of concrete depends on the existing normal stress on it, *i.e.*, the shear capacity at a section depends on position of the pier on the overall load-deformation curve. Thus, neglecting axial load-moment-shear interaction may lead to unconservative estimate of the overall response of large bridge piers. A comprehensive investigation needs to be taken up to predict the actual load-deformation relation of large bridge piers with due consideration to axial load–moment–shear interaction. This will help in refining the actual response estimate and identifying the location of hinging/failure, particularly in non-prismatic piers that are commonly used in India nowadays.

The requirements of transverse reinforcement for different cases of slenderness, axial load levels, expected ductility levels, etc., predicted by such analytical means can be substantiated through experimentation, and design specifications may be prepared.

•••

References

AASHTO 1998, (1998), AASHTO LRFD Bridge Design Specifications, Second Edition, SI Edition, American Association of State Highway and Transportation Officials, Washington, D.C., USA

ACI 318-77, (1978), Building Code Requirements for Reinforced Concrete, ACI Committee 318, American Concrete Institute, Detroit.

ACI 318-89, (1992), Building Code Requirements for Reinforced Concrete and Commentary (Revised 1992), ACI Committee 318, American Concrete Institute, Detroit.

ACI 318-95, (1995), Building Code Requirements for Structural Concrete and Commentary, ACI Committee 318, American Concrete Institute, Farmington Hills, Michigan.

ASCE-ACI Joint Task Committee 426, (1973), "The Shear Strength of Reinforced Concrete Members," Journal of the Structural Division, ASCE, Vol. 99, No. ST6, pp 1091-1187.

Ang, B.G., Priestley, M.J.N., and Paulay, T., (1989), "Seismic Shear Strength of Circular Reinforced Concrete Columns," ACI Structural Journal, Vol.86, No.1, pp 45-59.

Azizinamini, A., and Kuska, S., (1994), "Seismic Behaviour of High-Strength Concrete Columns," Proceedings of the 5th US National Conference on Eathquake Engineering, Chicago, USA.

Bahn, B.Y., and Hsu, Cheng-Tzu T., (1998), "Stress-Strain Behaviour of Concrete under Cyclic Loading," ACI Materials Journal, Vol. 95, No. 2, pp 178-193.

Balan, T.A., Filippou, F.C., and Popov, E.P., (1998), "Hysteretic model of ordinary and high-strength steel," Journal of Structural Engineering, ASCE, Vol.124, No.3, pp 288-297.

CALTRANS 1995, (1995), Memo to Designers 20-4 Attachment B, California Department of Transportation, Sacramento, USA.

CALTRANS 1999, (1999), Seismic Design Criteria, Version 1.1, California Department of Transportation, Sacramento, USA.

Dasgupta, P, (2000), "Effect of Confinement on Strength and Ductility of Large RC Hollow Sections," Master of Technology Thesis, Department of Civil Engineering, Indian Institute of Technology Kanpur, India.

Davey, B.E., (1975), "Reinforced Concrete Bridge Piers Under Seismic Loading," Master of Engineering Report, Civil Engineering Department, University of Canterbury, Christchurch, New Zealand.

Dodd, L.L., and Cooke, N., (2000), "Capacity of Circular Bridge Columns Subjected to Base Excitation, " ACI Structural Journal, Vol.97, No.2, pp 297-307.

Ghali, A., and Neville, A.M., (1997), Structural Analysis: A unified classical and matrix approach, E and FN Spon, London.

IRC:6-2000, (2000), Standard Specifications and Code of Practice for Road Bridges, Section: II, Loads and Stresses, The Indian Road Congress, New Delhi.

IRC:21-1987, (1987), Standard Specifications and Code of Practice for Road Bridges, Section: III, Cement Concrete (Plain and Reinforced), The Indian Road Congress, New Delhi.

IRC:78-1983, (1983), Standard Specifications and Code of Practice for Road Bridges, Section: VII, Foundations and Substructure, The Indian Road Congress, New Delhi.

IS:456-2000, (2000), Code of Practice for Plain and Reinforced Concrete, Bureau of Indian Standards, New Delhi.

IS:1893-1984, (1984), Criteria for Earthquake Resistant Design of Structures, Indian Standards Institution, New Delhi.

Kent, D.C., and Park, R., (1971), "Flexural Members with Confined Concrete," Journal of Structural Engineering, ASCE, Vol. 97, No. 7, pp 1969-1990.

Kunnath, S.K., El-Bahy, A., Taylor, A., and Stone, W., (1997), "Cumulative Seismic Damage of Reinforced Concrete Bridge Piers," Technical Report NCEER-97-0006, National Centre for Earthquake Engineering Research, Buffalo.

Maiti, M.K., and Goyal, A., (1996), "Nonlinear Seismic Response of Reinforced Concrete Stack-like Structures," Bulletin of the Indian Society of Earthquake Technology, Vol. 33, No. 2, pp 195-213.

Mander, J.B., Priestley, M.J.N., and Park,R., (1988a), "Theoretical Stress-Strain Model for Confined Concrete," Journal of Structural Engineering, ASCE, Vol.114, No.8, pp 1804-1826.

Mander, J.B., Priestley, M.J.N., and Park,R., (1988b), "Observed Stress-Strain Behaviour of Confined Concrete," Journal of Structural Engineering, ASCE, Vol.114, No.8, pp 1827-1849.

Masukawa, J., Suda, K., and Maekawa, K., (2000), "Predicting Post-Peak Behaviour of High Bridge Pier with Hollow Section Using a New Model for Spalling of Cover Concrete and Buckling of Reinforcement," Proceedings of the 12th World Conference on Earthquake Engineering, Auckland, New Zealand, Paper No.1869.

Mau, S.T., (1990), "Effect of Tie Spacing on Inelastic Buckling of Reinforcing Bars," ACI Structural Journal, Vol.87, No.6, pp 671-677.

Munro, I.R.M., Priestley, M.J.N., and Park, R., (1976), "Seismic Behaviour of Reinforced Concrete Bridge Piers," Report No. 76-7, Department Civil Engineering, University of Canterbury, Christchurch, New Zealand.

Murty, C.V.R., and Hall, J.F., (1994), "Earthquake Collapse Analysis of Steel Frames," Earthquake Engineering and Structural Dynamics, Vol. 23, No. 11, pp 1199-1218.

NZ 3101: 1978, (1978), Draft Code of Practice for the Design of Concrete Structures, Standards Associations of New Zealand, Wellington.

NZS 3101: 1995, (1995), Concrete Structure Standard, Standards New Zealand, Wellington.

Park, R., Kent, D.C., and Sampson, R.A., (1972), "Reinforced Concrete Members with Cyclic Loading," Journal of the Structural Diviion, Proceedings of the American Society of Civil Engineers, Vol. 98, No. ST7, pp 1341-1359.

Park, R., and Paulay, T., (1975), Reinforced Concrete Structures, John Wiley and Sons, Inc., New York.

Park, R., Priestley, M.J.N., and Gill, W.D., (1982), "Dcutility of Square-Confined Concrete Columns," Journal of the Structural Division, ASCE, Vol. 108, No. ST4, pp 929-950.

Paulay, T., and Priestley, M.J.N., (1992), Seismic Design of Reinforced Concrete and Masonry Buildings, John Wiley and Sons, Inc., New York.

Popovics, S., (1973), "A Numerical Approach to the Complete Stress-Strain Curve of Concrete," Cement and Concrete Research, Vol. 3, pp 583-599.

Priestley, M.J.N., and Benzoni, G., (1996), "Seismic Performance of Circular Columns with Low Longitudinal Reinforcement Ratios," ACI Structural Journal, Vol.93, No.4, pp 474-485.

Priestley, M.J.N., Verma, R., and Xiao, Y., (1994), "Seismic Shear Strength of Reinforced Concrete Columns," Journal of Structural Engineering, ASCE, Vol. 120, No. 8, pp 2310-2329.

Priestley, M.J.N., Seible, F., and Calvi, G.M., (1996), Seismic Design and Retrofit of Bridges, John Wiley and Sons, Inc., New York.

PWRI 9810, (1998), Design Specifications of Highway Bridges, Part V-Seismic Design, Earthquake Engineering Division, Earthquake Disaster Prevention Research Centre, Public Works Research Institute, Japan.

Razvi,S.R., and Saatcioglu,M., (1999a), "Confinement Model for High-Strength Concrete," Journal of Structural Engineering, ASCE, Vol.125, No.3, pp 281-289.

Razvi,R.S., and Saatcioglu,M., (1999b), "Analysis and Design of Concrete Columns for Confinement," Earthquake Spectra, EERI, Vol.15, No.4, pp 791-811.

Saatcioglu,M., and Razvi,S.R., (1992), "Strength and Ductility of Confined Concrete," Journal of Structural Engineering, ASCE, Vol.118, No.6, pp 1590-1607.

Saiidi, M.S., Wehbe, N.I., Sanders, D.H., and Caywood, C.J., (2001), "Shear Retrofit of Flared RC Bridge Columns Subjected to Earthquakes," Journal of Bridge Engineering, Vol. 6, No. 3, pp 189-197.

Santathadaporn, S., and Chen, W.F., (1972), "Tangent Stiffness Method for Biaxial Bending," Journal of the Structural Division, ASCE, Vol. 98, No ST1, pp 153-163.

Shah, S.P., Fafitis, A., and Arnold, R., (1983), "Cyclic Loading of Spirally Reinforced Concrete," Journal of Structural Engineering, ASCE, Vol. 109, No. 7, pp 1695-1710.

Sheikh,S.A., and Uzumeri,S.M., (1982), "Analytical Model for Concrete Confinement in Tied Columns," Journal of Structural Engineering, ASCE, Vol.108, No.12, pp 2703-2722.

Sheikh,S.A., and Yeh,C.C., ((1992), "Analytical Moment Curvature Relations for Tied Concrete Columns," Journal of Structural Engineering, ASCE, Vol. 118, No.2, pp 529-544.

Sinha, B.P., Gerstle, K.H., and Tulin, L.G., (1967), "Stress-Strain Relations for Concrete under Cyclic Loading," Journal of the American Concrete Institute, February 1967, pp 195-211.

Suda,K., Masukawa,J., and Maekawa,K., (2000), "Models for Concrete Cover Spalling and Reinforcement Buckling of Reinforced Concrete," Proceedings of the 12th World Conference on Earthquake Engineering, New Zealand, Paper No.1437.

Warner, R.F., (1969), "Biaxial Moment Thrust Curvature Relations," Journal of the Structural Divison, ASCE, Vol. 95, No. ST5, pp 923-940.

Wehbe, N., Saiidi, M., Sanders, D., and Douglas, B., (1996), "Ductility of Rectangular Reinforced Concrete Bridge Columns with Moderate Confinement," Technical Report NCEER-96-0003, National Centre for Earthquake Engineering Research, Buffalo.

William, K.J., and Warnke, E.P., (1975), "Constitutive Model for the Triaxial Behaviour of Concrete," Proceedings, International Association for Bridge and Structural Engineering, Vol. 19, pp 1-30.

Wong, Y.L., Paulay, T., and Priestley, M.J.N., (1993), "Response of Circular Reinforced Concrete Columns to Multi-Directional Seismic Attack," ACI Structural Journal, Vol. 90, No. 2, pp 180-191.

Yeh, Y.K., Mo, Y.L., and Yang, C.Y., (2001), "Seismic Performance of Hollow Circular Bridge Piers," ACI Structural Journal, Vol. 98, No. 6, pp 862-87.

Zahn,F.A., Park,R., and Priestley,M.J.N., (1990), "Flexural Strength and Ductility of Circular Hollow Reinforced Concrete Columns without Confinement on Inside Face," ACI Structural Journal, Vol.87, No.2, pp 156-166.

•••

Table 2.1: Properties of specimens analytically studied for validation of developed program.

Specimen	L	f_c'	Longitudinal Reinforcement			Transverse Reinforcement		
			Diameter	f_y	f_{su}	Diameter	f_y	Spacing
	(m)	(MPa)	(mm)	(MPa)	(MPa)	(mm)	(MPa)	(mm)
A1	2.355	27.2	19	465.0	684.4	6,8.24,10	448.9	110
PI2-C	3.5	30.9	22	418.2	626.5	10	410.0	200

Table 2.2: Comparison of response quantities from analyses with experimental values.

Specimen	Maximum Force			Ultimate Displacement		
	Experimental	Analytical	Error	Experimental	Analytical	Error
	(kN)	(kN)	(%)	(kN)	(kN)	(%)
A1	362.5	310.8	-14.2	122.0	110	-10.0
PI2-C	2356.4	2488.6	+5.6	102.6	100	-2.5

Table 3.1: Results of analyses of four types of piers comparing shear capacity and demand, and showing final form of failure.

Pier ($L=5m$)	Section (m)	Area (m^2)	Long. Reinf.	Trans. Reinf.	Shear Capacity (kN)	Shear Demand (kN)	Failure Mode
CSWG	1.80 ϕ	2.54	54Y22	Y8@260	1379	2471	Buckling of long. steel
CSSG	1.80 ϕ	2.54	54Y22	Y12@110	2197	2494	---
RSWG	2.5×1.0	2.50	46Y25	Y8@300	1823	4236	Buckling of long. steel
RSSG	2.5×1.0	2.50	46Y25	Y10@200	2607	4283	---
CHWG	2.4(OD), 1.7(ID)	2.25	57Y22	Y10@140	2464	3834	Buckling of long. steel
CHSG	2.4(OD), 1.7(ID)	2.25	57Y22	Y10@140	2464	3834	Buckling of long. steel
RHWG	1.2×3.0(OD), 0.5×2.3(ID)	2.45	100Y16	Y10@140	3726	5057	Buckling of long. steel
RHSG	1.2×3.0(OD), 0.5×2.3(ID)	2.45	100Y16	Y10@140	3726	5057	Buckling of long. steel

Table 3.2: Transverse reinforcement requirement to prevent shear failure in piers of four types of cross-section in investigation on effect of geometry.

Pier	Shear Capacity (kN)	Shear Demand (kN)	Transverse Reinforcement Provided ρ_s^p	Transverse Reinforcement Required ρ_s^r	Ratio ρ_s^r/ρ_s^p
CSWG	1379	2471	4.47×10^{-4}	3.04×10^{-3}	6.67
CSSG	2197	2494	2.39×10^{-3}	3.12×10^{-3}	1.30
RSWG	1823	4236	1.42×10^{-3}	5.24×10^{-3}	3.70
RSSG	2607	4283	3.33×10^{-3}	6.17×10^{-3}	1.85
CHWG	2464	3834	4.16×10^{-3}	9.30×10^{-3}	2.22
CHSG	2464	3834	4.16×10^{-3}	9.30×10^{-3}	2.22
RHWG	3726	5057	7.68×10^{-3}	8.79×10^{-3}	1.15
RHSG	3726	5057	7.68×10^{-3}	8.79×10^{-3}	1.15

Table 3.3: Results of analyses of four types of piers of three slenderness ratio comparing shear capacity with demand, and showing final form of failure.

Pier Name	L (m)	Section (m)	Area (m^2)	Long. Reinf.	Trans. Reinf.	Shear Capacity (kN)	Shear Demand (kN)	Failure Mode
CSWL-2	5.0	2.50 ϕ	4.91	66Y28	Y8@300	2333	6093	Buckling of long. steel
CSWL-6	15.0	2.50ϕ	4.91	66Y28	Y8@300	2333	1786	Buckling of long. steel
CSWL-10	25.0	2.50ϕ	4.91	84Y36	Y8@300	3118	1686	Buckling of long. steel
RSWL-2	6.0	3.0×1.6	4.80	64Y28	Y8@300	3114	6789	Buckling of long. steel
RSWL-6	18.0	3.0×1.6	4.80	64Y28	Y8@300	3114	1997	Buckling of long. steel
RSWL-10	30.0	3.0×1.6	4.80	64Y32	Y8@300	3357	1290	Buckling of long. steel
CHWL-2	7.0	3.5(OD), 2.5(ID)	4.71	84Y25	Y10@100	4554	6726	Comp. of concrete
CHWL-6	21.0	3.5(OD), 2.5(ID)	4.71	84Y25	Y10@100	4554	1980	Comp. of concrete
CHWL-10	35.0	3.5(OD), 2.5(ID)	4.71	90Y28	Y10@100	5021	1303	----
RHWL-2	8.0	2.8×4.0(OD), 2.0×3.2(ID)	4.80	156Y20	Y10@130	6419	8648	----
RHWL-6	24.0	2.8×4.0(OD), 2.0×3.2(ID)	4.80	156Y20	Y10@130	6419	2579	----
RHWL-10	40.0	2.8×4.0(OD), 2.0×3.2(ID)	4.80	156Y20	Y10@130	6419	1398	----

Table 3.4: Transverse reinforcement requirement to prevent shear failure in piers in investigation on effect of slenderness.

Pier	Shear Capacity (kN)	Shear Demand (kN)	Transverse Reinforcement Provided ρ_s^p	Transverse Reinforcement Required ρ_s^r	Ratio ρ_s^r/ρ_s^p
CSWL-2	2333	6093	2.77×10^{-4}	5.16×10^{-3}	18.61
CSWL-6	2333	1786	2.77×10^{-4}	2.77×10^{-4}	1.00
CSWL-10	3118	1686	2.77×10^{-4}	2.77×10^{-4}	1.00
RSWL-2	3114	6789	1.35×10^{-3}	3.85×10^{-3}	2.85
RSWL-6	3114	1997	1.35×10^{-3}	1.35×10^{-3}	1.00
RSWL-10	3357	1290	1.35×10^{-3}	1.35×10^{-3}	1.00
CHWL-2	4554	6726	3.74×10^{-3}	7.98×10^{-3}	2.13
CHWL-6	4554	1980	3.74×10^{-3}	3.74×10^{-3}	1.00
CHWL-10	5021	1303	3.74×10^{-3}	3.74×10^{-3}	1.00
RHWL-2	6419	8648	6.04×10^{-3}	8.00×10^{-3}	1.32
RHWL-6	6419	2579	6.04×10^{-3}	6.04×10^{-3}	1.00
RHWL-10	6419	1398	6.04×10^{-3}	6.04×10^{-3}	1.00

Table 3.5: Results of analyses of solid circular pier with three axial load ratio and three different circular hoops with percentage lateral drift.

Pier (L=10.0m)	Section (m)	Area (m^2)	Long. Reinf.	Trans. Reinf.	Shear Capacity (kN)	Shear Demand (kN)	Axial Load Ratio	Drift (%)
CSWP-05-1	2.0 ϕ	3.14	44Y28	Y8 @300	1590	1464	0.05	1.85
CSWP-10-1	2.0 ϕ	3.14	44Y28	Y8 @300	1590	1661	0.10	1.50
CSWP-30-1	2.0 ϕ	3.14	44Y28	Y8 @300	1590	2122	0.30	0.90
CSSP-05-2	2.0 ϕ	3.14	44Y28	Y10@130	2055	1472	0.05	2.25
CSSP-10-2	2.0 ϕ	3.14	44Y28	Y10@130	2055	1674	0.10	2.00
CSSP-30-2	2.0 ϕ	3.14	44Y28	Y10@130	2055	2159	0.30	0.95
CSSP-05-3	2.0 ϕ	3.14	44Y28	Y12@130	2343	1474	0.05	2.70
CSSP-10-3	2.0 ϕ	3.14	44Y28	Y12@130	2343	1676	0.10	2.15
CSSP-30-3	2.0 ϕ	3.14	44Y28	Y12@130	2343	2172	0.30	1.15

Table 3.6: Transverse reinforcement requirement to prevent shear failure in piers in investigation on effect of axial load.

Pier	Shear Capacity (kN)	Shear Demand (kN)	Transverse Reinforcement Provided ρ_s^p	Transverse Reinforcement Required ρ_s^r	Ratio ρ_s^r/ρ_s^p
CSWP-05-1	1590	1464	3.49×10^{-4}	3.49×10^{-4}	1.00
CSWP-10-1	1590	1661	3.49×10^{-4}	7.44×10^{-4}	2.13
CSWP-30-1	1590	2122	3.49×10^{-4}	1.68×10^{-3}	4.82

Table 3.7: Results of analyses of hollow circular piers with and without radial links, comparing percentage lateral drift.

Pier	L (m)	Section (m) OD	ID	Area (m²)	Longitudinal Reinforcement	Transverse Reinforcement	Ratio ρ_s^2/ρ_s^1	Drift (%)
CHWG	5.0	2.4	1.7	2.25	57Y22	Y10@140 $(\rho_s^1 = 4.16 \times 10^{-3})$	---	1.34
CHWG-L	5.0	2.4	1.7	2.25	57Y22	Y10@140 + 19 Y8 Radial Links $(\rho_s^2 = 5.22 \times 10^{-3})$	1.25	2.24
CHWL-2	7.0	3.5	2.5	4.71	84Y25	Y10@100 $(\rho_s^1 = 3.74 \times 10^{-3})$	---	1.86
CHWL-2-L	7.0	3.5	2.5	4.71	84Y25	Y10@100 + 28 Y8 Radial Links $(\rho_s^2 = 5.23 \times 10^{-3})$	1.40	3.43

Table 3.8: Details of critical conditions along lateral load-deformation relations of piers.

Pier	Critical Conditions				
	Yielding of longitudinal reinforcement in outmost layer(s) on tension side (% Drift and Location)	Spalling of cover concrete on compression side (% Drift and Location)	Compression failure of core concrete on compression side (% Drift and Location)	Buckling of longitudinal reinforcement in outmost layer on compression side (% Drift and Location)	Compression failure of core concrete on compression side (% Drift and Location)
Effect of Geometry					
CSWG	0.52%; 0.55D	1.16%; 0.55D 1.30%; 1.67D		1.16%; 0.55D	1.30%; 0.55D
CSSG	0.52%; 0.55D	1.16%; 0.55D	---	---	---
RSWG	0.40%; 0.50D	1.06%; 0.50D 1.28%; 1.50D		1.08%; 0.50D	1.28%; 0.50D
RSSG	0.40%; 0.50D	1.12%; 0.50D	---	---	---
CHWG/ CHSG	0.40%; 0.52D	1.30%; 0.52D	1.40%; 0.52D	1.50%; 0.52D	
RHWG/ RHSG	0.40%; 0.42D	0.32%; 0.42D	1.12%; 0.42D	1.80%; 0.42D	

Table 3.8: contd...

Pier	Critical Conditions				
	Yielding of longitudinal reinforcement in outmost layer(s) on tension side (% Drift and Location)	Spalling of cover concrete on compression side (% Drift and Location)	Compression failure of core concrete on compression side (% Drift and Location)	Buckling of longitudinal reinforcement in outmost layer on compression side (% Drift and Location)	Compression failure of core concrete on compression side (% Drift and Location)
Effect of Slenderness					
CSWL-2	0.40%; 0.5D	1.12%; 0.5D		1.16%; 0.5D	1.20%; 0.5D
CSWL-6	0.93%; 0.5D 1.20%; 1.0D 1.93%; 1.5D	2.07%; 0.5D		2.13%; 0.5D	2.20%; 0.5D
CSWL-10	1.68%; 0.5D 1.92%; 1.0D 2.24%; 1.5D	2.88%; 0.5D	2.96%; 0.5D	3.12%; 0.5D	
RSWL-2	0.37%; 0.5D	1.43%; 0.5D	·	1.47%; 0.5D	1.67%; 0.5D
RSWL-6	0.92%; 0.5D 1.17%; 1.0D 1.75%; 1.5D	2.50%; 0.5D	·	2.50%; 0.5D	2.75%; 0.5D
RSWL-10	1.47%; 0.5D 1.67%; 1.0D 2.00%; 1.5D 2.40%; 2.0D 3.20%; 2.5D	3.47%; 0.5D		3.93%; 0.5D	4.10%; 0.5D
CHWL-2	0.43%; 0.5D	1.50%; 0.5D	1.71%; 0.5D	---	
CHWL-6	0.95%; 0.5D 1.19%; 1.0D 1.79%; 1.5D	2.62%; 0.5D	2.86%; 0.5D	---	
CHWL-10	1.49%; 0.5D 1.66%; 1.0D 1.94%; 1.5D 2.40%; 2.0D 3.07%; 2.5D	3.71%; 0.5D	3.86%; 0.5D	---	
RHWL-2	0.38%; 0.5D	2.44%; 0.5D	---	---	---
RHWL-6	0.83%; 0.5D 1.08%; 1.0D 1.67%; 1.5D	3.75%; 0.5D	---	---	---
RHWL-10	1.38%; 0.5D 1.56%; 1.0D 1.81%; 1.5D 2.24%; 2.0D 3.06%; 2.5D 5.04%; 3.0D	5.24%; 0.5D	---	---	---

Table 3.8: contd...

Pier	Critical Conditions				
	Yielding of longitudinal reinforcement in outmost layer(s) on tension side (% Drift and Location)	Spalling of cover concrete on compression side (% Drift and Location)	Compression failure of core concrete on compression side (% Drift and Location)	Buckling of longitudinal reinforcement in outmost layer on compression side (% Drift and Location)	Compression failure of core concrete on compression side (% Drift and Location)
Effect of Axial Load					
CSWP-05-1	0.80%; 0.5D 1.15%; 1.0D	1.75%; 0.5D		1.80%; 0.5D	1.85%; 0.5D
CSWP-05-2	0.80%; 0.5D 1.15%; 1.0D	1.80%; 0.5D	---	---	---
CSWP-05-3	0.80%; 0.5D 1.15%; 1.0D	1.80%; 0.5D	---	---	---
CSSP-10-1	0.80%; 0.5D 1.35%; 1.0D	1.45%; 0.5D		1.45%; 0.5D	1.50%; 0.5D
CSSP-10-2	0.80%; 0.5D 1.30%; 1.0D	1.45%; 0.5D	---	---	---
CSSP-10-3	0.80%; 0.5D 1.30%; 1.0D	1.50%; 0.5D	---	---	---
CSSP-30-1	0.90%; 0.5D	0.90%; 0.5D	---	---	---
CSSP-30-2	0.95%; 0.5D	0.95%; 0.5D	---	---	---
CSSP-30-3	0.95%; 0.5D	0.95%; 0.5D	---	---	---
Effect of Radial Links					
CHWG	0.40%; 0.52D	1.30%; 0.52D	1.40%; 0.52D	1.50%; 0.52D	
CHWG-L	0.40%; 0.52D	1.30%; 0.52D	2.10%; 0.52D	2.30%; 0.52D	
CHWL-2	0.43%; 0.5D	1.50%; 0.5D	1.71%; 0.5D	---	
CHWL-2-L	0.43%; 0.5D	1.57%; 0.5D	3.00%; 0.5D	---	

•••
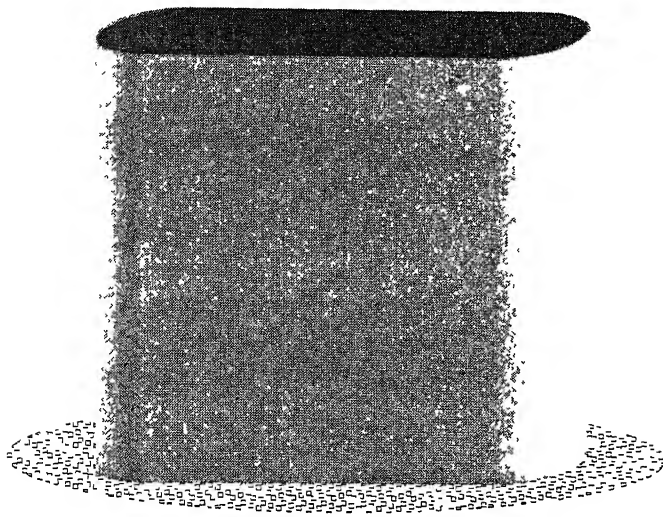
(a) Wall Type
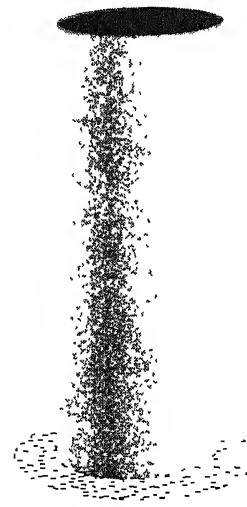
(b) Single Column Type

(c) Multiple-column Frame Type
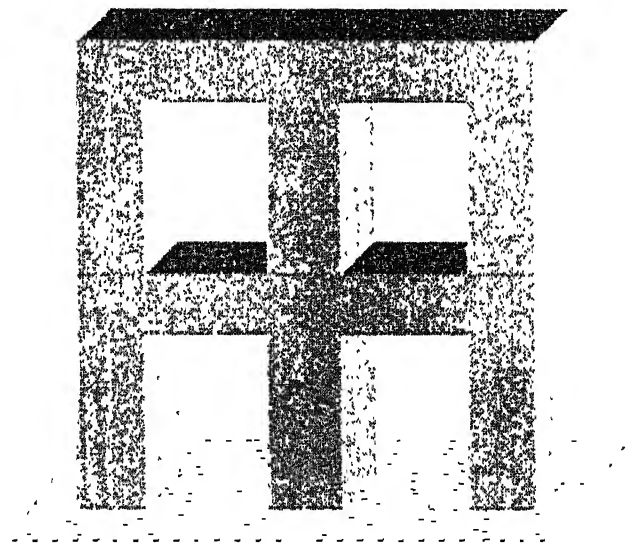
(d) Linked-column Frame Type

Figure 1.1: Different types of RC bridge piers.
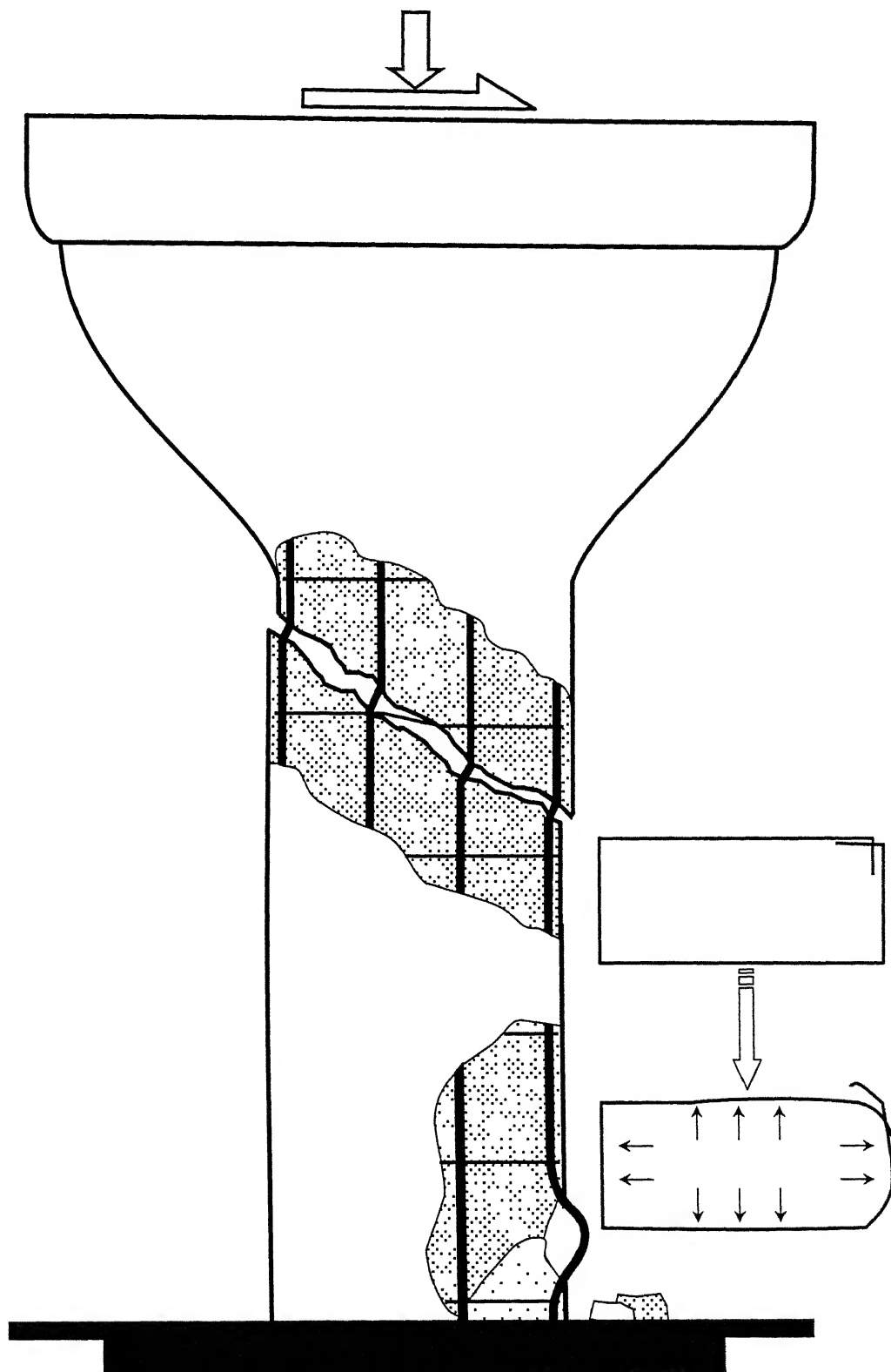
Figure 1.2: Single column type bridge pier with possible structural damages under strong seismic shaking.
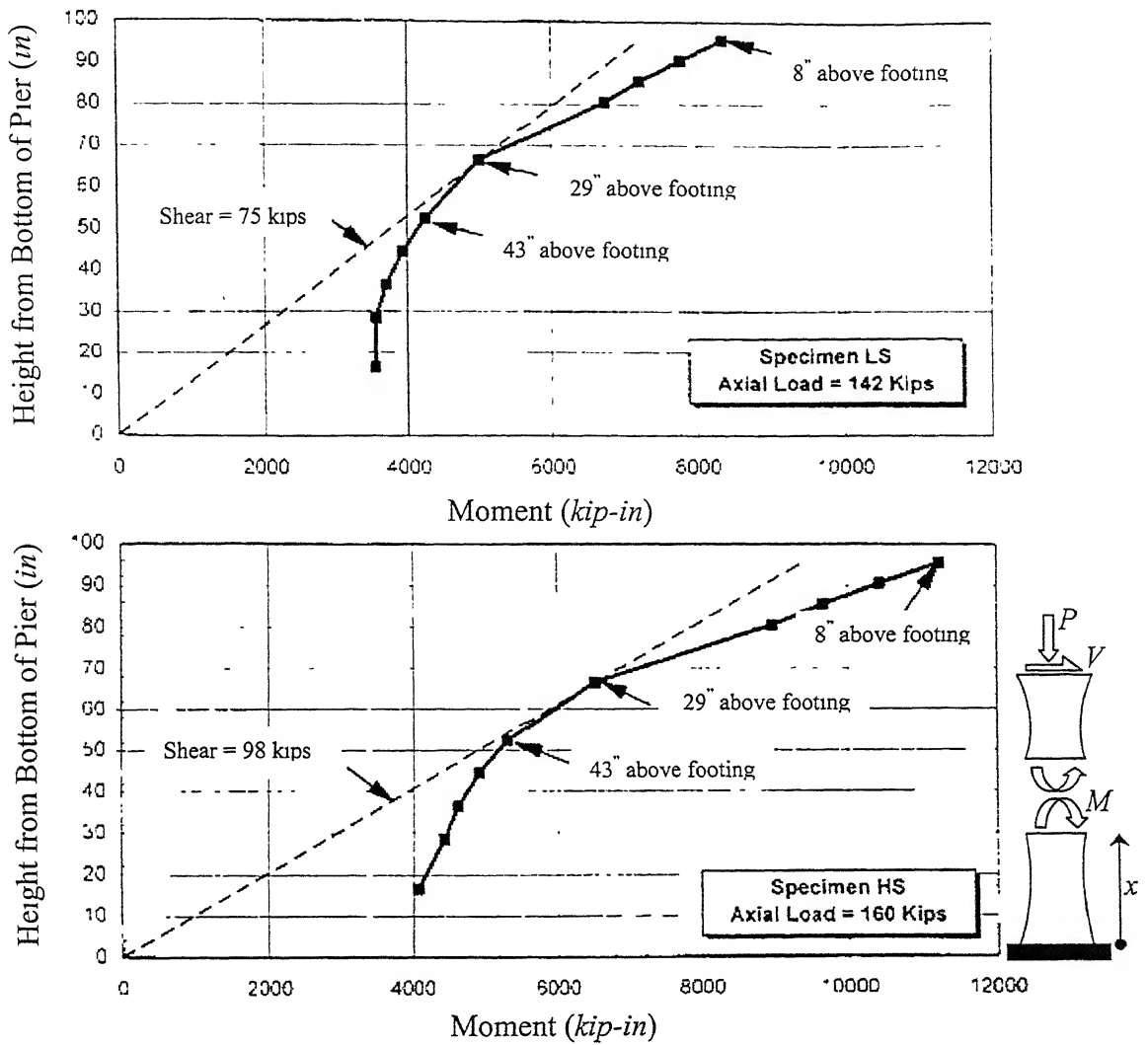
Figure 1.3: Identification of critical shear in a flared pier [Saiidi *et al.*, 2001].
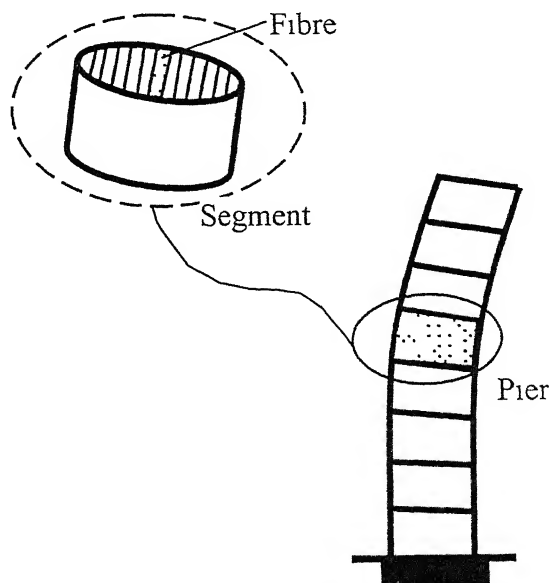
Figure 1.4: Discretisation of a pier into segments and segments into fibres in the Fibre Model.
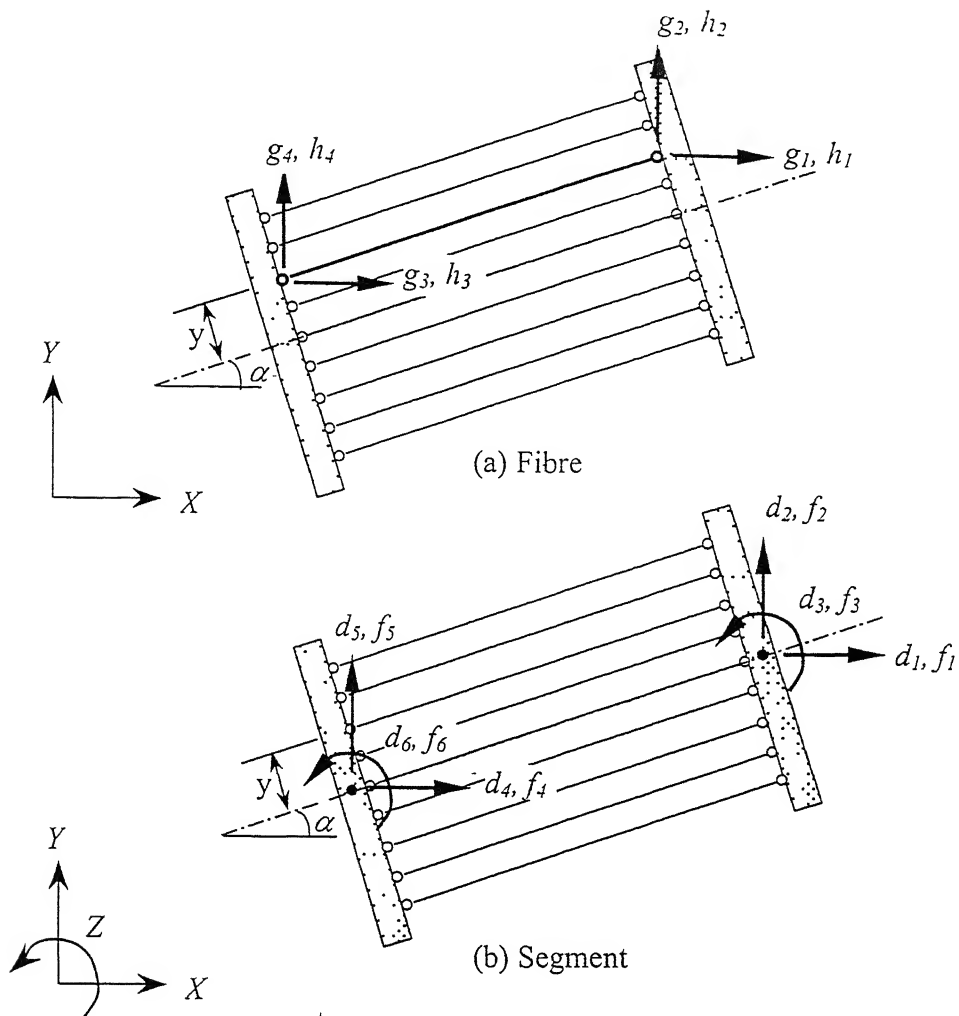
Figure 1.5: Global degrees of freedom and end-forces on (a) a fibre, and (b) a segment used in the Fibre Model
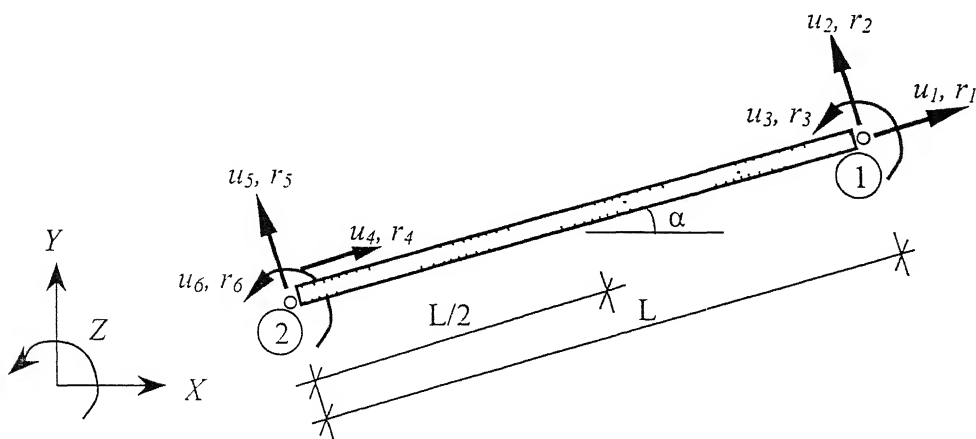
Figure 1.6: Local degrees of freedom and end-forces on a segment used in the Fibre Model.
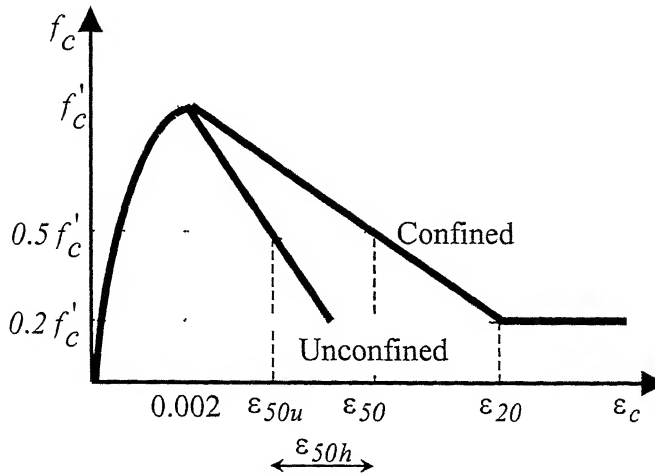
Figure 1.7: Kent and Park model for confined concrete stress-strain curve [Kent and Park, 1971].
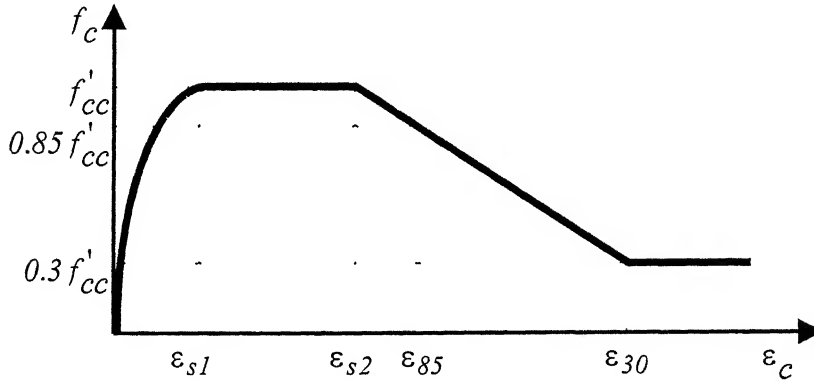
Figure 1.8: Sheikh and Uzumari model for confined concrete stress-strain curve [Sheikh and Uzumari, 1982].
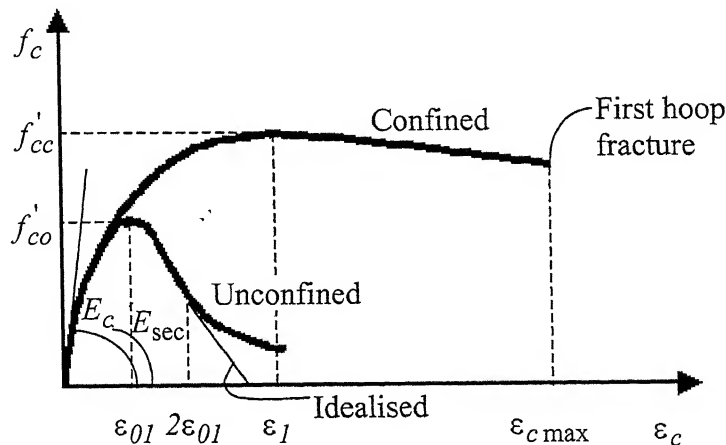
Figure 1.9: Mander model for confined concrete stress-strain curve [Mander *et al.*, 1988].
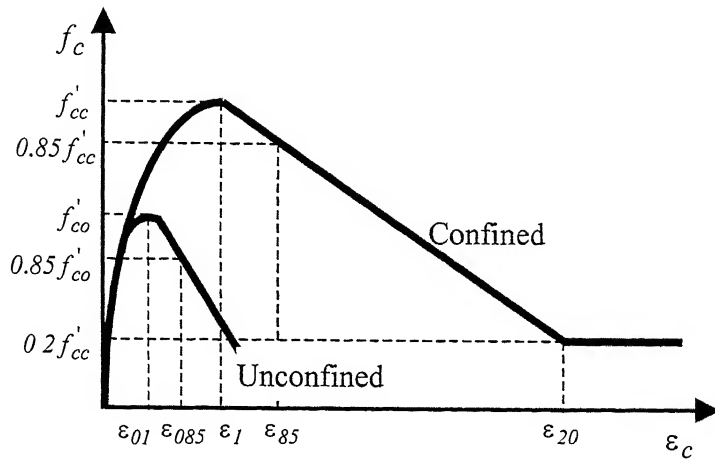
Figure 1.10: Saatcioglu and Razvi model for confined concrete stress-strain curve [Saatcioglu and Razvi, 1992].
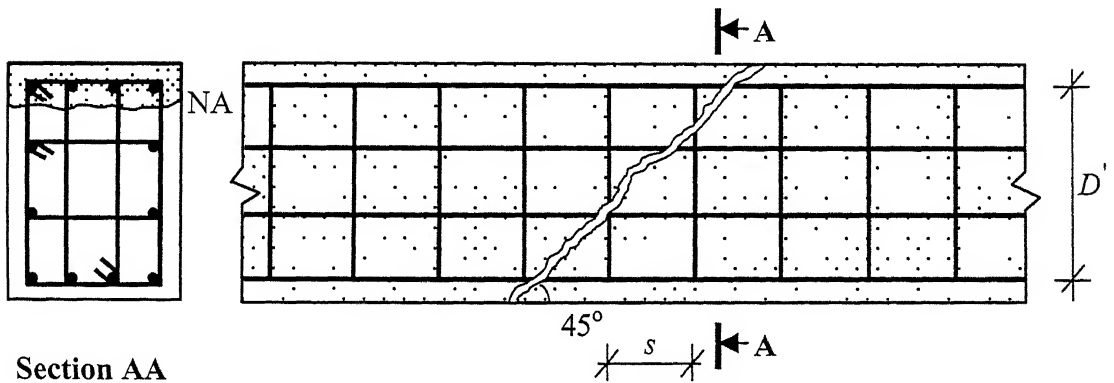
(a) Solid rectangular section
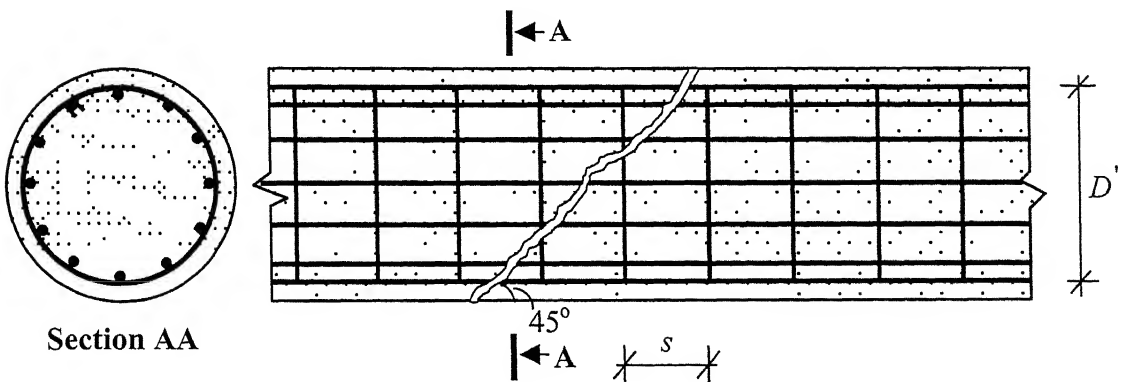
(b) Solid circular section

Figure 1.11: Definition of D' for strength provided by transverse steel V_{us} in (a) solid rectangular section, (b) solid circular section.
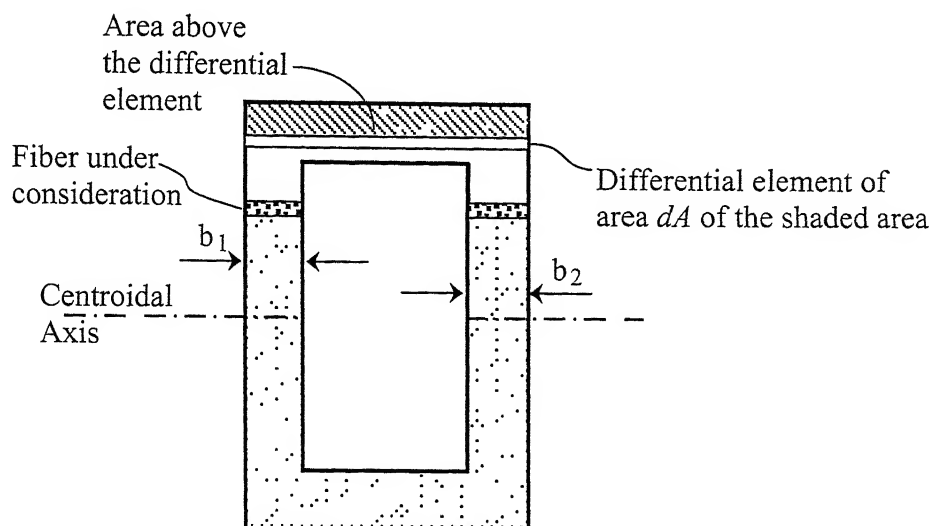
I = Second moment of the whole cross-section area about the axis of bending

Q = First moment of the area above the fiber under consideration about the axis of bending

b = Breadth of cross-section at the level of fibre under consideration

$= b_1 + b_2$

Figure 2.1: Quantities involved in calculation of shear area.
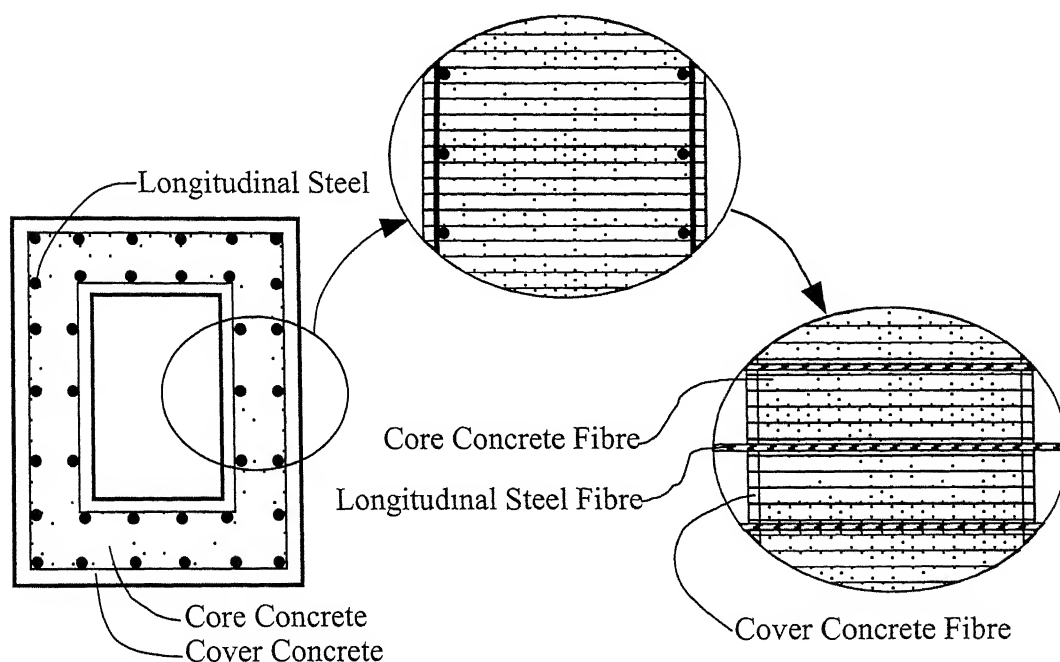
Figure 2.2: Discretisation of RC section into concrete (core and cover) and longitudinal steel fibres.
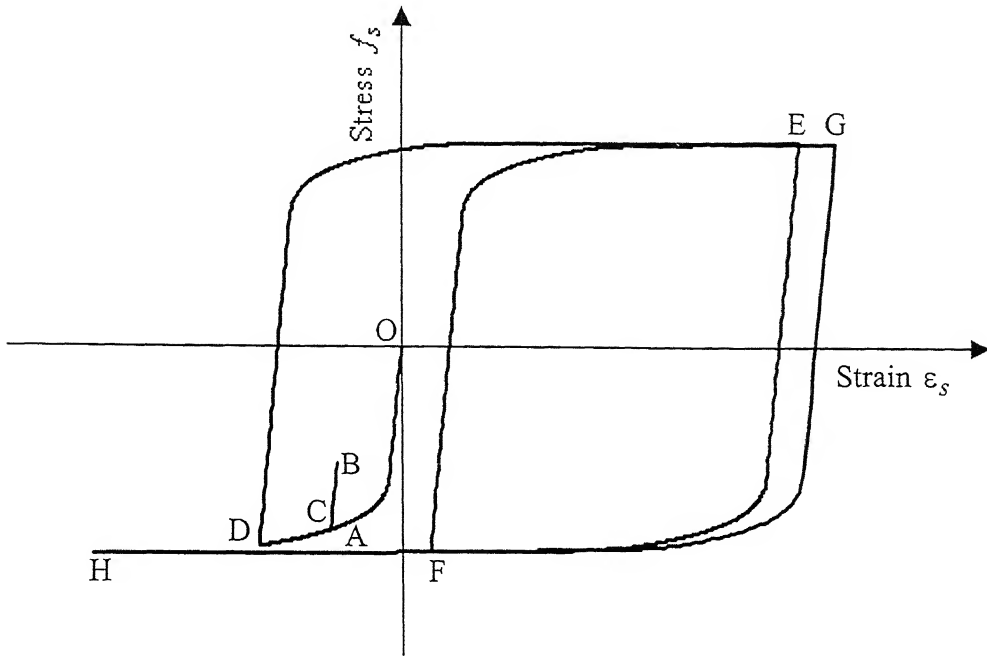
Figure 2.3: Proposed cyclic steel stress-strain curve model for HYSD bars showing possible strain path starting at O.
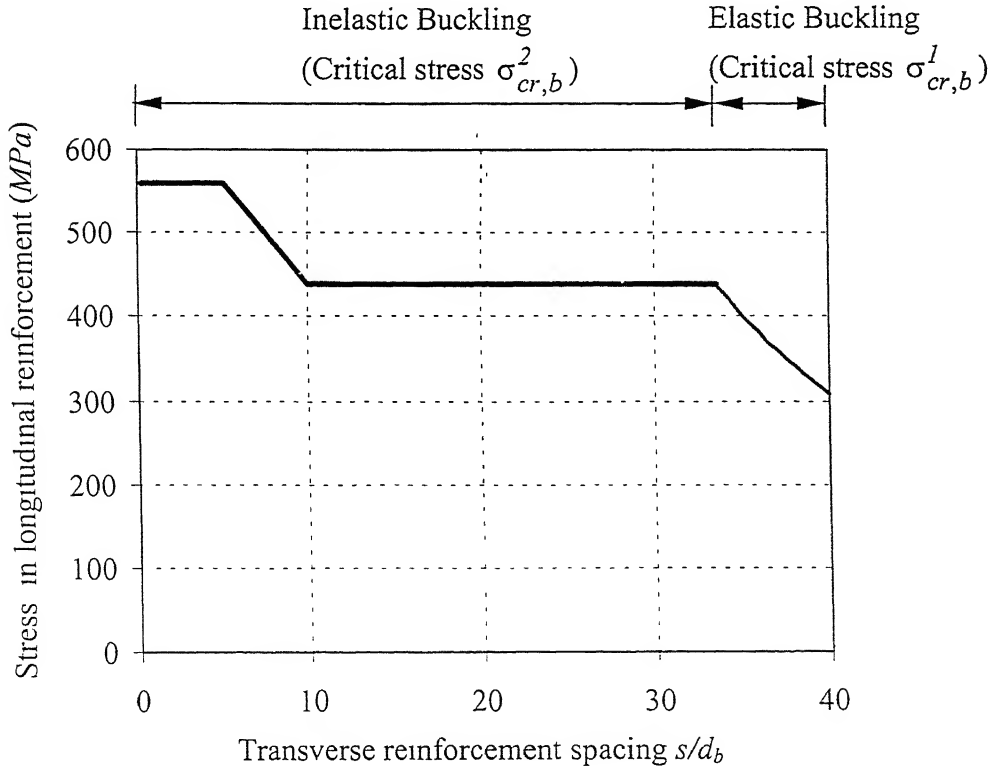
Figure 2.4: Critical buckling stress for longitudinal reinforcement.
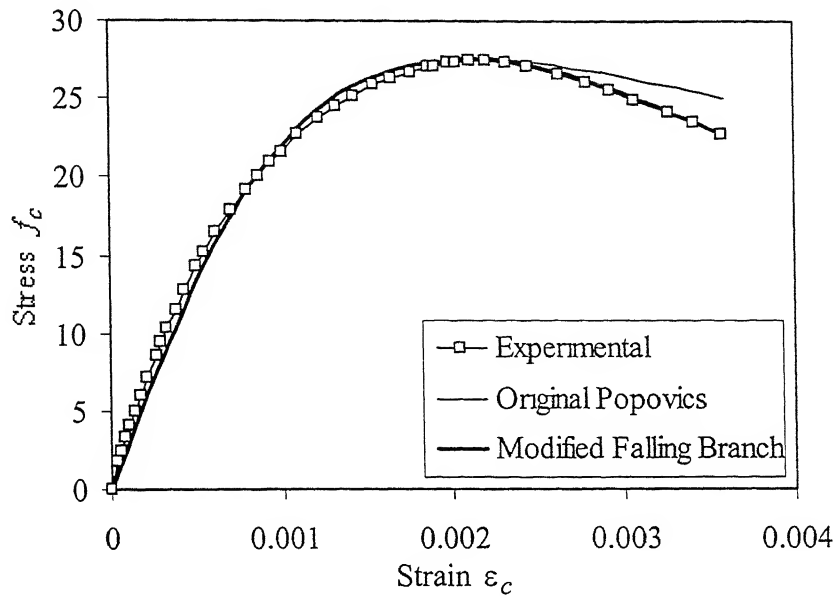
Figure 2.5: Comparison of experimental concrete stress-strain curve [Kunnath *et al.*, 1997] using Popovics' equation with modification for falling branch.
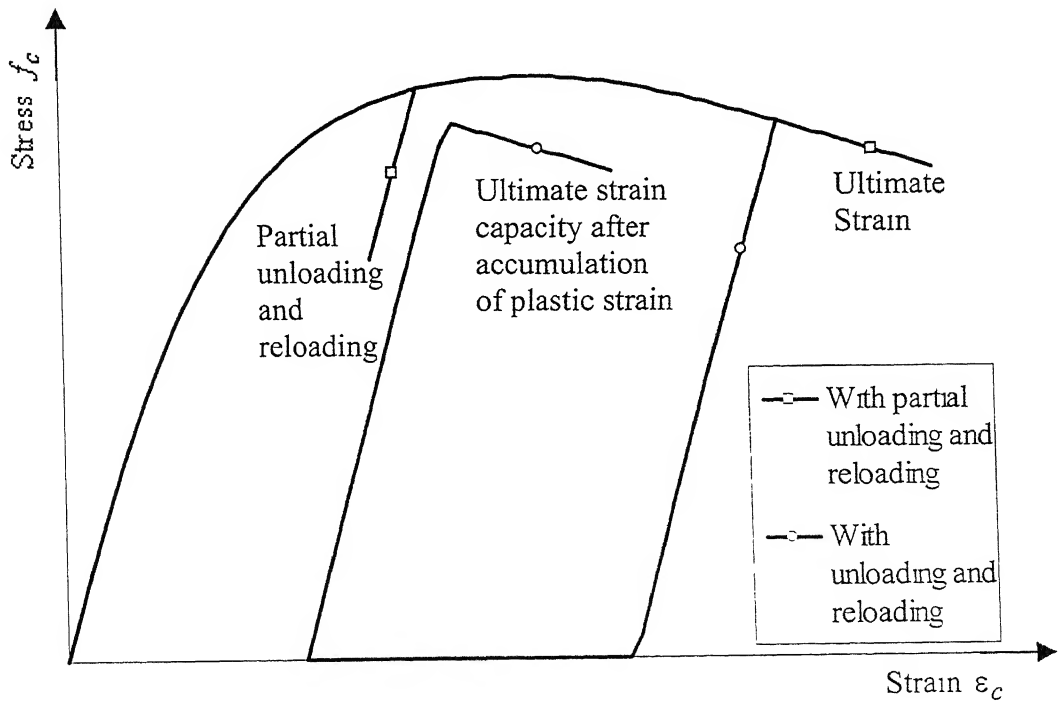
Figure 2.6: Proposed cyclic stress-strain model for concrete in compression.
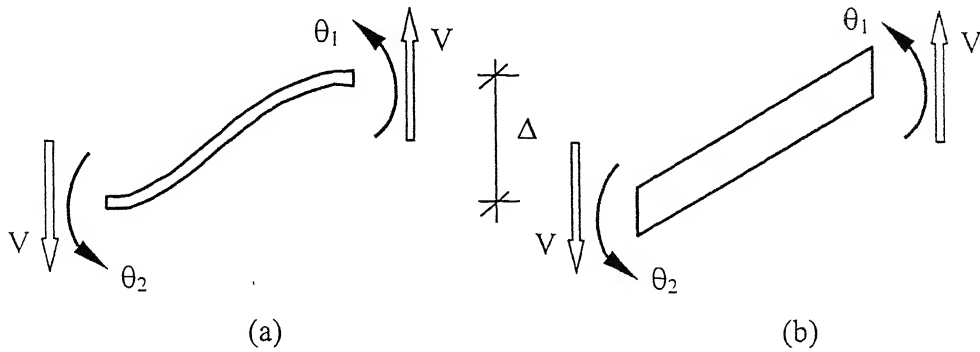
Figure 2.7: Pure lateral translational deformation in (a) flexure, and (b) shear.
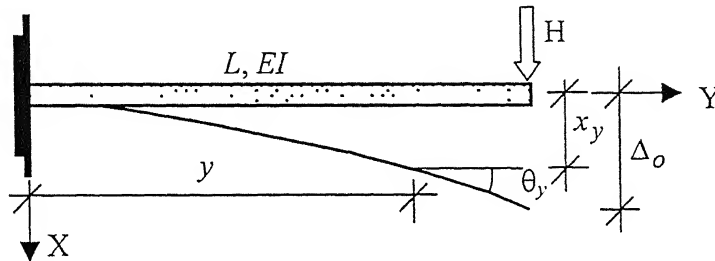
Figure 2.8: Initial lateral and rotational deformation of cantilever pier section for specified tip displacement.

Deformed Profile at the end of displacement step r, $^r\{x\}$

Target Deformation Profile for displacement step $(r+1)$,

$$^{r+1}\{x\} = \left(\frac{\Delta_{r+1}}{\Delta_r}\right)^r\{x\}$$
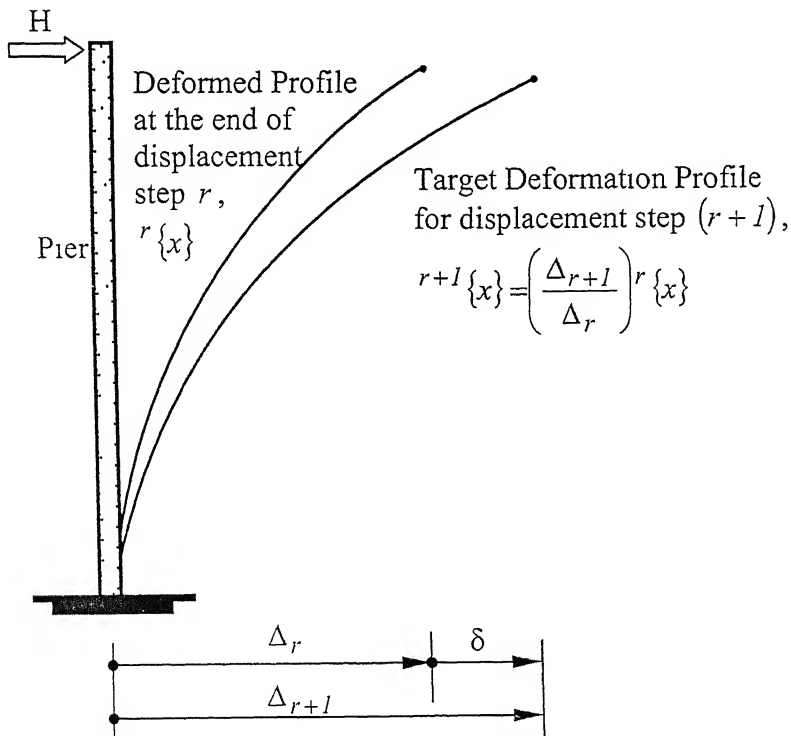
Figure 2.9: Target displacement profile of pier for next displacement step in pushover analysis

GCA : Gross cross-section centroidal axis   — · — · — · —
NA : Neutral axis   ————————
ECA : Effective centroidal axis   — — — — — — —
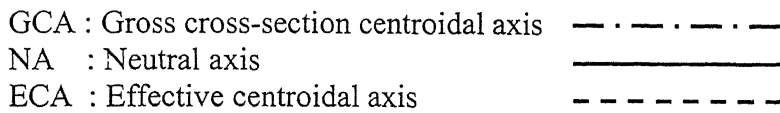
Figure 2.10: Effective centroidal axis in cracked section.
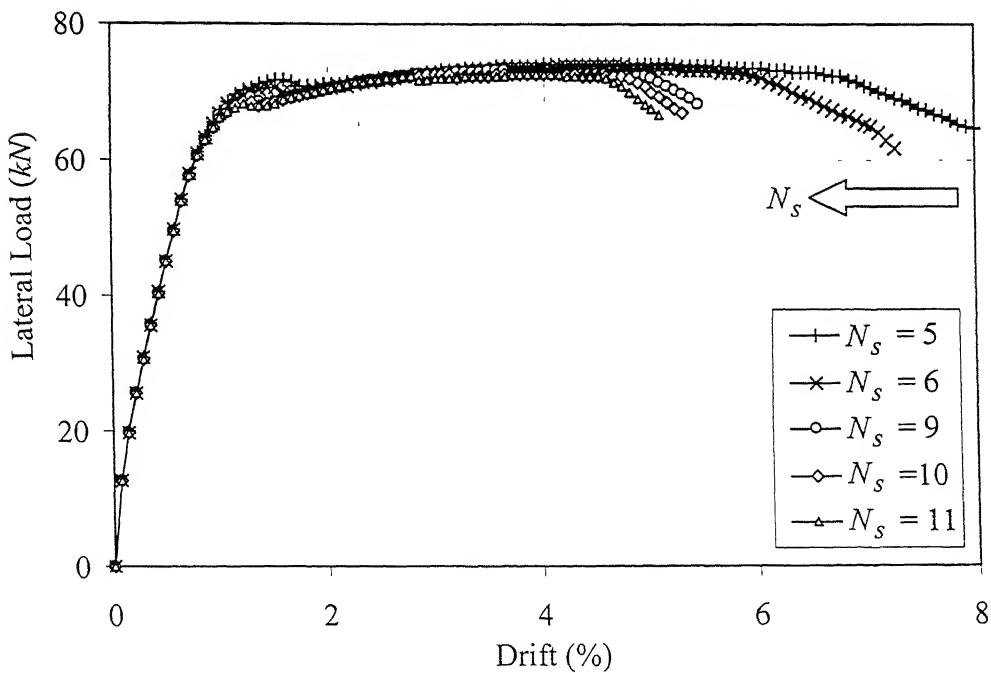
Figure 2.11: Effect of discretisation on the lateral load demand and drift capacity of a *305mm* diameter *1375mm* long specimen column.

Side View

Front View
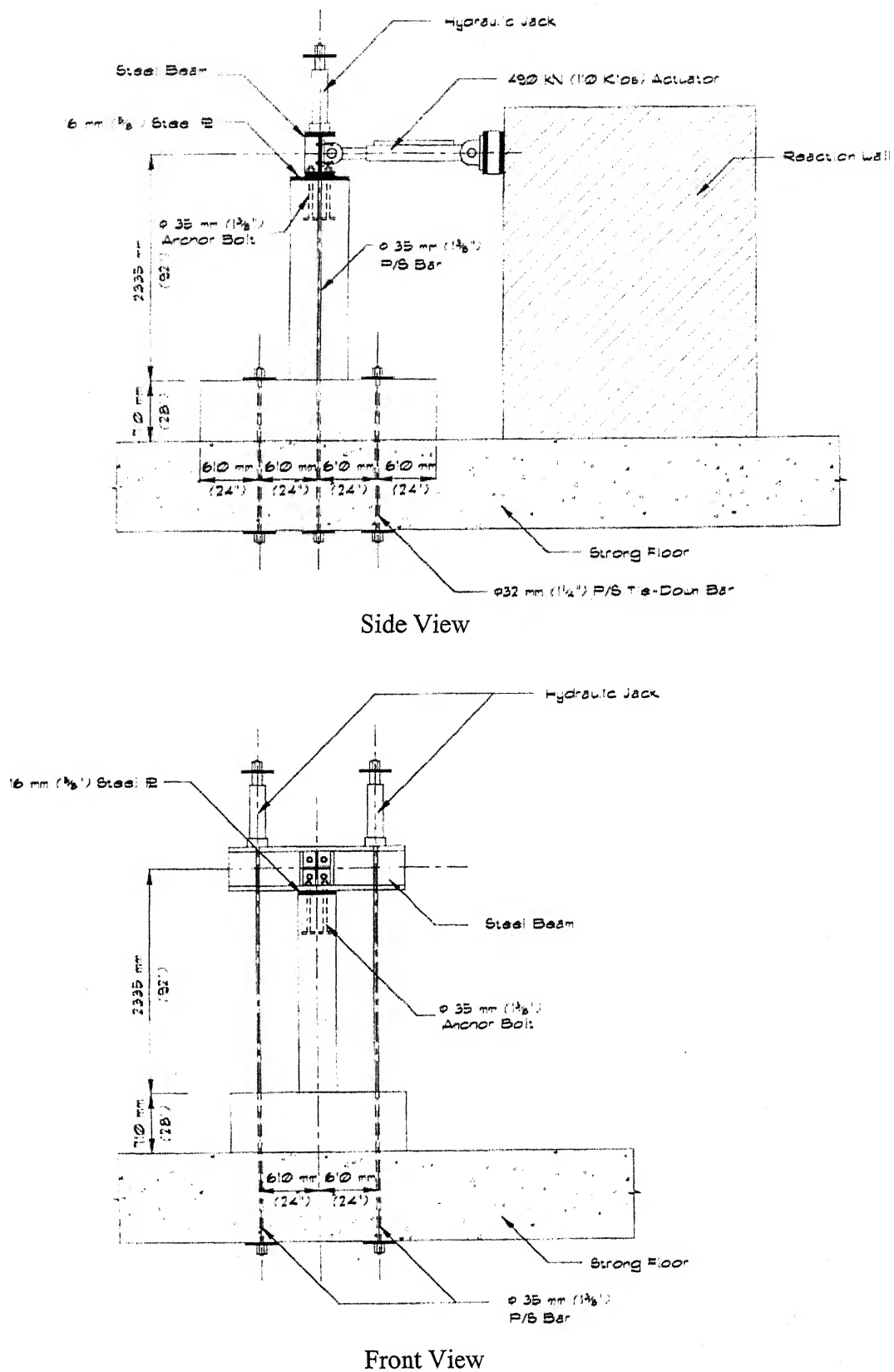
Figure 2.12: Experimental setup for specimen A1 [Wehbe *et al.*, 1996].
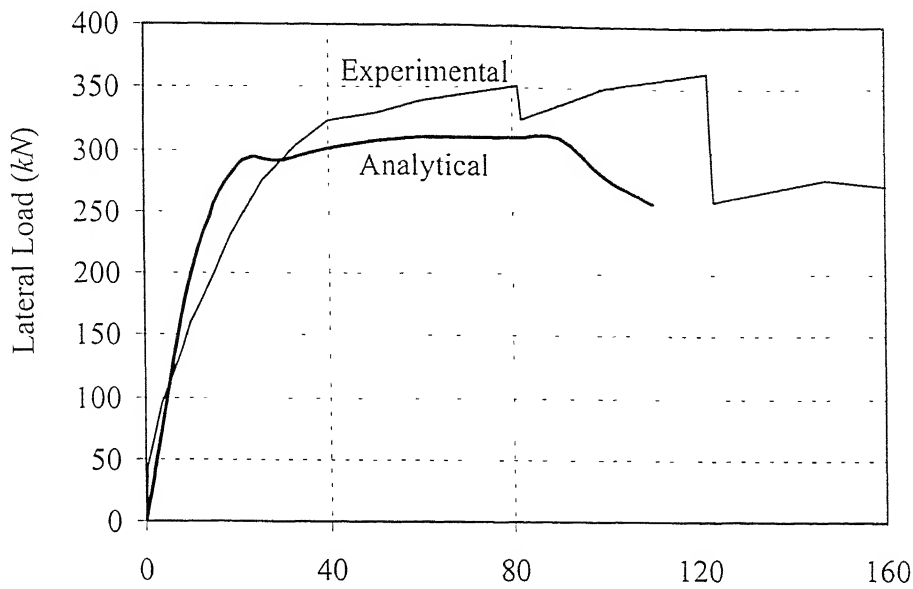
Figure 2.13: Comparison of experimental and analytical lateral load-deformation relation of a solid rectangular column [Wehbe *et al.*, 1996].
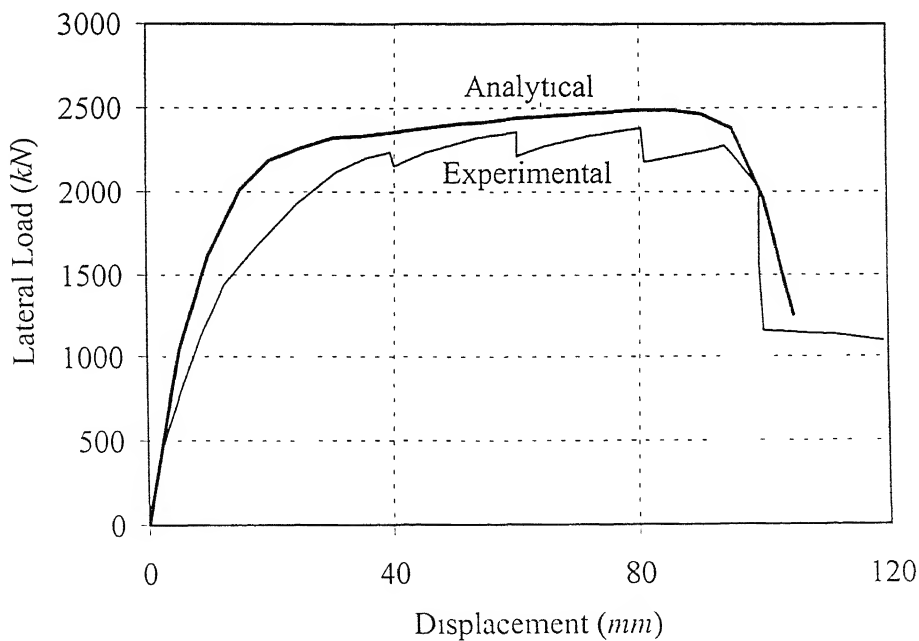
Figure 2.14: Comparison of experimental and analytical lateral load-deformation relation of a hollow circular pier [Yeh *et al.*, 2001]

Section AA

(a) Hollow rectangular section

Section AA

(b) Hollow circular section
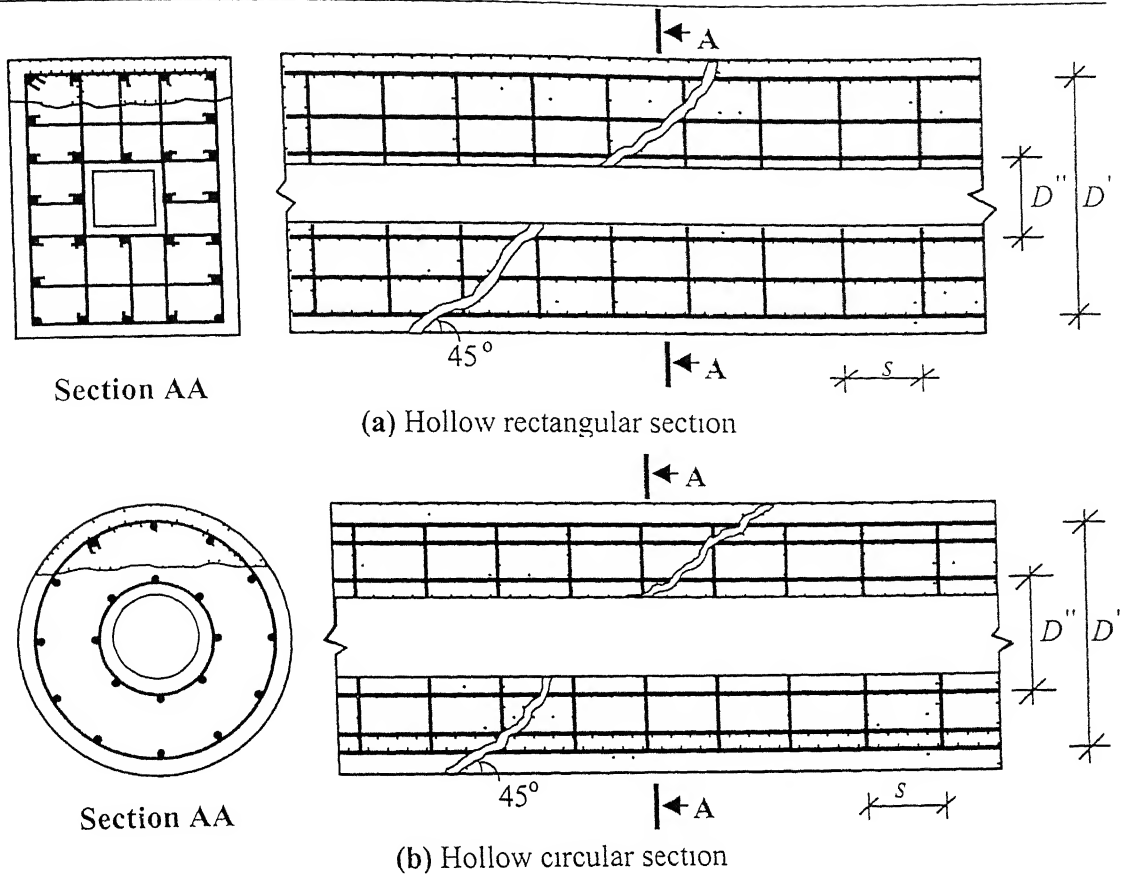
Figure 3.1: Definition of D' and D'' for strength provided by transverse steel V_{us} in (a) hollow rectangular section, (b) hollow circular section
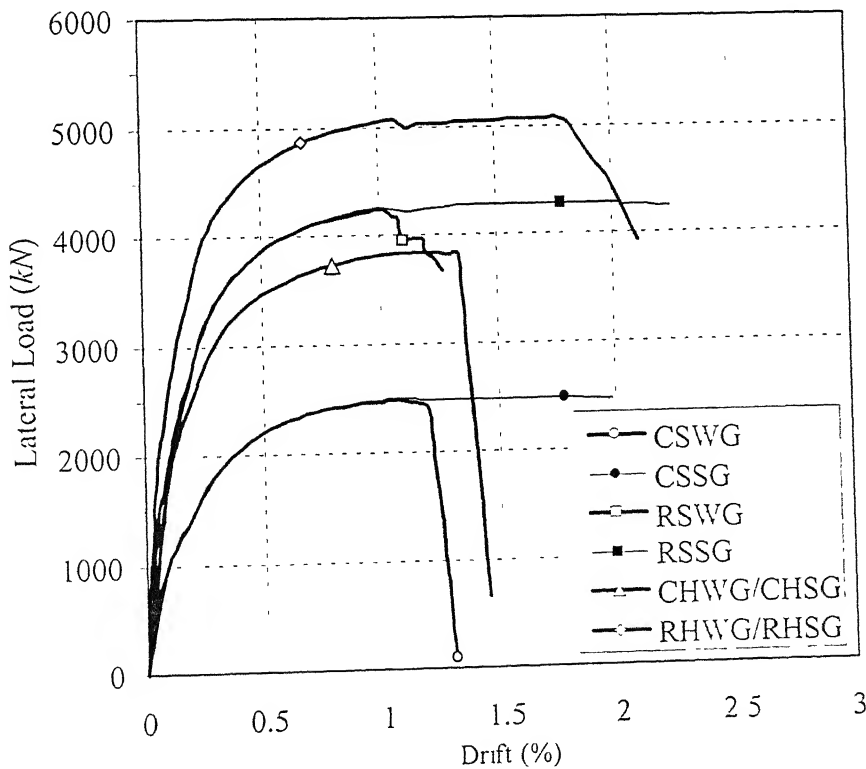
Figure 3.2: Lateral load-deformation relations of *5m* tall piers in investigation on effect of cross-section geometry.
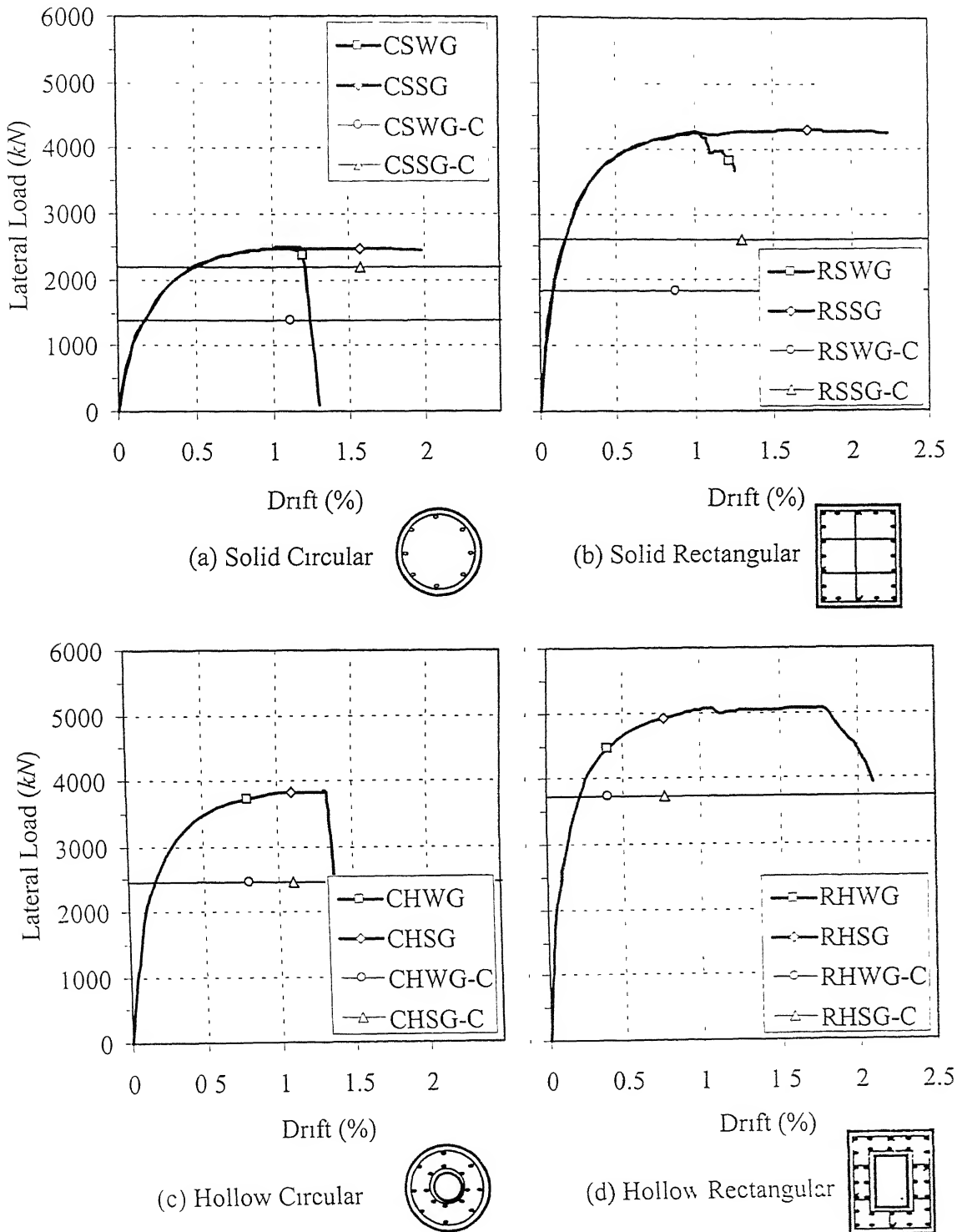
Figure 3.3: Lateral load-deformation relations of *5m* tall piers with corresponding nominal shear capacity levels in investigation of effect of section geometry
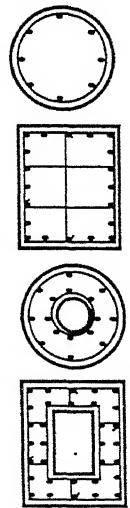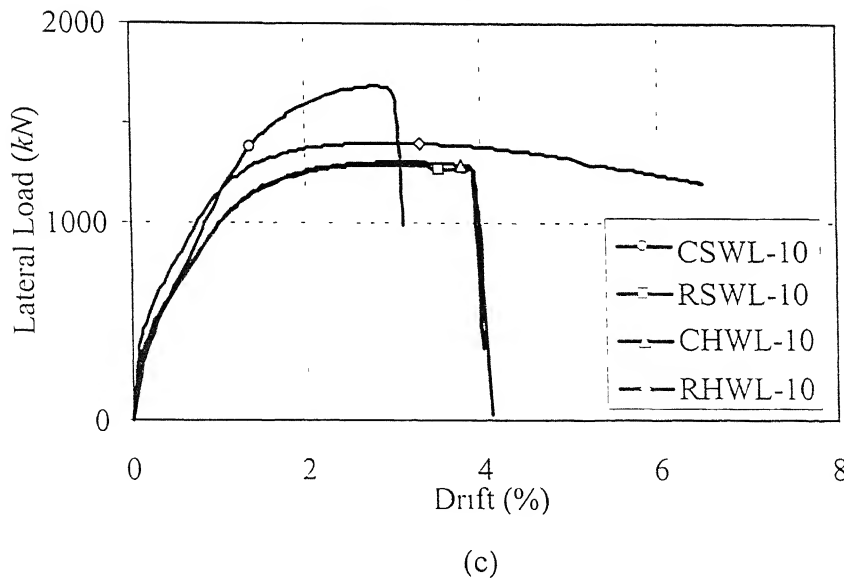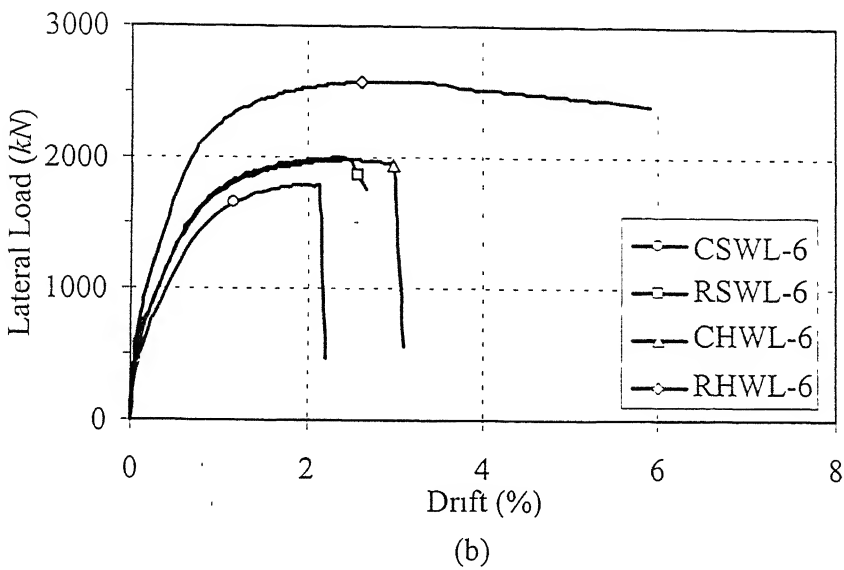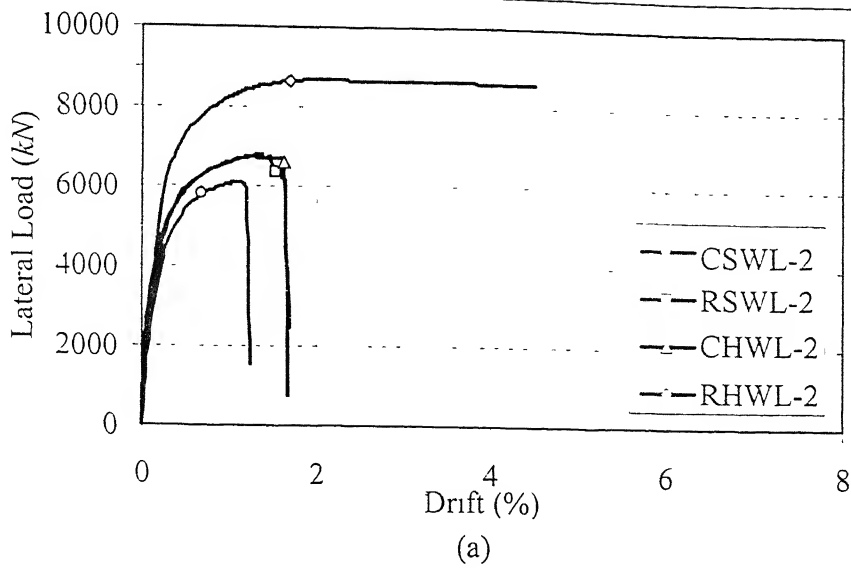
Figure 3.4: Lateral load-deformation relations of piers of slenderness ratio (a) *2*, (b) *6*, and (c) *10* in investigation on effect of slenderness.
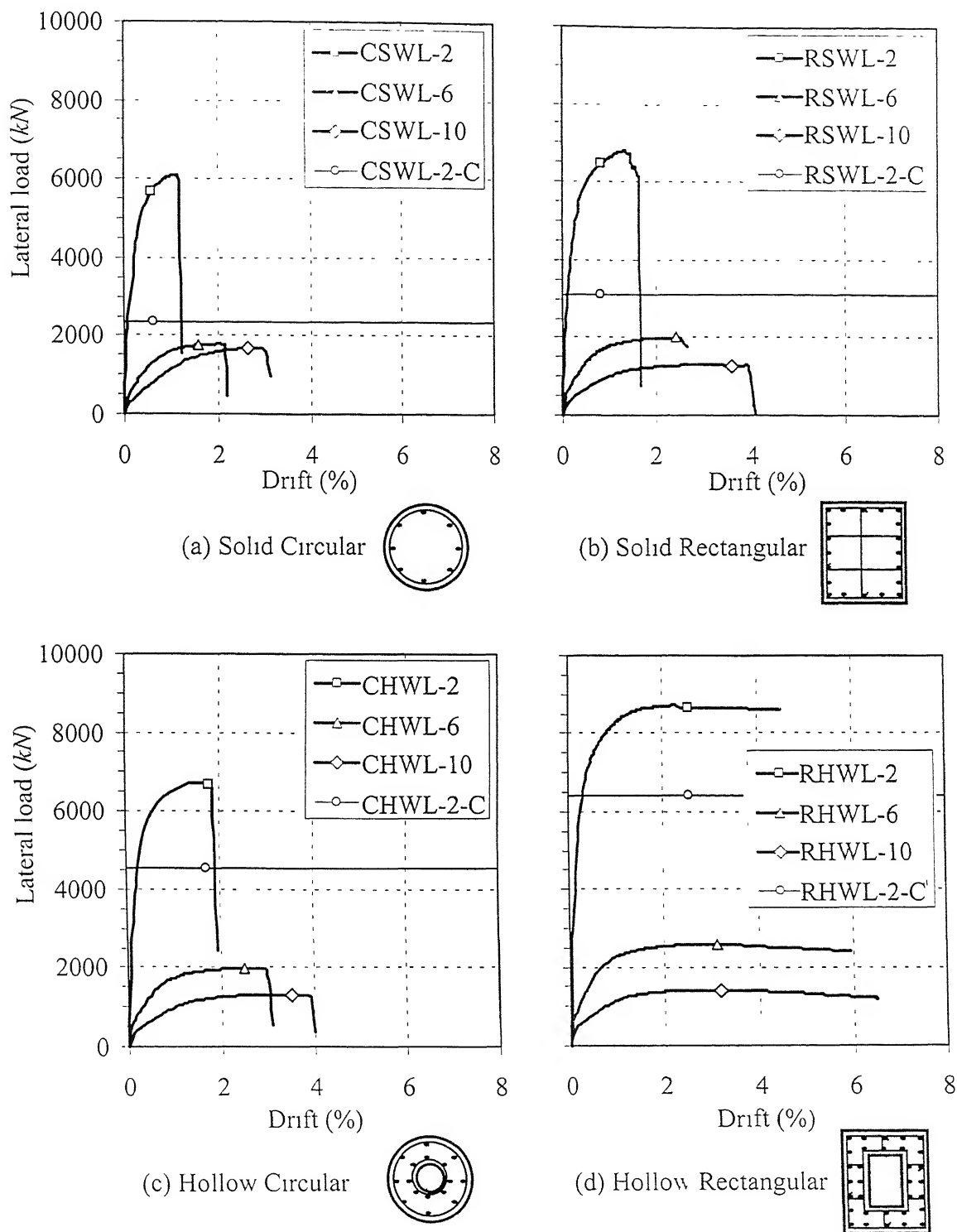
Figure 3.5: Lateral load-deformation relations of (a) solid circular, (b) solid rectangular, (c) hollow circular, and (d) hollow rectangular piers of slenderness ratios *2, 6* and *10*, with corresponding nominal shear capacities
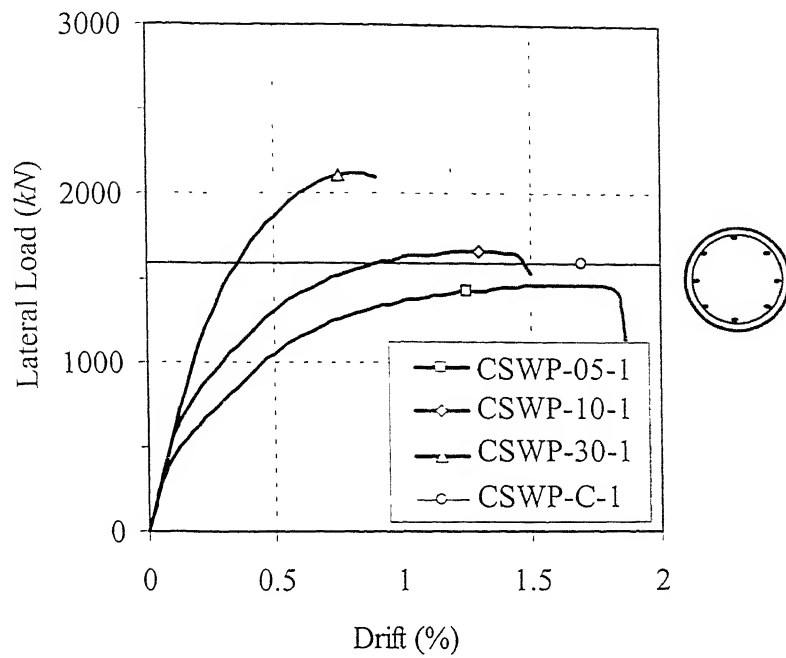
Figure 3.6: Lateral load deformation relations of solid circular pier with three axial load levels with corresponding nominal shear capacity level.
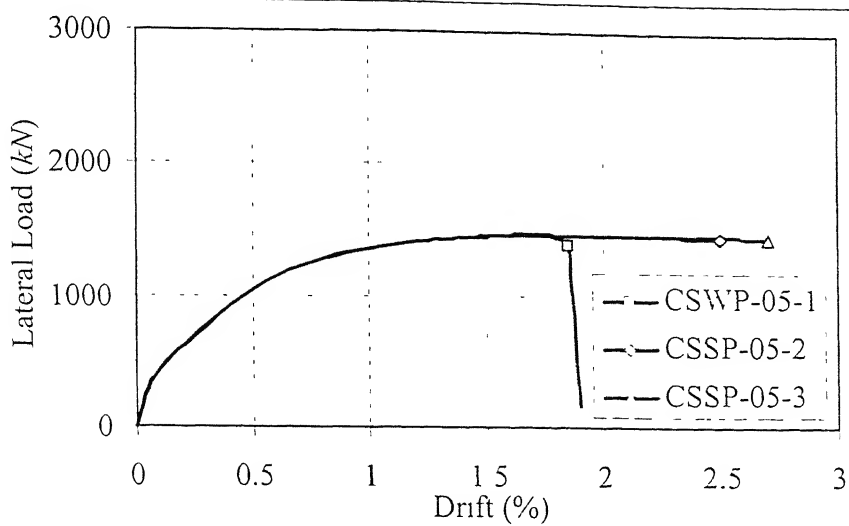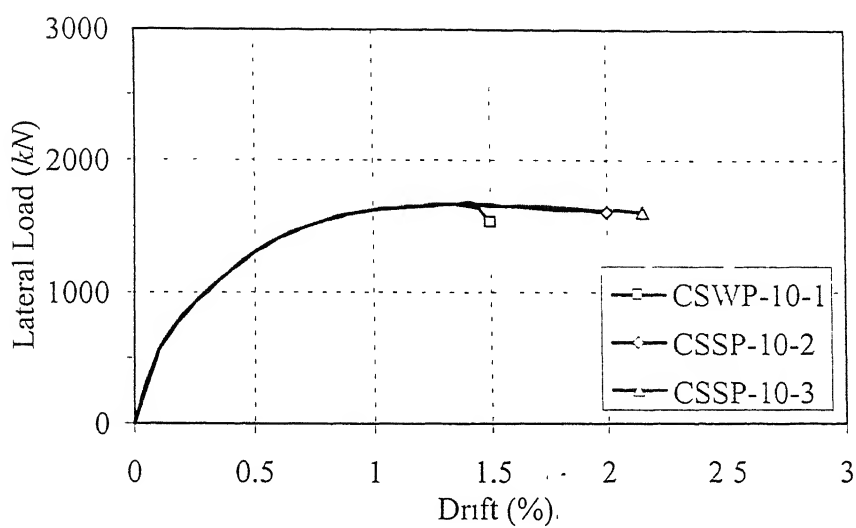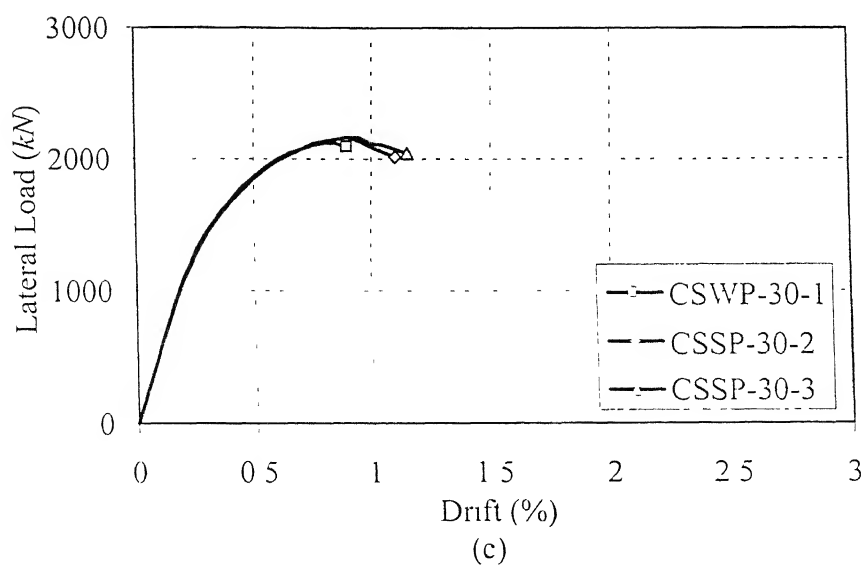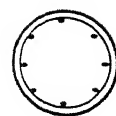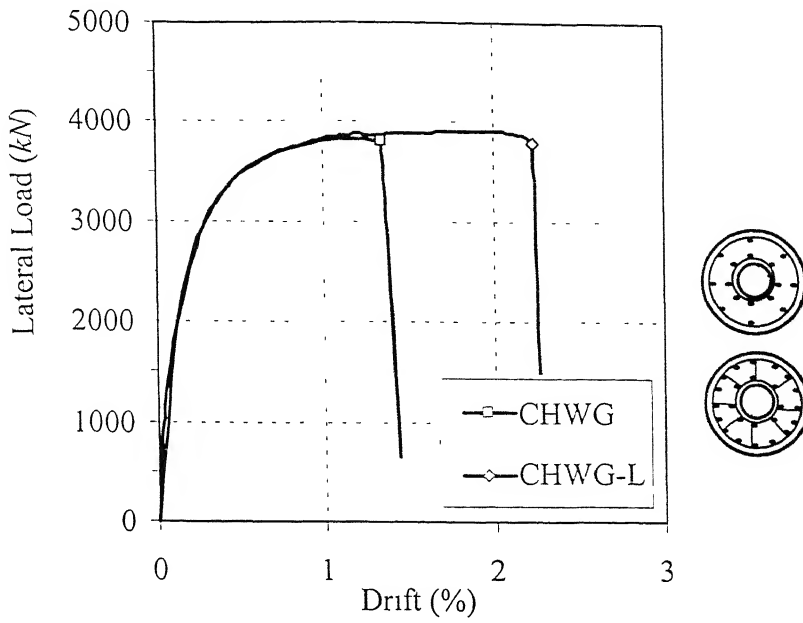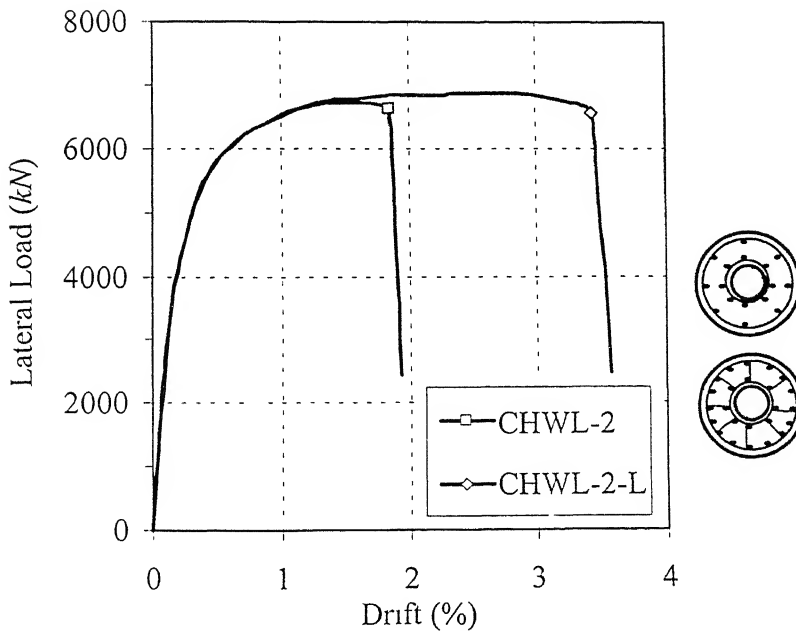
Figure 3.7: Lateral load deformation relations of solid circular pier with axial load ratio of (a) *0 05*, (b) *0 10*, and (c) *0 30* with three different hoop reinforcements.

(a) CHWG

(b) CHWL-2

Figure 3.8: Lateral load deformation relations of hollow circular piers (a) CHWG, and (b) CHWL-2 with and without radial links

• • •

Appendix A

Stress-Strain Curve for
High Yield Strength Deformed Steel Bars

A1 STRESS-STRAIN CURVE FOR HYSD BARS

The stress-strain curve of HYSD steel bars [Dasgupta, 2000] conforming to IS:1786-1979 consists of three parts [Figure A-1]. The first one was given by a straight line through the origin with a slope E_s, upto a stress of $0.8f_y$, where E_s and f_y are Young's modulus and 0.2% proof stress of the steel, respectively.
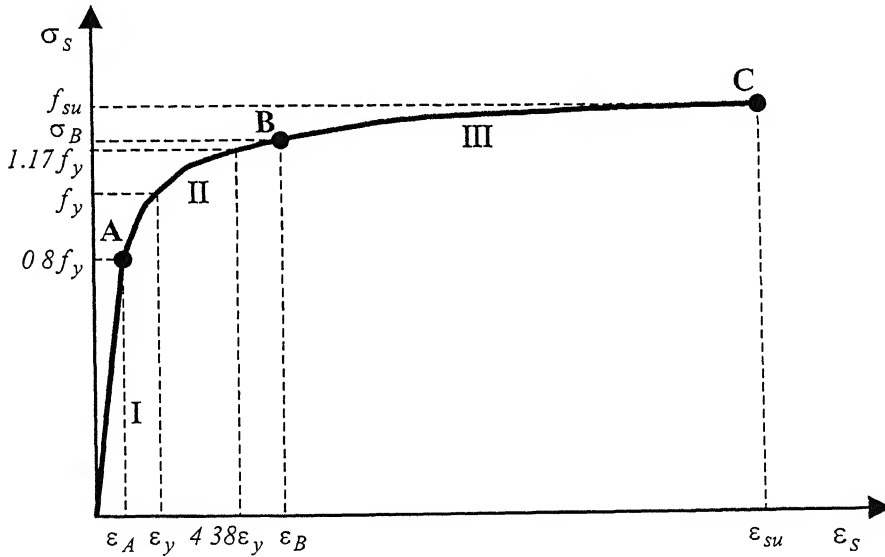
Figure A-1: Stress-Strain Curve of HYSD Steel Bars [Dasgupta, 2000].

The second part was given by a cubic ellipse as

$$-\frac{(\varepsilon - \varepsilon_{II})^3}{a_{II}^3} + \frac{(\sigma - \sigma_{II})^3}{b_{II}^3} = 1,\qquad\text{(A-1)}$$

where ε_{II} and σ_{II} are the coordinates of the centre of the ellipse and a_{II} and b_{II} are the semi-major and semi-minor axes of the ellipse, respectively. These four quantities were evaluated from the four boundary conditions

$$\sigma\big|_{\varepsilon=\varepsilon_A} = 0.8 f_y$$

$$\frac{\partial\sigma}{\partial\varepsilon}\bigg|_{\varepsilon=\varepsilon_A} = E_s$$

$$\sigma\big|_{\varepsilon=\varepsilon_y} = f_y \qquad , \tag{A-2}$$

$$\frac{\partial\sigma}{\partial\varepsilon}\bigg|_{4.38\varepsilon_y} = E_{sh}$$

where

$$\varepsilon_A = \frac{0.8 f_y}{E_s}. \tag{A-3}$$

In Eq.(A-2), ε_y and E_{sh} are the yield strain and the strain-hardening slope of the steel stress-strain curve, respectively. ε_y is given by

$$\varepsilon_y = 0.002 + \frac{f_y}{E_s}, \tag{A-4}$$

The four unknowns in Eq.(A-1) were calculated as

$$\varepsilon_{II} = \varepsilon_A - \psi_4, \tag{A-5}$$

$$\sigma_{II} = 0.8 f_y - \psi_2, \tag{A-6}$$

$$a_{II} = \sqrt[3]{\frac{\psi_2^3 \psi_4^2}{E_s \psi_2^2} - \psi_4^3} \text{ , and} \tag{A-7}$$

$$b_{II} = a_{II} \sqrt[3]{\frac{E_s \psi_2^2}{\psi_4^2}}, \tag{A-8}$$

where ψ_2 and ψ_4 were obtained by iterating through the following Eqs:

$$\psi_1 = \frac{E_s\left(3l\psi_4^2 + 3l^2\psi_4 + l^3\right)}{\psi_4^2}, \tag{A-9}$$

$$\psi_2 = \frac{-3m^2 - \sqrt{9m^4 - 4m^3(3m - \psi_1)}}{2(3m - \psi_1)}, \tag{A-10}$$

$$\psi_3 = \frac{E_{sh}}{E_s}\left(1 + \frac{q}{\psi_2}\right)^2 \text{, and} \tag{A-11}$$

$$\psi_4 = \frac{-2p - \sqrt{4p^2 - 4p^2(1 - \psi_3)}}{2(1 - \psi_3)}, \tag{A-12}$$

where

$$\begin{aligned}
l &= \varepsilon_y - \varepsilon_I \\
m &= 0.2f_y, \\
p &= 4.38\varepsilon_y - \varepsilon_I, \text{ and} \\
q &= 1.17f_y - 0.8f_y.
\end{aligned} \tag{A-13}$$

The third part was represented by another cubic ellipse having its centre at $(\varepsilon_{III}, \sigma_{III})$ and with semi-major and semi-minor axes as a_{III} and b_{III}. It starts at strain ε_B and continues upto rupture strain. The stress σ_B and slope E_B of the stress-strain curve at the starting point was found from the values given by the previous ellipse. The second ellipse reaches the rupture strain with a stress equal to the ultimate stress and with a zero slope. So, the boundary conditions were given by

$$\begin{aligned}
\sigma|_{\varepsilon = \varepsilon_B} &= \sigma_B \\
\frac{\partial \sigma}{\partial \varepsilon}\bigg|_{\varepsilon = \varepsilon_B} &= E_B \\
\sigma|_{\varepsilon = \varepsilon_{su}} &= f_{su} \\
\frac{\partial \sigma}{\partial \varepsilon}\bigg|_{\varepsilon = \varepsilon_{su}} &= 0
\end{aligned} \tag{A-14}$$

Solving for these boundary conditions, the four unknowns of the curve were obtained as

$$\varepsilon_{III} = \varepsilon_{su}, \tag{A-15}$$

$$\sigma_{III} = \sigma_B - \zeta_2, \tag{A-16}$$

$$b_{III} = f_{su} - \sigma_{III}, \text{ and} \tag{A-17}$$

$$a_{III} = b_{III} \sqrt[3]{\frac{\zeta_1^2}{\zeta_2^2 E_B}}, \tag{A-18}$$

where ζ_1 and ζ_2 are given by

$$\zeta_1 = 4\ 91\varepsilon_y - \varepsilon_{su}, \text{ and}$$

$$\zeta_2 = \frac{-3z^2 - \sqrt{9z^4 - 4z^3\left(3z + \zeta_1 E_B\right)}}{2\left(3z + \zeta_1 E_B\right)}. \tag{A-19}$$

In Eq.(A-19), z is given by

$$z = f_{su} - \sigma_B. \tag{A-20}$$

Thus, the whole stress-strain curve was given by,

$$\sigma = \begin{cases} \varepsilon E_s & 0 \le \varepsilon \le \varepsilon_A \\[2em] \sigma_{II} + b_{II}\sqrt[3]{1 + \left(\dfrac{\varepsilon - \varepsilon_{II}}{a_{II}}\right)^3} & \varepsilon_A < \varepsilon \le \varepsilon_B \\[2em] \sigma_{III} + b_{III}\sqrt[3]{1 + \left(\dfrac{\varepsilon - \varepsilon_{III}}{a_{III}}\right)^3} & \varepsilon_B < \varepsilon \le \varepsilon_{su} \end{cases} \tag{A-21}$$

$\bullet\bullet\bullet$